PARTITION OF UNITY ISOGEOMETRIC ANALYSIS FOR SINGULARLY PERTURBED PROBLEMS AND FOURTH ORDER DIFFERENTIAL EQUATIONS CONTAINING SINGULARITIES

by

Sinae Kim

A dissertation submitted to the faculty of
The University of North Carolina at Charlotte
in partial fulfillment of the requirements
for the degree of Doctor of Philosophy in
Applied Mathematics

Charlotte

2016

Approved by:

_____

Dr. Hae-soo Oh

_____

Dr. Joel Avrin

_____

Dr. Shaozhong Deng

_____

Dr. Churlzu Lim

ABSTRACT

SINAE KIM. Partition of Unity Isogeometric Analysis for singularly Perturbed problems and fourth order differential equations containing singularities. (Under the direction of DR. HAE-SOO OH)

Our aim in this research is to develop the numerical solutions of singularly perturbed convection-diffusion problems and heat equations in a circular domain, and fourth-order PDEs containing singularities, avoiding fine mesh around the boundary layer or singular zone. To resolve the oscillations of classical numerical solutions of our problems, we construct boundary layer elements via boundary layer analysis for the perturbed problem. We also construct singular functions by the known solution on the crack domain for the fourth-order equations containing singularities. We modify the boundary layer elements and singular functions using partition of unity function with flat-top, which absorb the boundary layer or crack singularities and do not affect outside the boundary layer zone or singular zone. Using B-spline Isogeometric Finite element space enriched with the boundary layer elements and singular functions, we obtain an accurate numerical scheme on the exact geometry, in a circular domain. As for the perturbed problems, we develop the boundary layer element on the reference domain through the geometry mapping which can capture the boundary layer singularity. As for the fourth-order equations containing singularities, since we already know the singular functions on the physical domain not reference domain, we add the singular functions directly or introduce the Mapping Method to generate those singular functions. We obtain an accurate numerical methods in IGA setting, using partition of unity functions and enrichment functions.

ACKNOWLEDGMENTS

TABLE OF CONTENTS

LIST OF FIGURES

LIST OF TABLES

CHAPTER 1: INTRODUCTION

By Isogeometric Analasis, we can use the design geometry directly for analysis without modifying the geometry for analysis purpose. By using the geometry mapping, we could approximate the solution on parametric domain for any physical domain. In Isogeometric Analysis, we use B-spline as the basis functions that allows us to construct them with any regularity. However, general Isogeometric Analysis does not give accurate solutions to perturbed problems or fourth-order equations with singularities. Therefore, we enrich Isogeometric Finite Element Space by adding boundary layer element or singular functions into boundary layer or singular zone using Partion of Unity with flat-top. We call this approach Partion of Unity Isogeometric Analysis. (PU-IGA) See [48] and [49]

Most of the numerical methods to solve the singular perturbed problems are based on domain decomposition or refined meshes near boundary layer in [35], [50], [51], and [68], etc. In [27], the authors approximated the problem using a quasi-uniform triangulation and P_1 finite element space enriched with boundary layer correctors in a rectangle and circle. In this paper, we similarly derive the boundary layer element via boundary layer analysis [40] and use that element as enriched function in B-spline based Isogeometric setting. Without using fine mesh and without modification of geometry, using boundary layer element which absorbs the singularity behavior, we aim to approximate the solution. We extend the boundary layer analysis to the

problem on other geometry, an ellipse to develop boundary layer elements.

This Enriched PU-IGA is extended to solve a singularly perturbed parabolic problems on a circular domain.One can find numerical results for parabolic perturbed problems in [9], [12], [33], [39] , and [69] etc. The authors utilized mesh refinement near boundary and mainly focused on the finite difference method in a rectangular domain. In [29], the author approximates the perturbed parabolic problem on circular domain using a quasi-uniform triangulation and P_1 finite element space enriched with boundary layer correctors constructed near the circular boundary. In this paper, we aim to approximate the problem using B-spline based Isogeometric Finite Element Space enriched with boundary layer elements via boundary layer analysis. We avoid the costly mesh refinements at the boundary using the boundary layer element modified by the partition of unity with flat-top.

As for perturbed problems, we develop the enrichment function on the reference domain which can capture the singularity. While, we consider the fourth-order equation with singularities whose singular solution is known on a physical domain. For example, the solution behavior of crack singularity is well known [23] . In [42], the authors introduced the mapping technique called the Method of Auxiliary Mapping (MAM) into conventional $p-$FEM. In the similar way, we introduce a Mapping Method for fourth-order equations with singularities to generate the known singular functions on a physical domain. We construct a geometry mapping that generates singular functions resembling the singularities.

This paper is organized as follows. In Chaper 2, we review definitions, terminologies and properties of Isogeometric Analysis, B-splines and Partition of Unity. We also

briefly review Boundary Layer Analysis. In Chapter 3, we obtain error estimates and propose construction of basis functions of PU-IGA. In Chapter 4, we solve perturbed convection-diffusion problem on a circular domain. We define PU-IGA finite element space which incorporates the boundary layer elements. We present the results of numerical simulations. In Chapter 5, we solve 1D perturbed parabolic problem on a circular domain in PU-IGA enriched by the boundary layer elements. We present error estimates and numerical results. In Chapter 6, we solve fourth-order equations containing singularities in PU-IGA enriched by singular functions directly or PU-IGA with a mapping to generates singular functions. We compare the numerical results with general IGA. The conclusion follows.

CHAPTER 2: PRELIMINARIES

2.1   Isogeometric Analysis

Isogeometric analysis seeks to unify the fields of CAD(Computer-aided design) and FEA(Finite element Analysis). Analysis-suitable models are not automatically created or readily meshed from CAD geometry. There are many time consuming, preparatory steps involved. To break down the barriers between engineering design and analysis, Isogeometric Analysis focus on only one geometric model(CAD representation), which can be utilized directly as an analysis model. We follow notations and definitions in the books [16], [55] and [56].

NURBS-based isogeometric analysis

There are many computational geometry technologies that could serve as a basis for isogeometric analysis. The reason for selecting NURBS as our basis is compelling: It is the most widely used computational geometry technology, the industry standard, in engineering design.

The major strengths of NURBS are that they convenient for free-form surface modeling, can exactly represent all conic sections, and therefore circles, cylinders, spheres, ellipsoids, etc., and that there exit many efficient and numerically stable algorithms to generate NURBS objects. They also possess useful mathematics properties, such as the ability to be refined through knot insertion, C^{p-1}-continuity of pth-order NURBS,
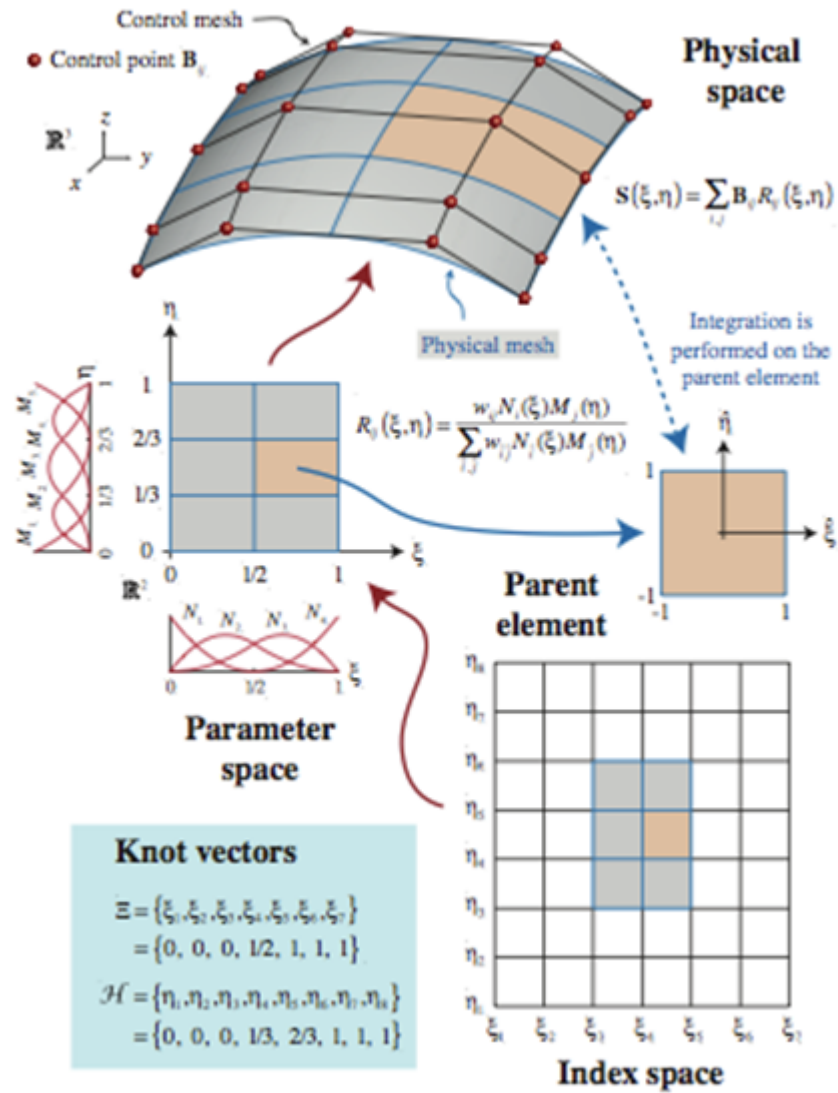
NURBS Object

Figure 1: Schematic illustration of NURBS object for a one-patch surface model [16]. Open knot vectors $\xrightarrow{p=2}$ quadratic C^1-continuous basis functions $\xrightarrow{B_i}$ geometrical objects

and the variation diminishing and convex hull properties.

NURBS Objects

In NURBS, the basis functions are usually not interpolatory. There are two notions of meshes, the control mesh and the physical mesh. The control points define the *Control Mesh*, and the control mesh interpolates the control points. The control mesh does not conform to the actual geometry. The control mesh may be severely distorted and even inverted to an extent, while at the same time for sufficiently smooth NURBS, the physical geometry may still remain valid.

The *Physical mesh* is a decomposition of the actual geometry. There are two notions of elements in the physical mesh, the patch and the knot span. The *patch* may be thought of as a macro-element or subdomain. Each patch has two representations, one in a parameter space and one in physical space.

Each patch can be decomposed into knot spans. Knot spans are bounded by knots. These define element domains where basis functions are smooth. Across knots, basis functions will be C^{p-m} where p is the degree of the polynomial and m is the multiplicity of the knot. Knot span may be thought of as micro-elements because they are the smallest entities we deal with. They also have representations in both a parameter space and physical space.

We have an *Index space* of a patch. It uniquely identifies each knot and discriminates among knots.A schematic illustration of the ideas is presented in Figure 2.1 for a NURBS surface in R^3 from[16].

2.2   B-splines and NURBS

NURBS are built from B-splines and so a discussion of B-splines is a natural starting point. The B-spline parameter space is local to patches rather than elements. That is, the B-spline mapping takes a patch of multiple elements in the parameter space into the physical space, as seen in Figure 1. Each element in the physical space is the image of a corresponding element in the parameter space, but the mapping itself is global to the whole patch.

Knot vectors

A *Knot vector* in one dimension is a non-decreasing set of coordinates in the parameter space, written $\Xi = \{\xi_1, \xi_2, ..., \xi_{n+p+1}\}$, where $\xi_i \in R$ is the ith knot, i is the knot index, $i = 1, 2, ..., n + p + 1$, p is the polynomial order, and n is the number of basis functions used to construct the B-spline curve. The knots partition the parameter space into elements. In the case of B-splines, the functions are piecewise polynomials where the different pieces join along knot lines. In this way the functions are C^∞ within an element.

Knot vectors may be *uniform* if the knots are equally space in the parameter space. If they are unequally space, the knot vector is *non-uniform*. Knot values may be repeated, that is, more than one knot may take on the same value. The multiplicities of knot values have important implications for the continuity of the basis function across knots.

A knot vector is said to be *open* if its first and last knot values appear $p + 1$ times. Open knot vectors are the standard in the CAD literature. In one dimension,

basis functions formed from open knot vectors are interpolatory at the ends of the

parameter space.

Basis functions

With a knot vector, the B-spline basis functions are defined recursively starting

with piecewise constants$(p = 0)$:

$$N_{i,0} = \begin{cases} 1 & \text{if } \xi_i \leq \xi < \xi_{i+1} \\ \\ 0 & \text{otherwise} \end{cases} \tag{1}$$

For $p = 1, 2, 3, ...$, they are defined by

$$N_{i,p}(\xi) = \frac{\xi - \xi_i}{\xi_{i+p} - \xi_i} N_{i,p-1}(\xi) + \frac{\xi_{i+p+1} - \xi}{\xi_{i+p+1} - \xi_{i+1}} N_{i+1,p-1}(\xi) \tag{2}$$

This is referred to as the *Cox-de Boor recursion formula*[Cox, 1971; de Boor, 1972].

The results of applying (1) and (2) to a uniform vector are presented in Figure 2

There are several important features of B-spline basis functions.

- Partition of unity, that is,

$$\sum_{i=1}^{n} N_{i,p}(\xi) = 1, \qquad \forall \xi$$

- Nonnegative, that is,

$$N_{i,p} \geq 0, \qquad \forall \xi$$

- $p - m$ continuous derivatives of pth order functions across boundary (across the

  knot), where m is the multiplicity of the knot value

- $p + 1$ span (support) of pth order B-spline functions
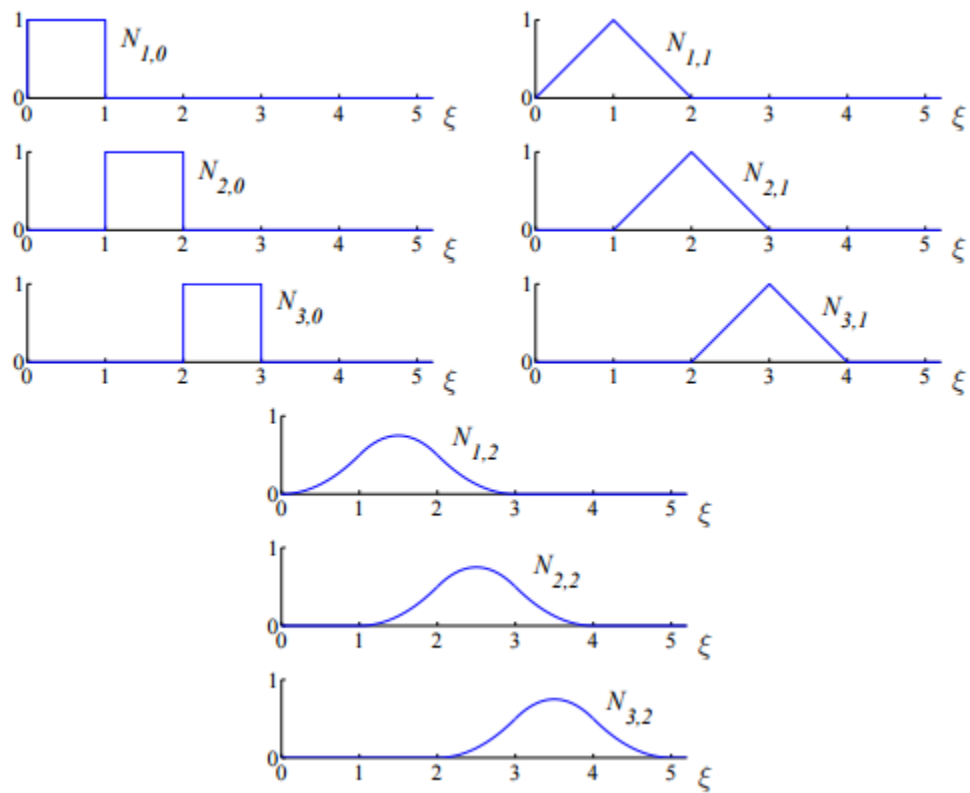
Figure 2: Basis functions of order 0, 1, and 2 for uniform knot vector $\Xi = \{0, 1, 2, 3, 4, ...\}$ [16]

- Any given function shares support with $2p + 1$ functions including itself.

B-spline geometries

Given n basis functions, $N_{i,p}, i = 1, 2, ..., n$ and corresponding control points $B_i \in R^d, i = 1, 2, ..., n$ (vector-valued coefficients), a piecewise-polynomial *B-spline curve* is given by

$$C(\xi) = \sum_{i=1}^{n} N_{i,p}(\xi) B_i$$

Given a *control net* $B_{i,j}, i = 1, 2, ..., n, j = 1, 2, ..., m$, polynomial order p and q, and knot vectors $\Xi = \{\xi_1, \xi_2, ..., \xi_{n+p+1}\}$, and $\Im = \{\eta_1, \eta_2, ..., \eta_{m+q+1}\}$, a tensor product *B-spline surface* is defined by

$$S(\xi, \eta) = \sum_{i=1}^{n} \sum_{j=1}^{m} N_{i,p}(\xi) M_{j,q}(\eta) B_{i,j}$$

where $N_{i,p}(\xi)$ and $M_{j,q}(\eta)$ are univariate B-spline basis functions of order p and q, corresponding to knot vectors Ξ and $\Im$, respectively. Given a *control lattice* $\{B_{i,j,k}\}, i = 1, 2, ..., n, j = 1, 2, ..., m, k = 1, 2, ..., l$, polynomial orders p, q, and r, and knot vectors $\Xi = \{\xi_1, \xi_2, ..., \xi_{n+p+1}\}$, $\Im = \{\eta_1, \eta_2, ..., \eta_{m+q+1}\}$, and $\Re = \{\zeta_1, \zeta_2, ..., \zeta_{l+r+1}\}$, a B-spline solid is defined by

$$S(\xi, \eta, \zeta) = \sum_{i=1}^{n} \sum_{j=1}^{m} \sum_{k=1}^{l} N_{i,p}(\xi) M_{j,q}(\eta) L_{k,r}(\zeta) B_{i,j,k}$$

B-spline geometries have following properties:

- *Affine covariance*, the ability to apply an affine transformation to a curve by applying it directly to the control points

- A curve will have at least as many continuous derivatives across an element

boundary boundary as its basis functions have across the corresponding knot value.

- Moving a single control point can affect the geometry of no more than $p + 1$ elements of the curve.

- B-spline curve is completely contained within the convex hull defined by its control points.

- As the polynomial order increases, the curve become smoother and the effect of each individual control point is diminished.

- B-spline curves also possess a variation diminishing property.(no variation diminishing property for surface)

<div align="center">Non-Uniform Rational B-Splines</div>

Non-Uniform Rational B-Splines (NURBS) has the ability to exactly represent a wide array of objects that cannot be exactly represented by B-splines (polynomials). Define *weighting function*

$$W(\xi) = \sum_{i=1}^{n} N_{i,p}(\xi)w_i$$

where w_i is the ith *weight*. NURBS basis is given by

$$R_i^p(\xi) = \frac{N_{i,p}(\xi)w_i}{W(\xi)} = \frac{N_{i,p}(\xi)w_i}{\sum_{\hat{i}=1}^{n} N_{\hat{i},p}(\xi)w_{\hat{i}}}$$

which is clearly a piecewise rational function. A NURBS curve is defined by

$$C(\xi) = \sum_{i=1}^{n} R_i^p(\xi)B_i$$

This form is identical to that for B-splines.

Rational surfaces and solids are defined analogously in terms of the rational basis functions

$$R_{i,j}^{p,q}(\xi,\eta) = \frac{N_{i,p}(\xi)M_{j,q}(\eta)w_{i,j}}{\sum_{\hat{i}=1}^{n}\sum_{\hat{j}=1}^{m}N_{\hat{i},p}(\xi)M_{\hat{j},q}(\eta)w_{\hat{i},\hat{j}}}$$

$$R_{i,j,k}^{p,q,r}(\xi,\eta,\zeta) = \frac{N_{i,p}(\xi)M_{j,q}(\eta)L_{k,r}(\zeta)w_{i,j,k}}{\sum_{\hat{i}=1}^{n}\sum_{\hat{j}=1}^{m}\sum_{\hat{k}=1}^{l}N_{\hat{i},p}(\xi)M_{\hat{j},q}(\eta)L_{\hat{k},r}(\zeta)w_{\hat{i},\hat{j},\hat{k}}}$$

These rational basis functions bear much in common with their polynomial B-splines such as the continuity of the functions, their support, a partition of unity, and point-wise nonnegativity, and convex hull property.

2.3   Refinement

There are many ways in which the basis may be enriched while leaving the under-lying geometry and its parameterization intact. We have control over the element size and the order of the basis and the continuity of the basis.

Knot insertion

The first mechanism by which one can enrich the basis is *knot insertion*. Knots may be inserted without changing a curve geometrically or parametrically. Given a knot vector $\Xi = \{\xi_i, \xi_2, ..., \xi_{n+p+1}\}$, we have an *extended* knot vector $\bar{\Xi} = \{\bar{\xi}_1 = \xi_1, \bar{\xi}_2, ..., \bar{\xi}_{n+m+p+1} = \xi_{n+p+1}\}$, such that $\Xi \subset \bar{\Xi}$. The new $n + m$ basis functions are formed by applying the cox-de Boor recursion formula and the new $n + m$ control points are formed from linear combinations of the original control points by

$$\bar{B} = T^p B$$

where

$$
T_{ij}^0 = \begin{cases} 1 & \bar{\xi}_i \in [\xi_j, \xi_{j+1}) \\ \\ 0 & \text{otherwise} \end{cases}
$$

$$
T_{ij}^{q+1} = \frac{\bar{\xi}_{i+q} - \xi_j}{\xi_{j+q} - \xi_j} T_{ij}^q + \frac{\xi_{j+q+1} - \bar{\xi}_{i+q}}{\xi_{j+q+1} - \xi_{j+1}} T_{ij+1}^q \qquad \text{for } q = 0, 1, 2, ..., p-1
$$

This process may be repeated to enrich the solution space by adding more basis functions of the same order while leaving the curve unchanged. Insertion of new knot values clearly has similarities with the classical h-refinement strategy in finite element analysis as it splits existing elements into new ones. However, it differs in the number of new functions that are created, as well as in the continuity of the basis across the newly created element boundaries. To perfectly replicate h-refinement, one would need to insert each of the new knot values p times so that the functions will be C^0 across the new boundary. See Figure 3.

Order elevation

The second mechanism by which one can enrich the basis is *order elevation*. This process involves raising the polynomial order of the basis functions used to represent the geometry. The basis has $p - m_i$ continuous derivatives across element boundaries. When p is increased, m_i must also be increased if we are to preserve the discontinuities in the various derivatives already existing in the original curve. During order elevation, the multiplicity of each knot value is increased by one, but no new knot values are added. As with knot insertion, neither the geometry nor the parameterization are changed. The process is as followings.

- replicate existing knots until their multiplicity is equal to the polynomial order

$\Xi = \{0,0,0,1,1,1\}$ $\Xi = \{0,0,0,.5,1,1,1\}$

Original curve and control points   Refined curve and control points

Original one element mesh   Refined two element mesh

Original basis functions   New basis functions
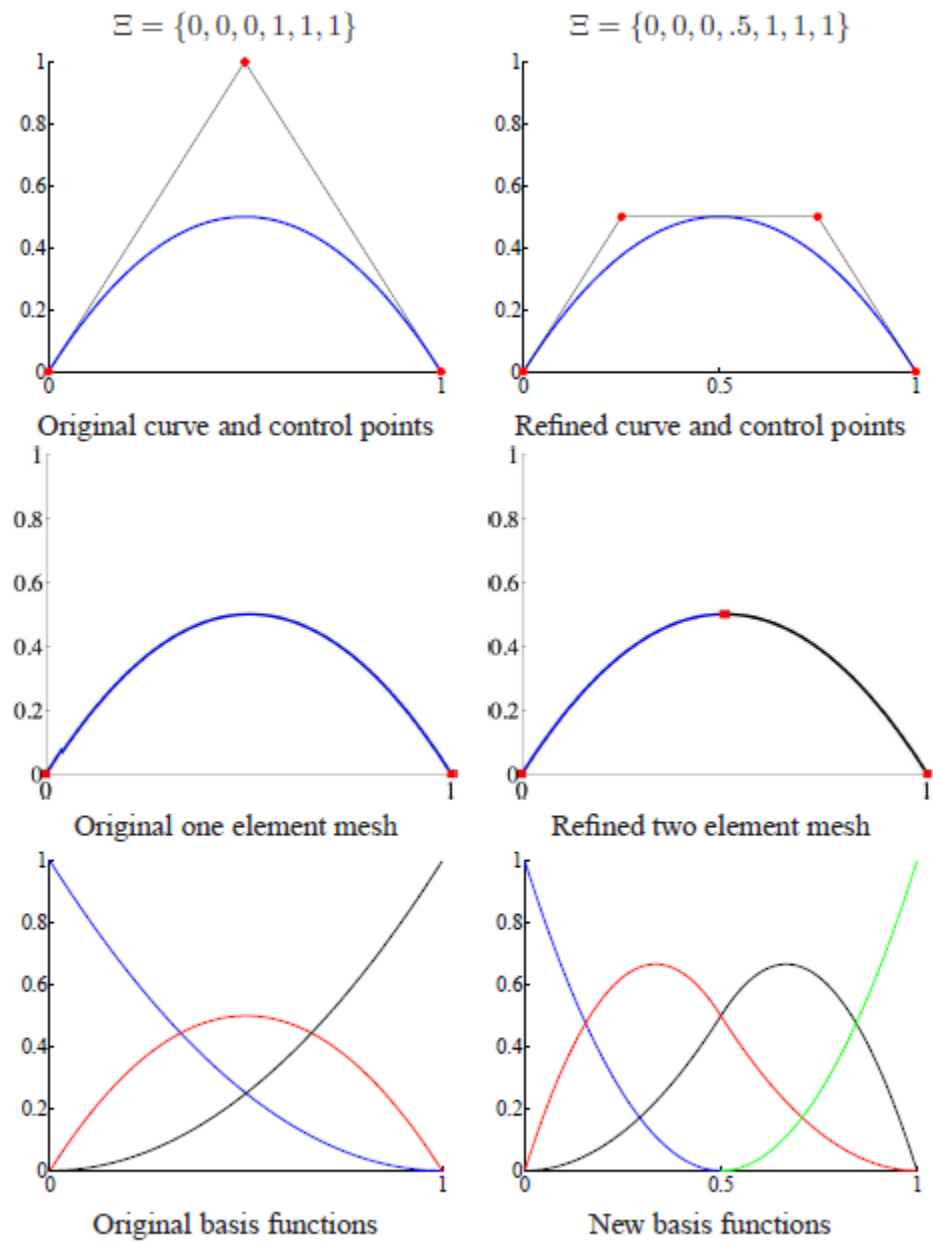
Knot insertion. Control points are denoted by •'s. The knots, which define a mesh by partitioning the curve into elements, are denoted by ■'s.

Figure 3: [16]

- elevate the order of the polynomial on each of individual segments

- excess knots are removed to combine the segments into one, order-elevated, B-spline curve.

Order elevation clearly has much in common with the classical p-refinement strategy in finite element analysis as it increases the polynomial order of the basis. The major difference is that p-refinement always begins with a basis that is C^0 everywhere, while order elevation is compatible with any combination of continuities that exist in the unrefined B-spline mesh. See Figure 4.

k-refinement

We can insert new knot values with multiplicities equal to one to define new elements across whose boundaries functions will be C^{p-1}. We can also repeat existing knot values to lower the continuity of the basis across existing element boundaries. This makes knot insertion a more flexible process than simple h-refinement, Similarly, we have a more flexible higher-order refinement as well.

K-refinement procedure is that we elevate the order of the orginal, coarsest curve to q degree, and then insert the unique knot value $\bar{\xi}$. The basis would have $q-1$ continuous derivatives at $\bar{\xi}$. There is no analogous practice in standard finite element analysis. See Figure 5.

In summary, Pure k-refinement keeps h fixed but increases the continuity along with the polynomial order. Pure p-refinement increases the polynomial order while the basis remains C^0. Inserting new knot values with a multiplicity of p results in classical h-refinement, whereby new elements are introduced that have C^0 boundaries.

$\Xi = \{0, 0, 0, 1, 1, 1\}$

$\Xi = \{0, 0, 0, 0, 1, 1, 1, 1\}$

Original curve and control points

Refined curve and control points

Original one element mesh

Refined one element mesh

Original basis functions

New basis functions
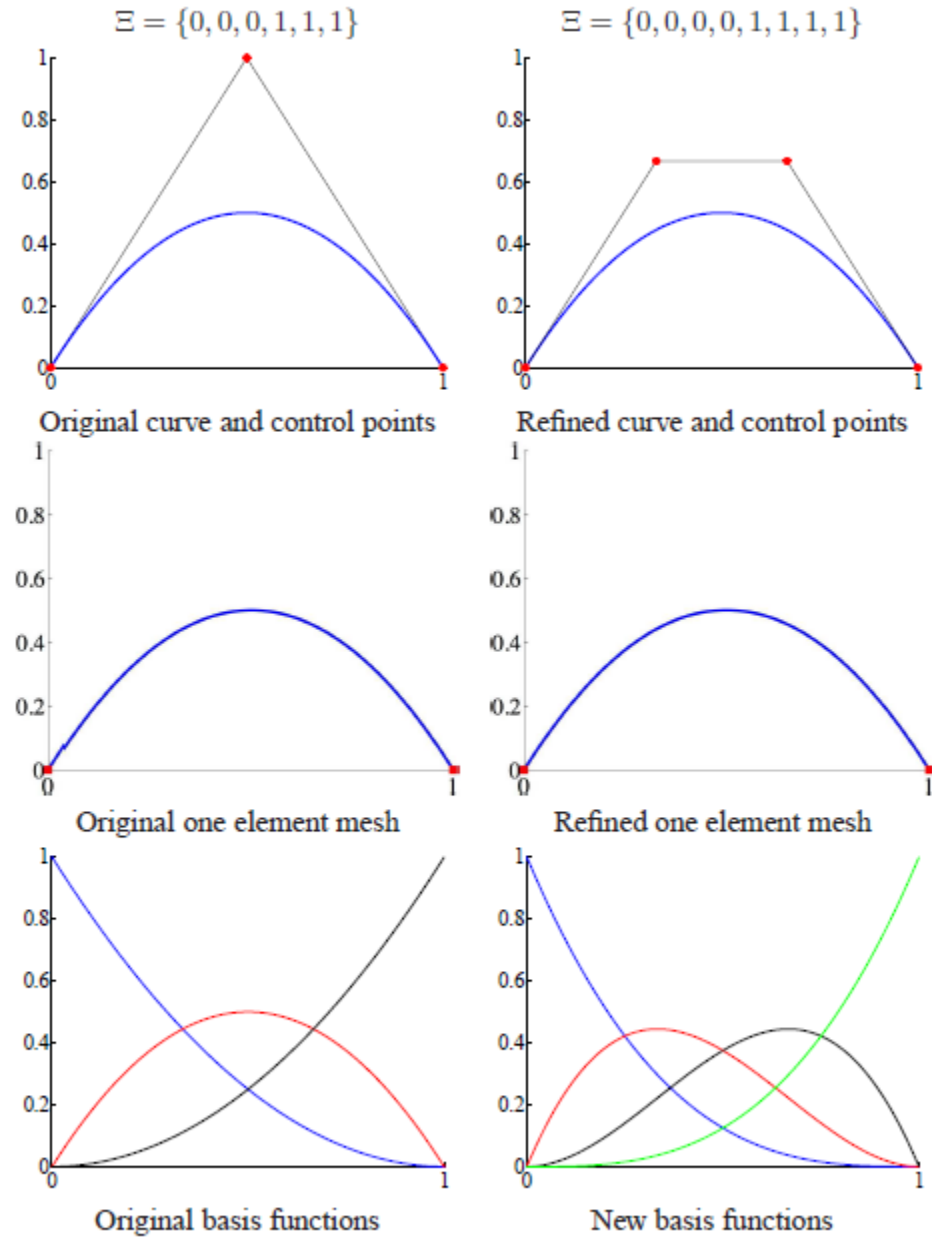
Order elevation. Control points are denoted by •'s. The knots, which define a mesh by partitioning the curve into elements, are denoted by ■'s.

Figure 4: [16]

A multitude of refinement options can be obtained beyond simple h, p, k-refinement by knot insertion and order elevation.

2.4   Partition of Unity

A family $\{U_k : \text{ open subsets of } R^d \mid k \in \mathcal{D}\}$ is said to be *a point finite open covering* of $\Omega \subset R^d$ if there is M such that any $x \in \Omega$ lies in at most M of the open sets U_k and $\Omega \subseteq \bigcup\limits_{k \in \mathcal{D}} U_k$.

For a point finite open covering $\{U_k \mid k \in \mathcal{D}\}$ of a domain, suppose there is a family of Lipschitz functions $\{\phi_k \mid k \in \mathcal{D}\}$ on Ω satisfying the following conditions:

- For $k \in \mathcal{D}, \ 0 \le \phi_k(x) \le 1, \quad x \in R^d$

- The support of ϕ_i is contained in $\bar{U}_k$, for each $k \in \mathcal{D}$

- $\sum_{k \in \mathcal{D}} \phi_k(x) = 1$ for each $x \in \Omega$

Then $\{\phi_k \mid k \in \mathcal{D}\}$ is called *a partition of unity (PU)* subordinate to the covering $\{U_k \mid k \in \mathcal{D}\}$. The covering sets $\{U_k\}$ are called *patches.*

A weight function, or window function, is a non-negative continuous function with compact support and is denoted by $w(x)$. Consider the following conical window function: For $x \in R$,

$$w(x) = \begin{cases} (1 - x^2)^l, & |x| \le 1 \\ \\ 0, & |x| > 1 \end{cases}$$

where l is an integer. $w(x)$ is z C^{l-1} function. In R^d the weight function $w(x)$ can be constructed from a one dimensional weight function as $w(x) = \prod_{i=1}^{d} w(x_i)$, where

18

$\Xi = \{0,0,0,\frac{1}{3},\frac{1}{3},\frac{2}{3},\frac{2}{3},1,1,1\},\ p=2$ $\Xi = \{0,0,0,\frac{1}{3},\frac{2}{3},1,1,1\},\ p=2$

$\Xi = \{0,0,0,0,\frac{1}{3},\frac{1}{3},\frac{1}{3},$
$\frac{2}{3},\frac{2}{3},\frac{2}{3},1,1,1,1\},\ p=3$ $\Xi = \{0,0,0,0,\frac{1}{3},$
$\frac{2}{3},1,1,1,1\},\ p=3$

$\Xi = \{0,0,0,0,0,\frac{1}{3},\frac{1}{3},\frac{1}{3},\frac{1}{3},$
$\frac{2}{3},\frac{2}{3},\frac{2}{3},\frac{2}{3},1,1,1,1,1\},\ p=4$ $\Xi = \{0,0,0,0,0,\frac{1}{3},$
$\frac{2}{3},1,1,1,1,1\},\ p=4$

$\Xi = \{0,0,0,0,0,0,\frac{1}{3},\frac{1}{3},\frac{1}{3},\frac{1}{3},\frac{1}{3},$
$\frac{2}{3},\frac{2}{3},\frac{2}{3},\frac{2}{3},\frac{2}{3},1,1,1,1,1,1\},\ p=5$ $\Xi = \{0,0,0,0,0,0,\frac{1}{3},$
$\frac{2}{3},1,1,1,1,1,1\},\ p=5$

(a)   (b)
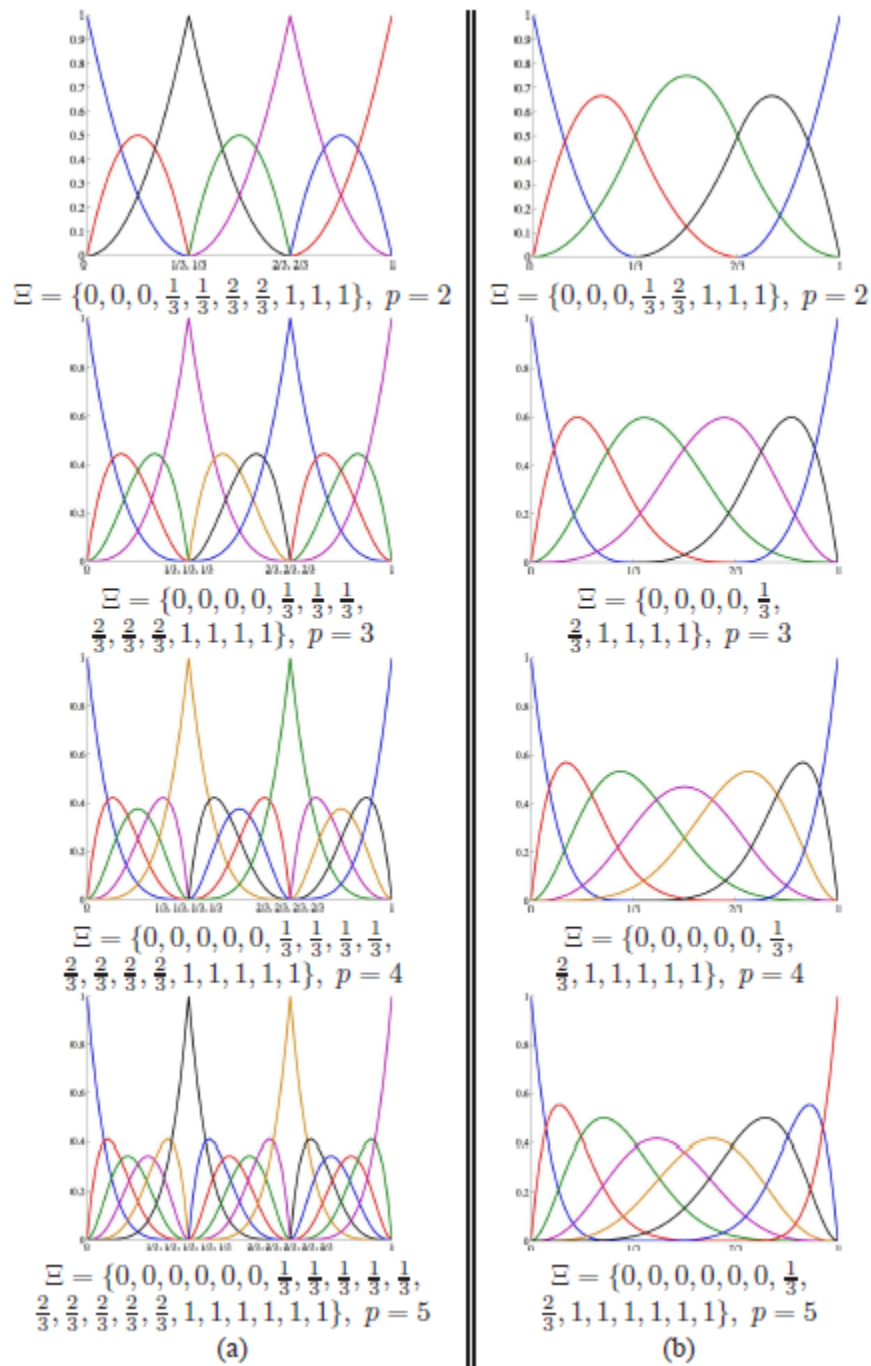
Figure 5: Three element, higher-order meshes for p- and k-refinement. a) The p-refinement approach results in many functions that are C^0 across element boundaries. b) In comparison, k-refinement results in a much smaller number of functions, each of which is C^{p-1} across element boundaries

$x = (x_1, ..., x_d)$. We use the normalized window function defined by

$$w_\delta^l(x) = Aw(\frac{x}{\delta}), \qquad A = \frac{(2l+1)!}{2^{2l+1}(l!)^2\delta} \tag{3}$$

where A is the constant such that $\int_R w_\delta^l(x)dx = 1$; refer to [24].

<div align="center">Partition of Unity functions with flat-top</div>

We first review one dimensional partition of unity with flat-top; refer to [43].

For any positive integer n, C^{n-1} piecewise polynomial basic PU functions were constructed as follows: For integers $n \geq 1$, we define a piecewise polynomial function by

$$\phi_{g_n}^{(pp)}(x) = \begin{cases} \phi_{g_n}^L(x) = (1+x)^n g_n(x), & x \in [-1, 0] \\ \phi_{g_n}^R(x) = (1-x)^n g_n(-x), & x \in [0, 1] \\ 0, & |x| \geq 1 \end{cases} \tag{4}$$

where $g_n(x) = a_0^{(n)} + a_1^{(n)}(-x) + a_2^{(n)}(-x)^2 + ..., +a_{n-1}^{(n)}(-x)^{n-1}$ whose coefficients are inductively constructed by the following recursion formula:

$$a_k^{(n)} = \begin{cases} 1, & k = 0 \\ \sum_{j=0}^k a_j^{(n-1)}, & 0 < k \leq n - 2 \\ 2(a_{n-2}^{(n)}), & k = n - 1 \end{cases}$$

$\phi_{g_n}^{(pp)}$ is depicted in Fig. 6 for various regularities.

The $\phi_{g_n}^{(pp)}$ has the following properties; refer to [24]
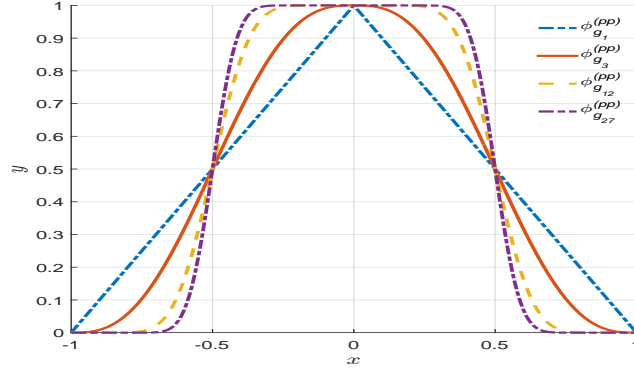
Figure 6: Reference PU functions $\phi_{g_n}^{(pp)}$ with respect to various regularities

-

$$\phi_{g_n}^{(pp)}(x) + \phi_{g_n}^{(pp)}(x-1) = 1, \quad \forall x \in [0,1] \tag{5}$$

Hence $\{\phi_{g_n}^{(pp)}(x-j) \mid j \in Z\}$ is a partition of unity on R.

- $\phi_{g_n}^{(pp)}$ is a C^{n-1} function

We can construct C^{n-1} PU function with flat-top whose support is $[a-\delta, b+\delta]$ with $a + \delta < b - \delta$ by the basic PU function $\phi_{g_n}^{(pp)}$.

$$\psi_{[a,b]}^{(\delta,n-1)}(x) = \begin{cases} \phi_{g_n}^L\left(\frac{x-(a+\delta)}{2\delta}\right), & x \in [a-\delta, a+\delta] \\\\ 1, & x \in [a+\delta, b-\delta] \\\\ \phi_{g_n}^R\left(\frac{x-(b-\delta)}{2\delta}\right), & x \in [b-\delta, b+\delta] \\\\ 0, & x \notin [a-\delta, b+\delta] \end{cases} \tag{6}$$

In order to make a PU function a flat-top, we assume $\delta \leq \frac{b-a}{3}$. See the figure 7.

This flat-top PU function $\psi_{[a,b]}^{(\delta,n-1)}$ is the convolution of the characteristic function
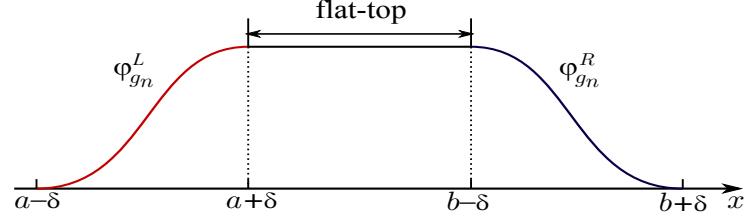
Figure 7: PU with flat-top $\psi_{[a,b]}^{(\delta,n-1)}(x)$

$\chi_{[a,b]}$ and the scaled window function w_δ^n by (2.11), that is,

$$\psi_{[a,b]}^{(\delta,n-1)} = \chi_{[a,b]}(x) * w_\delta^n(x)$$

By the first property of PU function $\phi_{g_n}^{(pp)}$,

$$\phi_{g_n}^R(\xi) + \phi_{g_n}^L(\xi - 1) = 1, \quad \xi \in [0,1]$$

If $\varphi : [-\delta, \delta] \to [0,1]$ is defined by

$$\varphi(x) = \frac{x + \delta}{2\delta}$$

then we have

$$\phi_{g_n}^R(\varphi(x)) + \phi_{g_n}^L(\varphi(x) - 1) = 1, \quad \xi \in [-\delta, \delta]$$

Construction of partition of unity functions with flat-top

The PU function with flat-top (6) can be constructed by either convolution or B-spline functions as follows:

- **PU functions constructed by convolutions** The PU function with flat-top (6) can be constructed by convolution, $\psi_{[a,b]}^{(\delta,n-1)}(x) = \chi_{[a,b]}(x) * w_\delta^n(x)$, the convolution of the characteristic function $\chi_{[a,b]}$ and the scaled window function

w_δ^n defined by (3). The characteristic function is defined by

$$\chi_{[a,b]}(x) = \begin{cases} 1 & \text{if } x \in [a,b], \\ 0 & \text{if } x \notin [a,b]. \end{cases}$$

- **PU functions constructed by B-splines** Using the partition of unity property of the B-splines,

the PU function (6) can also be constructed by B-spline functions.

1. For $\mathcal{C}^1$-continuous piecewise polynomial PU functions with flat-top, let $N_{i,4}(x), i = 1, \ldots, 12$ be B-splines of degree 3 that correspond to the open knot vector:

$$\left\{ \underbrace{0, .., 0}_{4}, \underbrace{a - \delta, a - \delta}_{2}, \underbrace{a + \delta, a + \delta}_{2}, \underbrace{b - \delta, b - \delta}_{2}, \underbrace{b + \delta, b + \delta}_{2}, \underbrace{1, .., 1}_{4} \right\}$$

A polynomial $P_3(x)$ of degree 3 defined on $[a - \delta, a + \delta]$ is uniquely determined by four constraints:

$$P_3(a - \delta) = 0, \quad P_3(a + \delta) = 1$$

$$\frac{d}{dx} P_3(a - \delta) = \frac{d}{dx} P_3(a + \delta) = 0$$

$\phi_{g_2}^L(\frac{x-(a+\delta)}{2\delta})$ satisfies the four constraints and also $N_{5,4}(x) + N_{6,4}(x)$ satisfies the four constraints. Therefore, we have

$$\phi_{g_2}^L\left(\frac{x - (a + \delta)}{2\delta}\right) = N_{5,4}(x) + N_{6,4}(x), \text{ for } x \in [a - \delta, a + \delta].$$

Similarly, we have

$$\phi_{g_2}^R\left(\frac{x - (b - \delta)}{2\delta}\right) = N_{7,4}(x) + N_{8,4}(x), \text{ for } x \in [b - \delta, b + \delta].$$

Using the partition of unity property of B-splines, we have

$$N_{5,4}(x) + N_{6,4}(x) + N_{7,4}(x) + N_{8,4}(x) = 1, \text{ for } x \in [a + \delta, b - \delta].$$

2. For $\mathcal{C}^2$-continuous piecewise polynomial PU functions with flat-top, let $N_{i,6}(x), i = 1, \ldots, 18$, be B-splines of degree 5 corresponding to the open knot vector,

$$\Big\{ \underbrace{0, .., 0}_{6}, \underbrace{a - \delta, .., a - \delta}_{3}, \underbrace{a + \delta, .., a + \delta}_{3}, \underbrace{b - \delta, .., b - \delta}_{3}, \underbrace{b + \delta, .., b + \delta}_{3}, \underbrace{1, .., 1}_{6} \Big\}.$$

A polynomial $P_5(x)$ of degree 5 defined on $[a - \delta, a + \delta]$ is uniquely determined by six constraints: three at $a - \delta$ and three at $a + \delta$,

$$P_5(a - \delta) = 0, \quad P_5(a + \delta) = 1$$

$$\frac{d}{dx}P_5(a - \delta) = \frac{d}{dx}P_5(a + \delta) = 0$$

$$\frac{d^2}{dx^2}P_5(a - \delta) = \frac{d^2}{dx^2}P_5(a + \delta) = 0$$

$\phi_{g3}^L(\frac{x-(a+\delta)}{2\delta})$ satisfies the six constraints and $N_{7,6}(x) + N_{8,6}(x) + N_{9,6}(x)$ also satisfies the six constraints. Therefore, we have

$$\phi_{g3}^L\Big(\frac{x - (a + \delta)}{2\delta}\Big) = N_{7,6}(x) + N_{8,6}(x) + N_{9,6}(x), \text{ for } x \in [a - \delta, a + \delta]$$

Similarly, we have

$$\phi_{g3}^R\Big(\frac{x - (b - \delta)}{2\delta}\Big) = N_{10,6}(x) + N_{11,6}(x) + N_{12,6}, \text{ for } x \in [b - \delta, b + \delta]$$

Moreover, we have

$$N_{7,6}(x) + N_{8,6}(x) + N_{9,6}(x) + N_{10,6}(x) + N_{11,6}(x) + N_{12,6} = 1, \text{ for } x \in [a+\delta, b-\delta].$$

3. In general, for each n, the $\mathcal{C}^{n-1}$-continuous piecewise polynomial PU function with flat-top can be constructed by the B-splines of degree $2n - 1$, $N_{i,2n}(x), i = 1, \ldots, 6n$, corresponding to the open knot vector:

$$\Big\{ \underbrace{0, .., 0}_{2n}, \underbrace{a - \delta, .., a - \delta}_{n}, \underbrace{a + \delta, .., a + \delta}_{n}, \underbrace{b - \delta, .., b - \delta}_{n}, \underbrace{b + \delta, .., b + \delta}_{n}, \underbrace{1, .., 1}_{2n} \Big\}.$$

We have

$$\psi_{[a,b]}^{(\delta,n-1)}(x) = \begin{cases} \sum_{k=1}^{n} N_{2n+k,2n}(x) & \text{if } x \in [a - \delta, a + \delta] \\ \sum_{k=1}^{2n} N_{2n+k,2n}(x) = 1 & \text{if } x \in [a + \delta, b - \delta] \\ \sum_{k=1}^{n} N_{3n+k,2n}(x) & \text{if } x \in [b - \delta, b + \delta] \\ 0 & \text{if } x \notin [a - \delta, b + \delta] \end{cases} \tag{7}$$

Since the two functions $\phi_{g_n}^R$ and $\phi_{g_n}^L$ defined by (4), satisfy the following relation:

$$\phi_{g_n}^R(\xi) + \phi_{g_n}^L(\xi - 1) = 1, \text{ for } \xi \in [0, 1],$$

if $\varphi : [-\delta, \delta] \to [0, 1]$ is defined by

$$\varphi(x) = (x + \delta)/(2\delta),$$

then we have

$$\phi_{g_n}^R(\varphi(x)) + \phi_{g_n}^L(\varphi(x) - 1) = 1, \text{ for } x \in [-\delta, \delta].$$

The gradient of the PU function with flat-top $\psi_{[a,b]}^{(\delta,n-1)}$ is bounded as follows:

$$\left| \frac{d}{dx} \left[\psi_{[a,b]}^{(\delta,n-1)}(x) \right] \right| \leq \frac{C}{2\delta} \tag{8}$$

Here the upper bounds C for various degrees of $\phi_{g_n}^{(pp)}$ are computed in Table 1 from [43].

Table 1: The upper bound of the gradient of the unscaled piecewise polynomial PU function $\phi_{g_n}^{(pp)}$ of (4) for various degrees.

degree	$n=2$	$n=3$	$n=5$	$n=7$	$n=10$	$n=15$	$n=20$	$n=30$
C	1.5	1.88	2.46	2.93	3.52	4.33	5.01	6.15

2.5   Boundary Layer Analysis

We follow the definitions and terminologies of [40]. Equations arising from mathematical models usually cannot be solved in exact form. Therefore, we often resort to approximation and numerical methods. Foremost among approximation techniques are perturbation methods. *Perturbation methods* lead to an approximate solution, to a problem when the model equations have terms that are small.

To fix the idea, consider a differential equation

$$F(x, y, y', y'', \epsilon) = 0 \tag{9}$$

where, x is the independent variable and y is the dependent variable. The appearance of a small parameter ϵ is shown explicitly, $\epsilon \ll 1$. (9) is called the *perturbed problem*. A *perturbation series* is a power series in ϵ of the form

$$y_0(x) + \epsilon y_1(x) + \epsilon^2 y_2(x)...$$

The basis of the *regular perturbation* method is to assume a solution of the differential equation of this form, where the functions $y_0, y_1, y_2...$ are found by substitution into the differential equation. The first few terms of such a series form an approximate solution, called a *perturbation solution*; usually no more than two or three terms are

taken. Generally, the method will be successful if the approximation is uniform.

The term y_0 in perturbation series is called the *leading order term*. The terms $\epsilon y_1, \epsilon^2 y_2, \ldots$ are regarded as higher-order correction terms that are expected to be small. If the method is successful, y_0 will be the solution of the *unperturbed problem*

$$F(x, y, y', y'', 0) = 0$$

in which ϵ is set to zero. A naive regular perturbation expansion does not always produce an approximate solution. There are several indicators that often suggest its failure.

- When the small parameter multiplies the highest derivative in the problem.

- When setting the small parameter equal to zero changes the character of the problem, as in the case of a partial differential equation changing type, or an algebraic equation changing degree. In other words, the solution for $\epsilon = 0$ is fundamentally different in character from the solutions for ϵ close to zero

- When problems occur on infinite domains, giving secular terms (correction term that is not small)

- When singular points are present in the interval of interest

- When the equations that model physical processes have multiple time or spatial scales

Such perturbation problems fall in the general category of *singular perturbation problems.* For differential equations, problems involving boundary layers are common.

The procedure is to determine whether there is a *boundary layer*, where the solution is changing very rapidly in a narrow interval, and where it is located. If there is a boundary layer, then the leading-order perturbation term found by setting $\epsilon = 0$ in the equation often provides a valid approximation in a large outer region(*outer layer*), away from the boundary layer. The inner approximation in the boundary layer is found by rescaling, which we must rescale the independent variable x in the boundary layer by selecting a small spatial scale that will reflect raid and abrupt changes and will force each term in the equation into its proper form in the rescaled variables.The *inner* and *outer* approximations can be matched to obtain a uniformly valid approximation over the entire interval of interest. The singular perturbation method applied in this context is called the method of *matched asymptotic expansions* or *boundary layer theory.*

Consider the boundary value problem

$$\epsilon y'' + (1 + \epsilon)y' + y = 0, \quad 0 < x < 1 \tag{10}$$

$$y(0) = 0, \quad y(1) = 1$$

where $0 < \epsilon \ll 1$.

Outer Approximation

In the region where $x = O(1)$, the solution could be approximated by setting $\epsilon = 0$ in the equation to obtain

$$y' + y = 0$$

and selecting the boundary condition $y(1) = 1$. This gives the outer approximation

$$y_o(x) = e^{1-x}$$

Inner Approximation

To analyze the behavior in the boundary layer, there is significant changes in y that take place on a very short spatial interval, which suggests a length scale on the order of a function of ϵ, say $\delta(\epsilon)$. If we change variable via

$$\xi = \frac{x}{\delta(\epsilon)}, \qquad y(x) = y(\delta(\epsilon)\xi) \equiv Y(\xi) \tag{11}$$

and use the chain rule, the differential equation (10) becomes

$$\frac{\epsilon}{\delta(\epsilon)^2}Y''(\xi) + \frac{(1+\epsilon)}{\delta(\epsilon)}Y'(\xi) + Y(\xi) = 0$$

where prime denotes derivatives with respect to ξ. Another way of looking at the rescaling is to regard (11) as a scale transformation that permits examination of the boundary layer close up, as under a microscope.

The coefficients of the four terms in the differential equation are

$$\frac{\epsilon}{\delta(\epsilon)^2}, \quad \frac{1}{\delta(\epsilon)}, \quad \frac{\epsilon}{\delta(\epsilon)}, \quad 1 \tag{12}$$

If the scaling is correct, each will reflect the order of magnitude of the term in which it appears. To determine the scale factor $\delta(\epsilon)$ we estimate these magnitudes by considering all possible dominant balances between pairs of terms in (4.3). (*dominant balancing*) In the pairs we include the first term because it was ignored in the outer layer, and it is known that it plays a significant role in the boundary layer. Because

Table 2: Three cases to consider for Dominant Balancing

	Same Order	Small in comparison
i.	$\epsilon/\delta(\epsilon)^2 \sim 1/\delta(\epsilon)$	$\epsilon/\delta(\epsilon), \ 1$
ii.	$\epsilon/\delta(\epsilon)^2 \sim 1$	$1/\delta(\epsilon), \ \epsilon/\delta(\epsilon)$
iii.	$\epsilon/\delta(\epsilon)^2 \sim \epsilon/\delta(\epsilon)$	$1/\delta(\epsilon), \ 1$

the goal is to make a simplification in the problem we do not consider dominant

balancing of three terms. If all four terms are equally important, not simplification

can be made at all. Therefore there are three cases to consider in Table 2.

In case i, $\epsilon/\delta(\epsilon)^2 \sim 1/\delta(\epsilon)$ forces $\delta(\epsilon) = O(\epsilon)$; then $\epsilon/\delta(\epsilon)^2$ and $1/\delta(\epsilon)$ are both

order $1/\epsilon$, which is large compared to $\epsilon/\delta(\epsilon)$ and 1. Therefore, a consistent scaling is

possible if we select $\delta(\epsilon) = O(\epsilon)$; hence, we take

$$\delta(\epsilon) = \epsilon$$

Therefore, the scaled differential equation (11) becomes

$$Y'' + Y' + \epsilon Y' + \epsilon Y = 0 \tag{13}$$

Now, (2.17) is amenable to regular perturbation. Because we are interested only

in the leading-order approximation, which we denote by Y_i, we set $\epsilon = 0$ in (13) to

obtain

$$Y_i'' + Y_i' = 0$$

The general solution is

$$Y_i(\xi) = C_1 + C_2 e^{-\xi}$$

Because the boundary layer is located near $x = 0$, we apply the boundary condition

$y(0) = 0$, or $Y_i(0) = 0$. This yields $C_2 = -C_1$, and so

$$Y_i(\xi) = C_1(1 - e^{-\xi})$$

In terms of y and x,

$$y_i(x) = C_1(1 - e^{-x/\epsilon})$$

This is the inner approximation for $x = O(\epsilon)$.

In summary, we have the approximate solution

$$y_o(x) = e^{1-x}, \quad x = O(1)$$

$$y_i(x) = C_1(1 - e^{-x/\epsilon}), \quad x = O(\epsilon)$$

each valid for an appropriate rage of x. There remains to determine the constant C_1, which is accomplished by the process of matching.

Matching

The inner and outer expansions should agree to some order in an overlap domain intermediate between the boundary layer and outer region. If $x = O(\epsilon)$, then x is in the boundary layer, and if $x = O(1)$, then x is in the outer region; therefore, this overlap domain could be characterized as values of x for which $x = O(\sqrt{\epsilon})$, for example, because $\sqrt{\epsilon}$ is between ϵ and 1 . This intermediate scale suggests a new scaled independent variable η in the overlap domain defined by

$$\eta = \frac{x}{\sqrt{\epsilon}}$$

The condition for matching is that the inner approximation, written in terms of the *intermediate variable* η, should agree with the outer approximation, written in terms of the intermediate variable η, in the limit as $\epsilon \to 0^+$. In symbols, for matching we require that for fixed η

$$\lim_{\epsilon \to 0^+} y_o(\sqrt{\epsilon}\eta) = \lim_{\epsilon \to 0^+} y_i(\sqrt{\epsilon}\eta)$$

For the present problem,

$$\lim_{\epsilon \to 0^+} y_o(\sqrt{\epsilon}\eta) = \lim_{\epsilon \to 0^+} e^{1-\sqrt{\epsilon}\eta} = e \tag{14}$$

and

$$\lim_{\epsilon \to 0^+} y_i(\sqrt{\epsilon}\eta) = \lim_{\epsilon \to 0^+} C_1(1 - e^{-\eta/\sqrt{\epsilon}}) = C_1$$

Therefore, matching requires $C_1 = e$ and the inner approximation becomes

$$y_i(x) = e(1 - e^{-x/\epsilon})$$

We have only introduced approximations of leading order. Higher-order approximations can be obtained by more elaborate matching schemes.

Uniform Approximations

To obtain a composite expansion that is uniformly valid throughout $[0, 1]$, we add the outer and inner approximations and then subtract the common limit (14) from the sum. In the intermediate or overlap region, both the inner and outer approximations are approximately equal to e. Therefore, in the overlap domain the sum of $y_o(x)$ and $u_i(x)$ gives $2e$, or twice the contribution. This is why we must subtract the common limit from the sum. In summary, $y_u(x)$ provides a uniform approximate solution

throughout the interval $[0, 1]$

$$y_u(x) = y_o(x) + y_i(x) - \text{common limit}$$

Substituting $y_u(x)$ into the differential equation shows that $y_u(x)$ satisfies the differential equation exactly on $(0, 1)$. Checking the boundary conditions, the left boundary condition is satisfied exactly and the right boundary condition holds up to $O(\epsilon^n)$, for any $n > 0$, because

$$\lim_{\epsilon \to 0^+} \frac{e^{1 - 1/\epsilon}}{\epsilon^n} = 0$$

for any $n > 0$. Consequently, y_u is a uniformly valid approximation on $[0, 1]$.

CHAPTER 3: PARTITION OF UNITY ISOGEOMETRIC ANALYSIS

We us Igogeometric Finite Element Setting in which we divide the domin into patches using Partion of Unity with flat-top so that we could have necessary basis functions on each patch. This is called Partion of Unity Isoeometric Analysis (PU-IGA). We develp error estimate for PU-IGA.

3.1   Error Analysis for PU-IGA

We estimate the error bound of PU-Galerkin method with respect to PU with flat-top modifying the proofs [2, 43].The proof of the higher dimensional case is similar to that of one dimensional case.

Let $\Omega = [\alpha, \beta]$ and $x_0 = \alpha < x_1 <, \ldots, x_N = \beta$ be a partition of Ω.

Let $\{\psi_i^\delta\}_{i=1}^N$ be Partition of Unity with flat-top and 2δ be the size of non flat-top zone. For each $i = 1, \ldots, N$, let

$$Q_i = [x_{i-1} - \delta, x_i + \delta]$$

$$\text{supp}(\psi_i^\delta) = Q_i \text{ and } \sum_{i=1}^N \psi_i^\delta(x) = 1 \text{ for all } x \in \Omega$$

$$\mathcal{V}_i = \text{span}\{f_k^i(x), k = 1, \ldots, n_i\} = \text{local approximation space on patch } Q_i$$

$$\mathcal{V} = \text{span}\{\psi_i^\delta(x)f_k^i(x) : k = 1, \ldots, n_i, i = 1, \ldots, N\} = \text{global approximation space on } \Omega$$

Let U^i be a local approximation of u on the patch Q_i. Then Galerkin approximation of the true solution u on the patch can be expressed as $\sum_{k=1}^{n_i} \xi_k^i f_k^i(x)$ on the patch.

The PU Galerkin approximation with respect to PU functions with flat-top $\psi_i^\delta(x)$ for the true solution $u(x)$ on the whole domain can be expressed as

$$u(x) \approx U(x) = \sum_{i=1}^{N} \psi_i^\delta(x) \Big(\sum_{k=1}^{n_i} \xi_k^i f_k^i(x) \Big)$$

for some constants $\xi_k^i, k = 1, \ldots, n_i, i = 1, \ldots, N$. The total number of global basis functions is $\sum_{i=1}^{N} n_i$.

Suppose for each i, there is $U^i \in \mathcal{V}_i$ such that

$$\|u - U^i\|_{L^2(Q_i \cap \Omega)} \le \varepsilon_0(i)$$

$$\|\frac{d}{dx}(u - U^i)\|_{L^2(Q_i \cap \Omega)} \le \varepsilon_1(i)$$

$$\|\frac{d^2}{dx^2}(u - U^i)\|_{L^2(Q_i \cap \Omega)} \le \varepsilon_2(i)$$

$$\|u - U^i\|_{L^2(Q_i^\delta \cap \Omega)} \le \varepsilon_0^\delta(i)$$

$$\|\frac{d}{dx}(u - U^i)\|_{L^2(Q_i^\delta \cap \Omega)} \le \varepsilon_1^\delta(i)$$

$$\|\frac{d^2}{dx^2}(u - U^i)\|_{L^2(Q_i^\delta \cap \Omega)} \le \varepsilon_2^\delta(i) \tag{15}$$

where $Q_i^\delta = [x_{i-1} - \delta, x_{i-1} + \delta] \cup [x_i - \delta, x_i + \delta] \subset Q_i = [x_{i-1} - \delta, x_i + \delta]$, and $\text{meas}(Q_i^\delta \cap \Omega) \le 4\delta$. The first three are local errors on the i-th patch Q_i. The last three are local errors on the i-th non flat-top zone Q_i^δ.

Theorem 1. Under the assumptions (15) we have the following error estimates:

$$(i) \quad \|u - U\|_{L^2(\Omega)} \le \sqrt{2} \Big\{ \sum_{i=1}^{N} [\varepsilon_0(i)]^2 \Big\}^{1/2}$$

$$(ii) \quad \|\frac{d}{dx}(u - U)\|_{L^2(\Omega)} \le 2 \Big\{ \sum_{i=1}^{N} \Big[[\frac{C_1}{2\delta}]^2 [\varepsilon_0^\delta(i)]^2 + [\varepsilon_1(i)]^2 \Big] \Big\}^{1/2}$$

$$(iii) \quad \|\frac{d^2}{dx^2}(u - U)\|_{L^2(\Omega)} \le \Big\{ 6 \sum_{i=1}^{N} \Big([\frac{C_2}{2\delta}]^2 [\varepsilon_0^\delta(i)]^2 + 4[\frac{C_1}{2\delta}]^2 [\varepsilon_1^\delta(i)]^2 + [\varepsilon_2(i)]^2 \Big) \Big\}^{1/2}$$

where $\quad C_1 = \|\frac{d\phi_{gn}^{(pp)}(x)}{dx}\|_\infty, \quad C_2 = \|\frac{d^2\phi_{gn}^{(pp)}(x)}{dx^2}\|_\infty, \quad \phi_{gn}^{(pp)}(x)$ is the unscaled reference

PU function defined by (4), and the size of δ is

$$\min\{0.05, 0.05 \cdot (h/3)\} \le \delta \le \min\{0.1, h/3\} \quad \text{in } [43]$$

Proof. (i) Consider the following new partition of Ω:

$$x_1^* = x_0, \quad x_k^* = (x_{k-1} + x_k)/2, \text{ for } k = 2, \ldots, N-1, \quad x_N^* = x_N.$$

Then, these two PU functions $\psi_k^\delta, \ \psi_{k+1}^\delta$ are non zero on the subinterval $[x_k^*, x_{k+1}^*]$, for

$k = 1, \ldots, N-1$. Thus, we have

$$
\begin{aligned}
\int_\Omega (u - U)^2 &= \int_\Omega \Big[(\sum_{i=1}^N \psi_i^\delta) u - \sum_{i=1}^N (\psi_i^\delta \sum_{k=1}^{n_i} \xi_k^i f_k^i) \Big]^2, \quad \text{by } \sum_{i=1}^N \psi_i^\delta = 1 \\
&= \sum_{k=1}^{N-1} \int_{[x_k^*, x_{k+1}^*]} \Big[\sum_{i=1}^N \psi_i^\delta \Big(u - U^i \Big) \Big]^2, \quad \text{by } U^i(x) = \sum_{k=1}^{n_i} \xi_k^i f_k^i(x) \\
&= \sum_{k=1}^{N-1} \int_{[x_k^*, x_{k+1}^*]} \Big[\psi_k^\delta \Big(u - U^k \Big) + \psi_{k+1}^\delta \Big(u - U^{k+1} \Big) \Big]^2 \\
&\le \sum_{k=1}^{N-1} \int_{[x_k^*, x_{k+1}^*]} 2 \Big[[\psi_k^\delta \Big(u - U^k \Big)]^2 + [\psi_{k+1}^\delta \Big(u - U^{k+1} \Big)]^2 \Big] \\
&= 2 \sum_{k=1}^{N-1} \int_{[x_k^*, x_{k+1}^*]} \sum_{i=1}^N [\psi_i^\delta \Big(u - U^i \Big)]^2 \\
&= 2 \int_\Omega \sum_{i=1}^N [\psi_i^\delta \Big(u - U^i \Big)]^2 \\
&\le 2 \sum_{i=1}^N \int_{Q_i \cap \Omega} \Big[u - U^i \Big]^2, \quad \text{by } 0 \le \psi_i^\delta \le 1 \\
&= 2 \sum_{i=1}^N [\varepsilon_0(i)]^2, \quad \text{by } \|u - U^i\|_{L^2(Q_i \cap \Omega)} = \varepsilon_0(i)
\end{aligned}
$$

(ii) Using a similar argument adopted in (i), we have

$$\int_\Omega [\frac{d}{dx}(u-U)]^2 = \int_\Omega \Big[\frac{d}{dx}\{(\sum_{i=1}^{N}\psi_i^\delta)u - \sum_{i=1}^{N}(\psi_i^\delta \sum_{k=1}^{n_i}\xi_k^i f_k^i)\}\Big]^2$$

$$= \int_\Omega \Big[\sum_{i=1}^{N}\frac{d}{dx}[\psi_i^\delta\big(u-U^i\big)]\Big]^2, \quad \text{by } U^i = \sum_{k=1}^{n_i}\xi_k^i f_k^i$$

$$= \int_\Omega \Big[\sum_{i=1}^{N}[\frac{d}{dx}\psi_i^\delta](u-U^i) + \sum_{i=1}^{N}\psi_i^\delta[\frac{d}{dx}(u-U^i)]\Big]^2$$

$$\leq 2\int_\Omega \Big(\sum_{i=1}^{N}[\frac{d}{dx}\psi_i^\delta](u-U^i)\Big)^2 + 2\int_\Omega \Big(\sum_{i=1}^{N}\psi_i^\delta[\frac{d}{dx}(u-U^i)]\Big)^2$$

$$\leq 4\int_\Omega \sum_{i=1}^{N}\Big([\frac{d}{dx}\psi_i^\delta](u-U^i)\Big)^2 + 4\int_\Omega \sum_{i=1}^{N}\Big(\psi_i^\delta[\frac{d}{dx}(u-U^i)]\Big)^2$$

$$\leq 4\sum_{i=1}^{N}\int_{Q_i\cap\Omega}\Big([\frac{d}{dx}\psi_i^\delta]^2(u-U^i)^2 + [\psi_i^\delta]^2[\frac{d}{dx}(u-U^i)]^2\Big)$$

$$\leq 4\sum_{i=1}^{N}\Big(\int_{Q_i\cap\Omega}[\frac{d}{dx}\psi_i^\delta]^2(u-U^i)^2 + \int_{Q_i\cap\Omega}[\frac{d}{dx}(u-U^i)]^2\Big), \quad \text{by } 0\leq\psi_i^\delta\leq 1$$

$$\leq 4\sum_{i=1}^{N}\Big([\frac{C}{2\delta}]^2\int_{Q_i^\delta\cap\Omega}(u-U^i)^2 + \int_{Q_i\cap\Omega}[\frac{d}{dx}(u-U^i)]^2\Big) \quad \text{by (16)}$$

$$\leq 4\sum_{i=1}^{N}\Big([\frac{C}{2\delta}]^2[\varepsilon_0^\delta(i)]^2 + [\varepsilon_1(i)]^2\Big)$$

where the constant C is the upper bound in Table 1.

$$\frac{d}{dx}\psi_i^\delta \leq \frac{d}{dx}\phi_{g_n}^L\big(\frac{x-(a+\delta)}{2\delta}\big) \leq \frac{1}{2\delta}\frac{d}{dx}\phi_{g_n}^L\big(\frac{x-(a+\delta)}{2\delta}\big) \leq \frac{C}{2\delta} \tag{16}$$

(iii) Using a similar argument adopted in (i) and (ii), we have

$$\int_\Omega [\frac{d^2}{dx^2}(u-U)]^2 = \int_\Omega \Big[\frac{d^2}{dx^2}\{\sum_{i=1}^N \psi_i^\delta u - \sum_{i=1}^N \psi_i^\delta U^i\}\Big]^2 = \int_\Omega \Big[\sum_{i=1}^N \frac{d^2}{dx^2}\big[\psi_i^\delta\big(u-U^i\big)\big]\Big]^2$$

$$= \sum_{k=1}^{N-1} \int_{[x_k^*,x_{k+1}^*]} \Big[\sum_{i=1}^N [\frac{d^2}{dx^2}\psi_i^\delta](u-U^i) + \sum_{i=1}^N 2\frac{d}{dx}\psi_i^\delta \frac{d}{dx}(u-U^i) + \sum_{i=1}^N \psi_i^\delta[\frac{d^2}{dx^2}(u-U^i)]\Big]^2$$

$$\leq 3\sum_{k=1}^{N-1} \int_{[x_k^*,x_{k+1}^*]} \Big\{\Big[\sum_{i=1}^N [\frac{d^2}{dx^2}\psi_i^\delta](u-U^i)\Big]^2 + \Big[2\sum_{i=1}^N \frac{d}{dx}\psi_i^\delta \frac{d}{dx}(u-U^i)\Big]^2 + \Big[\sum_{i=1}^N \psi_i^\delta[\frac{d^2}{dx^2}(u-U^i)]\Big]^2$$

$$\leq 6\int_\Omega \sum_{i=1}^N \Big\{\Big[[\frac{d^2}{dx^2}\psi_i^\delta](u-U^i)\Big]^2 + 4\Big[\frac{d}{dx}\psi_i^\delta \frac{d}{dx}(u-U^i)\Big]^2 + \Big[\psi_i^\delta[\frac{d^2}{dx^2}(u-U^i)]\Big]^2\Big\}$$

$$\leq 6\sum_{i=1}^N \int_{Q_i \cap \Omega} \Big\{\Big[[\frac{d^2}{dx^2}\psi_i^\delta](u-U^i)\Big]^2 + 4\Big[\frac{d}{dx}\psi_i^\delta \frac{d}{dx}(u-U^i)\Big]^2 + \Big[\psi_i^\delta[\frac{d^2}{dx^2}(u-U^i)]\Big]^2\Big\}$$

$$\leq 6\sum_{i=1}^N \Big([\frac{C_2}{2\delta}]^2[\varepsilon_0^\delta(i)]^2 + 4[\frac{C_1}{2\delta}]^2[\varepsilon_1^\delta(i)]^2 + [\varepsilon_2(i)]^2\Big),$$

$\square$

1. In Theorem 1, (ii) and (iii) shows that the error bound in the energy norm depends on the selection of δ, size of non flat-top zone. With small δ size, we might have small local errors, ε_0^δ, ε_1^δ, and ε_2^δ, but we could have big constant $C/2\delta$.

2. In Theorem 1, (i) shows that the error bound in the L^2-norm does not depend on the selection of δ.

3. We choose δ between 0.001 and 0.1. See [31] for the selection of δ

3.2   Total cost comparison of PU-IGA to IGA

The total cost for a numerical method is determined by the number of quadrature points, the polynomial degrees of the basis functions, the regularity of enrichment

functions, the number of elements, and the spatial dimension and etc. Extensive cost comparisons of IGA-Collocation and IGA-Galerkin with FEA-Galerkin were shown in [60].

We compare the cost of PU-IGA to that of IGA by bandwidth, operation counts and number of Gaussian points. When we compare them, we use one dimensional numerical examples of PU-IGA in later Chapter.

Let $N_{i,p+1}(x), i = 1, \ldots, m_k^p$, be $\mathcal{C}^{p-k}$-continuous B-spline functions of degree p corresponding to the open knot vector:

$$\Xi = \{\underbrace{0, \ldots, 0}_{p+1}, \underbrace{\xi_1, \ldots, \xi_1}_{k}, \underbrace{\xi_2, \ldots, \xi_2}_{k}, \ldots, \underbrace{\xi_{n-1}, \ldots, \xi_{n-1}}_{k}, \underbrace{\xi_n, \ldots, \xi_n}_{k}, \underbrace{1, \ldots, 1}_{p+1}\} \quad (17)$$

where $1 \le k \le p$ and $m_k^p = (nk + p + 1)$.

Suppose $AX = B$ is the algebraic system for a numerical solution of $-u'' = f$ using B-spline basis functions corresponding to (17).

- **Bandwidth**

  For a sparse matrix $A = [a_{ij}]_{1 \le i,j \le m_k^p}$, the smallest integers l_1 and l_2 such that $a_{ij} = 0$ for $i - j > l_1$ and $a_{ij} = 0$ for $j - i > l_2$ are called the lower and the upper bandwidth, respectively. The bandwidth of A is defined by $l_1 + l_2$.

  The bandwidth of the matrix A is $2p$ if $k = 1$ or $k = p$; $2p - 1$ otherwise. As for IGA, we use B-spline basis functions of high order, $p \ge 10$ in Table 5, for the numerical example. On the other hand, The author in [27] use the piecewise linear basis functions for the conventional FEM for the results in Table 5.

In this case, the bandwidth of A by IGA is orders of magnitude larger than that of A corresponding to piecewise linear basis functions. In PU-IGA, we choose the polynomial degrees of B-splines in patch-wise manner without sacrificing the regularity of local approximation functions. For example, we could choose $\mathcal{C}^9$- continuous B-spline basis functions of degree 10 on a patch Q_1, where we need higher order basis functions. Next we could select $\mathcal{C}^1$- continuous B-spline basis functions of degree 2 on another patch Q_2, where higher degree of basis functions are not required. If we use IGA without dividing the domain, then the bandwidth of A should be 20. However, if we use PU-IGA dividing patches and putting different degrees of basis functions into different patches, we could have block matrices of A with smaller bandwidth, like A_1 with bandwidth 4 and A_2 with bandwidth 20.

- **Operation Counts**

  Let k, multiplicity of (17) be 1 or p. Since the stiffness matrix A is symmetric, then operation counts for LU factorization and forward and back substitution is $p^2 \cdot m_p^k/2 + 2p \cdot m_p^k$, where m_p^k is the number of basis functions and p is the order of B-splines.

  If we choose selectively the order of B-spline functions and a set of B-splines in a patch-wise manner, then the number of basis functions could be reduced and also we could have smaller degrees on the different patches. Therefore, the number of operations can be reduced.

- **Number of quadrature points**

Suppose $f_l^i(x), l = 1, \ldots, n_i$, are local approximation polynomials of degree p on a patch $Q_i = [x_{i-1} - \delta, x_i + \delta]$ and $\psi_{Q_i}^\delta(x)$ is a $\mathcal{C}^1$-continuous PU function with flat-top of degree 3. Then $\psi_{Q_i}^\delta(x) f_l^i(x), l = 1, \ldots, n_i$, are polynomials of degree $p + 3$ on the non flat-top parts, $Q_i^\delta = [x_{i-1} - \delta, x_{i-1} + \delta] \cup [x_i - \delta, x_i + \delta]$, and are polynomials of degree p on the flat-top part, $[x_i + \delta, x_{i+1} - \delta]$. The number of quadrature points for the integral on the non flat-top part is $(p+4)/2$, while the number of quadrature points for the integral on the flat-top part is $(p + 1)/2$. Hence the total number of quadrature points for the integral of $\mathcal{C}^1$-continuous three piece-polynomial $\psi_{Q_i}^\delta(x) f_l^i(x)$ on Q_i is

$$\frac{p + 1}{2} + (p + 4)$$

because we have 2 parts of non flat-top parts. While IGA needs the number of quadrature points, $(p + 1)/2$. In PU-IGA, a few extra quadrature points are required for the integrals of polynomial local approximation functions defined on non flat-top zones. However, we choose selectively the order of B-spline functions and sets of B-spline functions in patch-wise manner, then the total quadrature points also can be reduced because we might use smaller degree on different patch.

3.3   Galerkin Method of Enriched PU-IGA

We use PU-IGA to deal with singularities. In this section, we describes how to construct basis functions in PU-IGA. Let

$$\hat{\Psi}_{ij}, \quad \text{for } i = 1, \ldots, N; j = 1, \ldots, M. \tag{18}$$

be $\mathcal{C}^{l-1}$-PU functions with flat-top

We use the following notations for the description of enriched PU-IGA:

1. $\text{supp}(\hat{\Psi}_{ij}) = [\xi_i - \delta, \xi_{i+1} + \delta] \times [\eta_j - \delta, \eta_{j+1} + \delta]$.

2. $\varphi_{ij} : \hat{\Omega} = [0, 1] \times [0, 1] \longrightarrow \text{supp}(\hat{\Psi}_{ij})$ is the linear mapping from the parameter domain onto a patch $\text{supp}(\hat{\Psi}_{ij}) \supset \hat{\Omega}_{ij}$.

3. $\hat{B}_{st}(\xi, \eta) = N_s(\xi) \times M_t(\eta)$, $1 \leq s \leq n_p$ and $1 \leq t \leq m_q$, are two-dimensional B-spline functions defined on $[0, 1] \times [0, 1]$, parameter domain.

4. $\tilde{B}_{st}^{(ij)} = \hat{B}_{st} \circ \varphi_{ij}^{-1}$, for $1 \leq i \leq N, 1 \leq j \leq M$, $1 \leq s \leq n_p, 1 \leq t \leq m_q$, are two-dimensional B-spline functions defined on each patch.

5. **Enriched PU-IGA** Let $G : \hat{\Omega} \longrightarrow \Omega$ be a design mapping. Suppose we know an enrichment function $h(x, y)$ that resembles either a boundary layer function or a singularity function on a subdomain $\Omega_{i_0, j_0} = G(\hat{\Omega}_{i_0 j_0})$ of physical domain Ω.

   We call $\hat{h} = (h \circ G)$ the **pullback** of the enrichment function h into the reference domain, and $h = \hat{h} \circ G^{-1}$ the **push-forward** of $\hat{h}$ into the physical domain.

The basis functions on the parameter domain are those in $\hat{\mathcal{V}}_1 \cup \hat{\mathcal{V}}_0$ that consist of

B-spline functions and an enrichment function modified by PU functions, where

$$
\hat{\mathcal{V}}_1 = \left\{ \begin{array}{l} \left(\hat{\Psi}_{ij} \cdot \tilde{B}_{st}^{(ij)} \right) \quad : \; 1 \le s \le n_i; 1 \le t \le n_j, \text{ and} \\[2mm] \qquad\qquad i = 1, \ldots, N; j = 1, \ldots, M, \; ij \neq i_0 j_0 \end{array} \right\}
$$

$$
\hat{\mathcal{V}}_0 = \left\{ \; \hat{h}(\xi, \eta) \cdot \hat{\Psi}_{i_0 j_0}(\xi, \eta), \quad \left(\hat{\Psi}_{i_0 j_0} \cdot \tilde{B}_{st}^{(i_0 j_0)} \right) \quad : \; 1 \le s \le n_{i_0}; 1 \le t \le n_{j_0} \; \right\}
$$

Now the approximation space $\mathcal{V}^h$ in the physical domain Ω enriched by $h(x, y)$ is

the vector space spanned by linearly independent basis functions in $\hat{\mathcal{V}}_1 \circ G^{-1} \cup \hat{\mathcal{V}}_0 \circ G^{-1}$.

That is,

$$
\mathcal{V}^h = \mathrm{span}\left(\hat{\mathcal{V}}_1 \circ G^{-1} \cup \hat{\mathcal{V}}_0 \circ G^{-1} \} \right).
$$

Then, This is the calculation of stiffness matrix by reference element approach. Let

$$
\nabla_x = (\frac{\partial}{\partial x}, \frac{\partial}{\partial y})^T, \quad \nabla_\xi = (\frac{\partial}{\partial \xi}, \frac{\partial}{\partial \eta})^T, \quad \mathbf{G} : \hat{\Omega}_{\mathbf{G}} = [0, 1] \times [0, 1] \longrightarrow \Omega.
$$

Suppose $\mathcal{B}(u, v) = \int_\Omega (\nabla_x v)^T \cdot (\nabla_x u)$. Then for two basis functions in $\mathcal{V}^h$ we have

$$
\mathcal{B}\left(\left(\hat{\Psi}_{ij} \cdot \tilde{B}_{s't'}^{(ij)} \right) \circ G^{-1}, \left(\hat{\Psi}_{lm} \cdot \tilde{B}_{st}^{(lm)} \right) \circ G^{-1} \right)
$$

$$
= \int_\Omega (\nabla_x \left(\hat{\Psi}_{lm} \cdot \tilde{B}_{s't'}^{(lm)} \right) \circ G^{-1})^T \cdot (\nabla_x \left(\hat{\Psi}_{ij} \cdot \tilde{B}_{st}^{(ij)} \right) \circ G^{-1}) dx dy
$$

$$
= \int_{\hat{\Omega}_{ij;lm}^*} (\nabla_\xi \left(\hat{\Psi}_{lm} \cdot \tilde{B}_{s't'}^{(lm)} \right))^T \cdot \left[(J(\mathbf{G})^{-1})^T \cdot J(\mathbf{G})^{-1} |J(\mathbf{G})| \right] (\nabla_\xi \left(\hat{\Psi}_{ij} \cdot \tilde{B}_{st}^{(ij)} \right)) d\xi d\eta
$$

where

$$
\hat{\Omega}_{ij;lm}^* = \mathrm{supp}\hat{\Psi}_{ij} \cap \mathrm{supp}\hat{\Psi}_{lm},
$$

$\hat{\Omega}^*_{ij;lm}$ is a slim rectangle with δ width or length   if $ij \neq lm$.

$\hat{\Omega}^*_{ij;lm}$ is a rectangle, the support of $\hat{\Psi}_{ij}$ if $ij = lm$.

Unlike PU-FEM and enriched IGA [48, 49], the intersection of supports of any two basis functions modified by PU function is always a rectangle on the reference domain so that we could integrate easily. That's one of strengths of PU-IGA.

CHAPTER 4: SINGULARY PERTURBED CONVECTION-DIFFUSION EQUATIONS IN A CIRCLE

4.1   Introduction

we consider singularly perturbed problems of the form, stationary convection-diffusion equation

$$
\begin{cases}
-\epsilon \triangle u - u_y = f(x,y) & \text{in } \Omega \\
\\
u = 0 & \text{on } \partial\Omega
\end{cases}
\tag{19}
$$

where $0 < \epsilon \ll 1$, Ω is the unit circle centered at $(0,0)$, and the function f is as smooth as needed.

The variational formulation of (19) reads: To find $u^\epsilon \in H_0^1(\Omega)$ such that

$$
a(u,v) := \epsilon(\nabla u, \nabla v) - (u_y, v) = (f, v)
\tag{20}
$$

for every $v \in H_0^1(\Omega)$

The specificity of problem (19) is that there are two characteristic points for the limit problem when $\epsilon = 0$, namely $(\pm 1, 0)$, and very complicated phenomena occur at these points. In [25] and [26], the problem under consideration in this paper was discussed analytically. It was shown that a boundary layer occurs around the lower half circle, $x^2 + y^2 = 1, y < 0$, and unless f satisfies certain compatibility conditions, singular behaviors can occur at the characteristic points $(\pm 1, 0)$

Most of the numerical methods to solve the singular perturbation problems like (19) are based on domain decomposition or refined meshes near boundary layers. See [35], [50], [51] and [68]. In [25] and [26], the authors have studied convection-diffusion equations in a rectangle and circular domain using uniform rectangular meshes incorporating boundary layer correctors. [27] showed the numerical solutions to the problem using a P-1 classical finite element space enriched by the boundary layer element. In this paper, developing boundary layer elements via boundary layer analysis in similar way, We approximate (19) in PU-IGA Finite Element Space enriched by the boundary layer elements multiplied by partition unity function.

We have better numerical results with less degree of freedom than that of [27].

Isogeometric analysis is a new approach that combines engineering design and finite element analysis, in which NURBS functions employed for the design are utilized as basis functions for analysis. If we could approximate boundary layer elements on some other domains through the geometry mapping, we could apply this Enriched PU-IGA on any other domain. We develop the boundary layer element on other geomery, ellipse in the last section of this chapter.

4.2   Geometry Mapping

We define the geometry mapping G from parametric domain to physical domain. The mapping $G : \hat{\Omega} \longrightarrow \Omega$ is defined by

$$G(\xi, \eta) = (x(\xi, \eta), y(\xi, \eta) = ((1 - \eta) \cos 2\pi\xi, (1 - \eta) \sin 2\pi\xi) \tag{21}$$
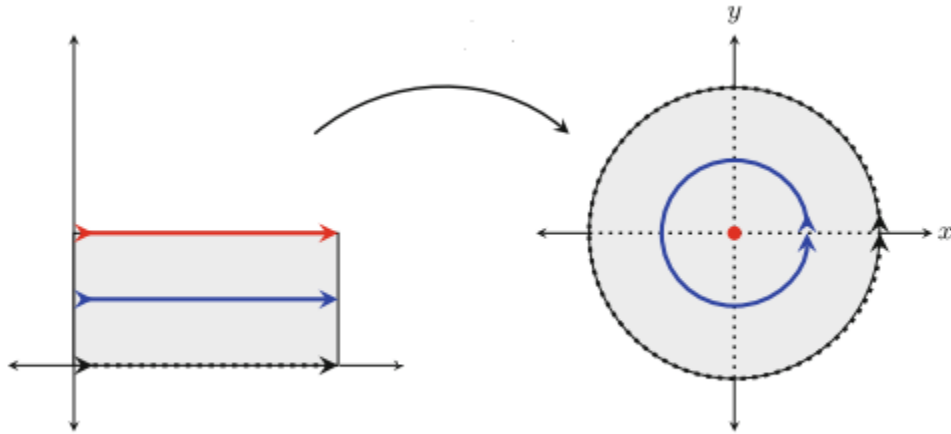
Figure 8: Parametrization of the mapping in [27]

where $\eta = 1 - r, r$ is the distance to the origin and $2\pi\xi$ is the polar angle from origin of the circle, Ω is the unit circle centered at $(0,0)$. We define the domains $\hat{\Omega} = [0,1] \times [0,1]$ in the parameter space. See Figure 8.

4.3   Boundary Layer Analysis

We analyze the boundary layer approximation on the parameter domain using the geometric mapping, $G(\xi, \eta)$ defined in (21). Let

$$\hat{u}(\xi, \eta) = u \circ G(\xi, \eta)$$

By chain rule,

$$\frac{\partial \hat{u}}{\partial \xi} = \frac{\partial u}{\partial x}(G(\xi, \eta))\frac{\partial x}{\partial \xi} + \frac{\partial u}{\partial y}(G(\xi, \eta))\frac{\partial y}{\partial \xi}$$
$$\frac{\partial \hat{u}}{\partial \eta} = \frac{\partial u}{\partial x}(G(\xi, \eta))\frac{\partial x}{\partial \eta} + \frac{\partial u}{\partial y}(G(\xi, \eta))\frac{\partial y}{\partial \eta}$$

We have

$$\frac{\partial u}{\partial x} = -\frac{\sin 2\pi\xi}{2\pi(1-\eta)}\frac{\partial \hat{u}}{\partial \xi} - \cos 2\pi\xi\frac{\partial \hat{u}}{\partial \eta}$$

$$\frac{\partial u}{\partial y} = -\frac{\cos 2\pi\xi}{2\pi(1-\eta)}\frac{\partial \hat{u}}{\partial \xi} - \sin 2\pi\xi\frac{\partial \hat{u}}{\partial \eta}$$

$$\triangle u = \frac{\partial^2 u}{\partial x^2} + \frac{\partial^2 u}{\partial y^2}$$

$$= \frac{\partial^2 \hat{u}}{\partial \eta^2} - \frac{1}{1-\eta}\frac{\partial \hat{u}}{\partial \eta} + \frac{1}{(1-\eta)^2}\frac{\partial^2 \hat{u}}{\partial \xi^2}$$

By this change of variables, the equation (3.1) becomes

$$-\epsilon\triangle u - u_y = -\epsilon\frac{\partial^2 \hat{u}}{\partial \eta^2} - \frac{\epsilon}{4\pi^2(1-\eta)^2}\frac{\partial^2 \hat{u}}{\partial \xi^2} + \frac{\epsilon}{1-\eta}\frac{\partial \hat{u}}{\partial \eta} \tag{22}$$

$$- \frac{\cos 2\pi\xi}{2\pi(1-\eta)}\frac{\partial \hat{u}}{\partial \xi} + \sin 2\pi\xi\frac{\partial \hat{u}}{\partial \eta} = f((1-\eta)\cos 2\pi\xi, (1-\eta)\sin 2\pi\xi)$$

We analyze the behavior in the boundary layer. There is significant changes in $\hat{u}$ taking place on a very short η interval, which suggest a length scale on the order of a function of ϵ, say ϵ^α. We introduce the stretched variable

$$\bar{\eta} = \frac{\eta}{\epsilon^\alpha}$$

The equation (22) is transformed to

$$-\epsilon^{1-2\alpha}\frac{\partial^2 \hat{u}}{\partial \bar{\eta}^2} - \frac{\epsilon}{4\pi^2(1-\epsilon^\alpha\bar{\eta})^2}\frac{\partial^2 \hat{u}}{\partial \xi^2} + \frac{\epsilon^{1-\alpha}}{1-\epsilon^\alpha\bar{\eta}}\frac{\partial \hat{u}}{\partial \bar{\eta}} - \frac{\cos 2\pi\xi}{2\pi(1-\epsilon^\alpha\bar{\eta})}\frac{\partial \hat{u}}{\partial \xi} + \sin 2\pi\xi\epsilon^{-\alpha}\frac{\partial \hat{u}}{\partial \bar{\eta}} = f(G^{-1})$$

The coefficients of the terms in the differential equation are

$$\epsilon^{1-2\alpha}, \quad \epsilon, \quad \epsilon^{1-\alpha}, \quad \epsilon^{-\alpha}$$

To determine α, we estimate these magnitudes by considering all possible dominant balances between pairs of terms in (4.3). If $\epsilon^{1-2\alpha}$ and $\epsilon^{-\alpha}$ are same order, both of them are order $1/\epsilon$, $\alpha = 1$, which is large compared to ϵ and $\epsilon^{1-\alpha}$. Therefore, a consistent scaling is possible if we select $\alpha = 1$. In other words, a reasonable boundary layer equation is determined by setting $\alpha = 1$ by dominating balancing. Hence, we have

$$-\epsilon^{-1}\frac{\partial^2 \hat{u}}{\partial \bar{\eta}^2} - \frac{\epsilon}{4\pi^2(1-\epsilon^\alpha\bar{\eta})^2}\frac{\partial^2 \hat{u}}{\partial \xi^2} + \frac{1}{1-\epsilon^\alpha\bar{\eta}}\frac{\partial \hat{u}}{\partial \bar{\eta}} - \frac{\cos 2\pi\xi}{2\pi(1-\epsilon^\alpha\bar{\eta})}\frac{\partial \hat{u}}{\partial \xi} + \sin 2\pi\xi\epsilon^{-1}\frac{\partial \hat{u}}{\partial \bar{\eta}} = f(G)$$

$$-\frac{\partial^2 \hat{u}}{\partial \bar{\eta}^2} - \frac{\epsilon^2}{4\pi^2(1-\epsilon^\alpha\bar{\eta})^2}\frac{\partial^2 \hat{u}}{\partial \xi^2} + \frac{\epsilon}{1-\epsilon^\alpha\bar{\eta}}\frac{\partial \hat{u}}{\partial \bar{\eta}} - \frac{\epsilon\cos 2\pi\xi}{2\pi(1-\epsilon^\alpha\bar{\eta})}\frac{\partial \hat{u}}{\partial \xi} + \sin 2\pi\xi\frac{\partial \hat{u}}{\partial \bar{\eta}} = \epsilon f(G)$$

$$(23)$$

Now, this is amenable to regular perturbation. Because we are interested only in the leading-order approximation, we set $\epsilon = 0$ in (23) to obtain

$$-\frac{\partial^2 \hat{u}}{\partial \bar{\eta}^2}\frac{\partial \hat{u}}{\partial \xi} + \sin 2\pi\xi\frac{\partial \hat{u}}{\partial \bar{\eta}} = 0$$

Because we are interested only in the leading-order approximation, we set $\epsilon = 0$ in (3.5) to obtain

$$-\frac{\partial^2 \hat{u}}{\partial \bar{\eta}^2} + \sin 2\pi\xi\frac{\partial \hat{u}}{\partial \bar{\eta}} = 0$$

The general solution is

$$\hat{u}(\xi, \bar{\eta}) = C_1 + C_2 e^{(\sin 2\pi\xi)\bar{\eta}}$$

Because the boundary layer is located around the lower half circle on the physical domain, near $\eta = 0$ and $1/2 < \xi < 1$ on the reference domain, we apply the boundary condition $\hat{u} = 0$ at $\eta = 0$ because the boundary condition $u = 0$ at $\partial\Omega$

$$C_2 = -C_1$$

$$\hat{u}(\xi, \bar{\eta}) = C_1(1 - e^{(\sin 2\pi\xi)\bar{\eta}}), \quad 1/2 < \xi < 1$$

In terms of ξ and η

$$\hat{u}(\xi, \bar{\eta}) = C_1(1 - e^{(\sin 2\pi\xi)\frac{\eta}{\epsilon}}), \quad 1/2 < \xi < 1$$

The boundary layer approximation can be written as

$$\hat{u}(\xi, \bar{\eta}) = C_1(1 - e^{(\sin 2\pi\xi)\frac{\eta}{\epsilon}})\chi_{[1/2,1]}(\xi)$$

where $\chi_A(\xi)$ is the characteristic function of A.

4.4   Approximation via finite elements

PU-IGA Finite Element Space

We define IGA finite element space, V_N and the enriched PU-IGA, $\bar{V}_N$, which includes the boundary layer element, φ_0.

$$V_N = \{\sum_{i=1}^{N} c_i R_i(x, y)\} \subset H_0^1(\Omega)$$

$$\bar{V}_N = \{\sum_{i=1}^{N} c_i R_i(x, y) + \sum_{i=1}^{M} d_i(\varphi_0(\xi, \eta) \circ G^{-1})(N_i(\xi) \circ G^{-1})\} \subset H_0^1(\Omega)$$

N is the number of B-splines corresponding the knot vectors in ξ and η directions, M is the number of basis functions along Γ_l, where $\Gamma_l = \{(x, y) =| x^2 + y^2 = 1, y < 0\}$, $R_i(x, y)$ is B-spline basis function in 2-dimensional space, $1 \leq i \leq N$, $N_i(\xi)$ is B-spline basis functions in 1-dimensional space, $1 \leq i \leq M$, $\varphi_0(\xi, \eta)$ is the boundary layer element defined by

$$\varphi_0(\xi, \eta) = (1 - \exp(\frac{\sin 2\pi\xi}{\epsilon}\eta))\psi(\eta)\chi_{[0.5,1]}(\xi) \tag{24}$$

: boundary layer approximation multiplied by PU with flat-top, $\psi(\eta)$ defined by

$$\psi(\eta) = \begin{cases} 0, & \text{if } \eta \in [b+\delta, 1] \\[2ex] \phi_{g_2}^R(\frac{\eta-(b-\delta)}{2\delta}, & \text{if } \eta \in [b-\delta, b+\delta] \\[2ex] 1, & \text{if } \eta \in [0, b-\delta] \end{cases}$$

We can now formulate the following discrete analogues of the problem (3.2) Find $u_h \in V_N$ and $\bar{u}_h \in \bar{V}_N$, respectively, such that

$$a(u_h, v) = (f, v), \quad \forall v \in V_N$$

$$a(\bar{u}_h, v) = (f, v), \quad \forall v \in \bar{V}_N$$

where $a(\cdot, \cdot)$ is as in (20).

4.5   Numerical Method

We present the results of numerical simulation of (1.1) using the general IGA and the enriched PU-IGA, which is enriched by the boundary layer element through boundary layer analysis.

We consider the finite element space V_N spanned by

$$\{R_1, R_2, ..., R_N\}$$

where N is the number of B-spline basis functions. To treat the boundary layers, we add the boundary layer elements in V_N. There are several ways to augment the basis of V_N by adding different boundary layer elements.

1. $\{\varphi_0(\xi_1, \eta)N_1(\xi), \varphi_0(\xi_2, \eta)N_2(\xi), ..., \varphi_0(\xi_M, \eta)N_M(\xi)\}$

2. $\{\varphi_0(0.75,\eta)N_1(\xi), \varphi_0(0.75,\eta)N_2(\xi), ..., \varphi_0(0.75,\eta)N_M(\xi)\}$

3. $\{\varphi_0(\xi,\eta)N_1(\xi), \varphi_0(\xi,\eta)N_2(\xi), ..., \varphi_0(\xi,\eta)N_M(\xi)\}$

where M is the number of B-splines in ξ direction on the lower semicircle. Here, φ_0 is the boundary layer element defined in (24). First, we have M different enrichment functions by plugging in different values in ξ direction. Second, we have only one enrichment function by plugging in one value in ξ direction. In the first and second one, we consider the boundary layer element as a function of η. Lastly, we have a boundary layer element as a function of ξ and η. For our implementation, we are going to use the second choice of boundary layer element which is plugging a specific value in ξ direction into the boundary layer element, namely,

$$\varphi_0(\eta) = (1 - \exp(\frac{-\eta}{\epsilon}))\psi(\eta)\chi_{[0.5,1]}(\xi)$$

Incorporating the boundary layer elements that absorb the singularity behavior in the finite space, we expect accurate numerical results in the PU-IGA setting. We do not use costly mesh refinements near the boundary. We also prevent propagation of the numerical errors along the characteristics inside of the domain Ω due to the convective term in the problem, by using PU with flat-top.

Basis Functions

We have flexibility of how to design the basis functions. We might divide the physical domain into several patches to apply different basis function in each patch. See Figure 10. In the outer region (away from the boundary layer), we could obtain optimal solution with general IGA. The boundary layer requires more sophisticated

basis function. That's one of reason to divide the patches to increase the flexibility. First, we only use one patch for the whole domain for simplicity. Next, we divide the domain into two patches to enrich boundary layer only with boundary layer approximation and use B-splines in regular zone.

Basis Functions on one patch

Let $\hat{M}_l(\eta)$ be the Berstein polynomials(special case of B-spline) of degree q defined on $[0, 1]$

$$\hat{M}_l(\eta) = \binom{q}{l}(1 - \eta)^{q-l}\eta^l, \quad l = 0, 1, 2, ..., q$$

Let $\hat{N}_k(\xi)$ be B-splines, corresponding to the open knot vector

$$\{\underbrace{0.....0}_{p+1}, \underbrace{1/4.....1/4}_{p-1}, \underbrace{1/2.....1/2}_{p-1}, \underbrace{3/4.....3/4}_{p-1}\underbrace{1.....1}_{p+1}\}$$

The first and the last B-spline functions are joined together to be one basis function so that the basis functions after push forward to the physical domain, can be periodic.

$$\hat{N}_1(\xi) = \begin{cases} (1 - 4\xi)^p, & \text{if } \xi \in [0, 1/4] \\ \\ 0, & \text{if } \xi \in [1/4, 3/4] \\ \\ (4\xi - 3)^p, & \text{if } \xi \in [3/4, 1] \end{cases}$$

Namely,

$$\hat{N}_1(\xi) = \hat{N}_1(\xi) + \hat{N}_{4p-2}(\xi)$$

We define the periodic B-spline basis function in 2-dimensional on the parametric domain as

$$\{\hat{N}_k(\xi)\hat{M}_l(\eta) \mid 1 \le k \le 4p - 3, \quad 0 \le l \le q\}$$
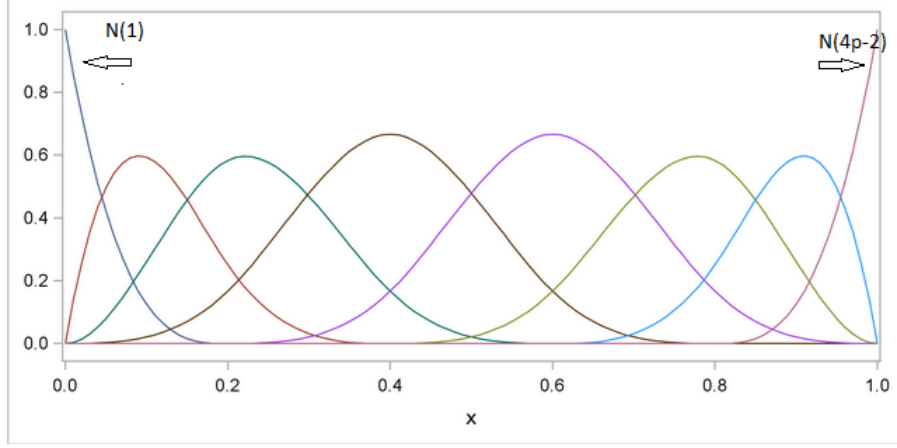
Figure 9: Periodic basis function

Notice that we use $4p-3$ of B-splines in ξ direction instead of $4p-2$ of them to make the B-splines periodic.

To prevent the influence of boundary layer element in outer region, we define the boundary layer element multiplying the PU-function with flat-top, $\psi(\eta)$.

$$\varphi_0(\eta) = (1 - \exp(\frac{-\eta}{\epsilon}))\psi(\eta)\chi_{[0.5,1]}(\xi)$$

$$\psi(\eta) = \begin{cases} 0, & \text{if } \eta \in [b+\delta, 1] \\ \phi_{g_2}^R(\frac{\eta-(b-\delta)}{2\delta}), & \text{if } \eta \in [b-\delta, b+\delta] \\ 1, & \text{if } \eta \in [0, b-\delta] \end{cases}$$

Here, δ will be between 0.01 and 0.1 and 2δ is the width of non flat-top part of the PU function. $\phi_{g_2}^R(x) = (1-x)^2(1+2x)$ from (2.12).

We introduce the basis function enriched with boundary layer element as following

$$\mathcal{V} := \{\hat{N}_k(\xi)\varphi_0(\eta)\psi(\eta) \mid 2p+1 \le k \le 4p-3\} \bigcup \{\hat{N}_k(\xi)\hat{M}_l(\eta) \mid 1 \le k \le 4p-3, \quad 0 \le l \le q\}$$

Notice that we augment the boundary layer elements along the lower half circle for $k = 2p + 1, ..., 4p - 3$.

The inverse of the geometry mapping G defined in (3.3) is

$$G^{-1}(x, y) = (\xi(x, y), \eta(x, y)) = (\frac{1}{2\pi} \tan^{-1} \frac{y}{x}, 1 - \sqrt{x^2 + y^2})$$

A family of enriched basis functions on the physical domain Ω is defined as $\mathcal{V} \circ G^{-1}$.

Basis functions on two patches

Partition of the Domain

We consider a covering of the physical domain consisting of two patches: one disk and one annular region shown in Fig. 10, that are defined as follows:

$$\begin{aligned}
\Omega_1^* &= \{(x, y) : 0 \le x^2 + y^2 \le (1 - (b - \delta))^2\} \\
\Omega_2^* &= \{(x, y) : (1 - (b + \delta))^2 \le x^2 + y^2 \le 1\}
\end{aligned}$$

To construct basis functions on these two patches, we need to construct PU functions with flat-top, Ψ_1, Ψ_2, defined on two patches Ω_1^*, Ω_2^*, respectively. For this end, we consider a covering of the parameter domain $\hat{\Omega}$ consisting of the following two patches:

$$\hat{\Omega}_1^* = [0, 1] \times [b - \delta, 1] \quad \hat{\Omega}_2^* = [0, 1] \times [0, b + \delta].$$

Construction of PU function

We define PU functions $\hat{\Psi}_i, i = 1, 2$, on rectangular patches $\hat{\Omega}_i^*, i = 1, 2$, respectively,

as follows:

$$
\hat{\Psi}_1(\xi, \eta) = \begin{cases} \phi_{g_2}^L\left(\frac{\eta - (b+\delta)}{2\delta}\right) & \text{if } \eta \in [b - \delta, b + \delta] \\ 1 & \text{if } \eta \in [b + \delta, 1] \\ 0 & \text{if } \eta \notin [b - \delta, 1], \end{cases}
$$

$$
\hat{\Psi}_3(\xi, \eta) = \begin{cases} \phi_{g_2}^R\left(\frac{\eta - (b-\delta)}{2\delta}\right) & \text{if } \eta \in [b - \delta, b + \delta] \\ 1 & \text{if } \eta \in [0, b - \delta] \\ 0 & \text{if } \eta \notin [0, b + \delta], \end{cases}
$$

where $\phi_{g_2}^R(x)$ and $\phi_{g_2}^L(x)$ are $\mathcal{C}^1$-continuous functions defined by

$$
\phi_{g_2}^R(x) = (1 - x)^2(1 + 2x), \quad \text{and} \quad \phi_{g_2}^L(x) = (1 + x)^2(1 - 2x).
$$

Then we use the following parameters, PU functions, and patches.

1. $\Omega_1^* = G(\hat{\Omega}_1^*), \quad \Omega_2^* = G(\hat{\Omega}_2^*)$

2. $\hat{\Psi}_1(\xi, \eta) + \hat{\Psi}_2(\xi, \eta) = 1$ for each $(\xi, \eta) \in [0, 1] \times [0, 1]$.

3. Let $\Psi_k \equiv \hat{\Psi}_k \circ G^{-1}, k = 1, 2$ Then their supports are two patches defined by
   (25): that is, $\text{supp}(\Psi_k) = \Omega_k, k = 1, 2$ shown in Fig. 10. In this figure, a narrow
   annuls is non flat-top part of the PU functions Ψ_k.

4. We choose different parameters b, and δ for different diffusion coefficients ε: for

example,

$$b = 0.05(0.005), \quad \delta = 0.01(0.001) \text{ when } \varepsilon = 10^{-3}(10^{-4}).$$
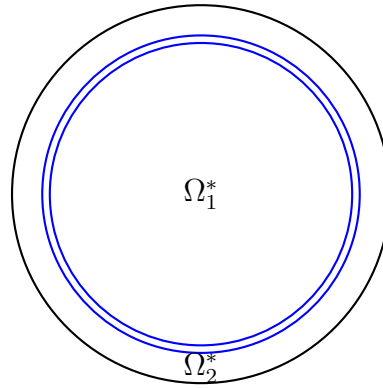
Figure 10: Diagram of supports of circular PU functions in the physical domain.
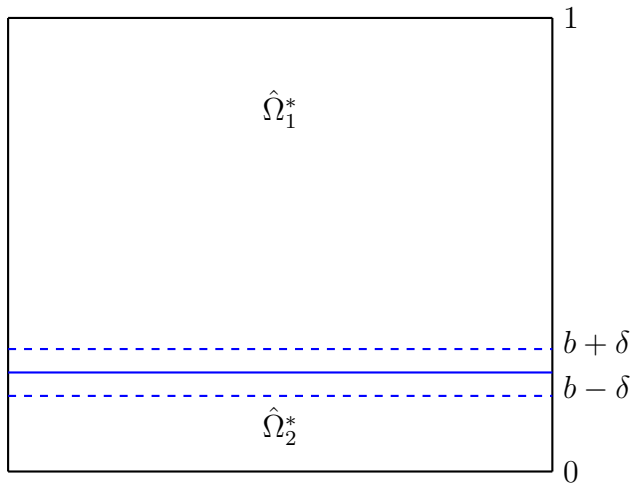
Figure 11: Schematic diagram of patches in the reference domain. $\hat{\Omega}_1^* = [0, 1] \times [b - \delta, 1], \hat{\Omega}_2^* = [0, 1] \times [0, b + \delta]$.

Basis functions on Ω_1^*

Let $T_1 : [b - \delta, 1] \longrightarrow [0, 1]$ be the bijective linear mapping. This is η directional

Berstein polynomial transformed by T_1.

$$\widetilde{M}_{k+1}^B(\eta) = {}_qC_k(1 - T_2(\eta))^{q-k}T_2(\eta)^k, \quad k = 0, 1, 2, \ldots, q \quad (q \geq 3).$$

Let $\hat{N}_k(\xi), k = 1, 2, \ldots, 4p - 2$, be B-splines, corresponding to an open knot vector

with $p \geq 3$

$$\{\underbrace{0\ldots0}_{p+1}, \underbrace{1/4\ldots1/4}_{p-1}, \underbrace{1/2\ldots1/2}_{p-1}, \underbrace{3/4\ldots3/4}_{p-1}, \underbrace{1\cdots1}_{p+1}\}.$$

Next, $\hat{N}_1$ and $\hat{N}_{4p-2}$, the first and the last B-spline functions, respectively, are joined

together to be one blending function denoted by $\hat{N}_1^B(\xi)$ so that they can be periodic

after push-forwarded to the innder disk Ω_1^* through the mapping G:

$$\hat{N}_1^B(\xi) \;\; = \;\; \begin{cases} (1 - 4\xi)^p & \text{if } \xi \in [0, 1/4] \quad (\hat{N}_1(\xi)) \\[2mm] 0 & \text{if } \xi \in [1/4, 3/4] \\[2mm] (4\xi - 3)^p & \text{if } \xi \in [3/4, 1] \quad (\hat{N}_{4p-2}(\xi)) \end{cases}$$

$$\hat{N}_k^B(\xi) \;\; = \;\; \hat{N}_k(\xi), k = 2, \ldots, 4p - 3$$

Now, the push-forward of the PU function $\hat{\Psi}_1$ of (25) onto the physical domain Ω

is denoted by

$$\Psi_1(x, y) = (\hat{\Psi}_1 \circ G^{-1})(x, y) = \hat{\Psi}_1(\xi(x, y), \eta(x, y)). \tag{25}$$

Then basis functions on the annular region Ω_1^* are the following functions of class $\mathcal{C}^0$:

$$\mathcal{V}^A = \left\{ \Psi_1(x,y) \cdot \left[\left(\hat{N}_k^B \times \widetilde{M}_l^B \right) \circ G^{-1} \right] (x,y) : 1 \leq k \leq 4p-3, 1 \leq l \leq q+1 \right\}$$

For the numerical methods for higher order equations, it is possible to modify the members of $\mathcal{V}^A$ to be $\mathcal{C}^1$ functions. Indeed, the basis functions in $\mathcal{V}^A$ are $\mathcal{C}^1$ except at points in $\{(x,0) : x \in (a-\delta, b+\delta)\}$, where $\left(\hat{N}_k^B \times \widetilde{M}_l^B \right) \circ G^{-1}(x,y)$ have discontinuous derivatives if $k=1$. We can modify the joined B-spline $(1-4\xi)^p$ and $(4\xi-3)^p$, to be $\mathcal{C}^1$- continuous function into $(1-4\xi)^{p-1}(1+(p-1)\xi)$ and $(4\xi)^{p-1}(p+1-4p\xi)$.

Enriched basis functions on Ω_2^*

Since the boundary layer occurs along the lower half of the unit circle, we enrich this region with the boundary layer function (24).

Let $T_2 : [0, a+\delta] \longrightarrow [0,1]$ be the bijective linear mapping. This is η directional Berstein polynomials transformed by T_2.

$$\widetilde{M}_{k+1}^C(\eta) = {}_qC_k(1-T_3(\eta))^{q-k}T_2(\eta)^k, \quad k=0,1,2,\ldots,q,$$

$\hat{N}_k^B(\xi)$ are same periodic B-spline functions for Ω_1^* corresponding to the knot vector (25). Then we have this augmented basis functions:

$$\hat{\mathcal{V}}_1^B = \left\{ \hat{N}_k^B(\xi) \cdot \hat{\varphi}_0(\eta) : k = 2p+1, \ldots, 4p-3 \right\}$$
$$\hat{\mathcal{V}}_2^B = \left\{ \hat{\Psi}_2(\xi, \eta) \cdot \left(\hat{N}_k^B(\xi) \cdot \widetilde{M}_l^C(\eta) \right) : 1 \leq k \leq 4p-3, \quad 2 \leq l \leq q+1 \right\}$$

where $\hat{\Psi}_2$ is defined in (25).

Since $\widetilde{M}_1^C(\eta) = 1$ for $\eta = 0$ and the boundary layer problem has the homogeneous

boundary condition along $\partial\Omega$, $\hat{\Psi}_2(\xi,\eta) \cdot \hat{N}_k^B(\xi) \cdot \widetilde{M}_1^C(\eta)$ are excluded in $\hat{\mathcal{V}}_2^S$.

We augment the enrichment function $\phi_0(\eta)$ along the lower half circle for $k = 2p+1, \ldots, 4p-3$ in $\hat{\mathcal{V}}_1^S$.

A family of enriched basis functions on the boundary layer region Ω_2^* is

$$\mathcal{V}^B = \left(\hat{\mathcal{V}}_1^B \circ G^{-1}\right) \cup \left(\hat{\mathcal{V}}_2^B \circ G^{-1}\right). \tag{26}$$

Then, combining these two sets $\mathcal{V}^A, \mathcal{V}^B$ of basis functions constructed in previous subsections, we have an approximation space $\mathcal{V}$ to deal with the boundary layer effects.

$$\mathcal{V} = \text{span}\left(\mathcal{V}^A \cup \mathcal{V}^B\right).$$

Note that $\mathcal{V}$ contains special boundary layer functions modified and scaled by PU functions with flat-top.

Galerkin method

The finite element method for (3.1) is formulated as *Galerkin's method*: Find $u_h \in \bar{V}_N$ such that

$$\epsilon(\nabla u, \nabla v) - (u_y, v) = (f, v), \quad \forall v \in \bar{V}_N$$

where $\bar{V}_N = \{\underbrace{\varphi_1, ..., \varphi_N}_{\text{B-spline}}, \underbrace{\varphi_{N+1}, ..., \varphi_{N+M}}_{\text{enriched}}\}$. Since

$$u_h(x, y) = \sum_{i=1}^{N+M} c_i \varphi_i(x)$$

We can write

$$\sum_{i=1}^{N+M} c_i[\epsilon(\nabla\varphi_i, \nabla\varphi_j) - (\frac{\partial\varphi_i}{\partial y}, \varphi_j)] = (f, \varphi_j), \quad j = 1, ..., N+M$$

In matrix form, the linear system (3.9) can be written as

$$Ac = b$$

where

$$A = \begin{bmatrix} a_{11} & \cdots & a_{1L} \\ \vdots & \vdots & \vdots \\ a_{L1} & \cdots & a_{LL} \end{bmatrix}, c = \begin{bmatrix} c_1 \\ \vdots \\ c_L \end{bmatrix}, b = \begin{bmatrix} b_1 \\ \vdots \\ b_L \end{bmatrix}$$

where L=M+N, $a_{ij} = \epsilon(\nabla\varphi_i, \nabla\varphi_j) - (\frac{\partial\varphi_i}{\partial y}, \varphi_j)$, and $b_i = (f, \varphi_i)$. The stiffness matrix

consists of four block matrices, A_1, A_2, A_3, A_4,

$$A = \begin{bmatrix} A_1 & A_2 \\ A_3 & A_4 \end{bmatrix}$$

The submatrix A_1 is composed of the terms involving only the B-splines whereas the

submatrices A_2, A_3 and A_4 involve the boundary layer elements. For $N+1 \leq i, j \leq$

$N+M$, the bilinear form in A_4 can be calculated as follows

$$a(\nabla\varphi_i, \nabla\varphi_j) = \epsilon \iint_{\Omega} \nabla\varphi_i\nabla\varphi_j - \frac{\partial\varphi_i}{\partial y}\varphi_j dxdy$$

$$= \iint_{\hat{\Omega}} (J(G)^{-1}\nabla(N_i(\xi)\varphi_0(\eta))^T (J(G)^{-1}\nabla(N_j(\xi)\varphi_0(\eta))|J(G)|d\xi d\eta$$

$$- \iint_{\hat{\Omega}} (J(G)_2^{-1}\nabla(N_i(\xi)\varphi_0(\eta))(N_j(\xi)\varphi_0(\eta))|J(G)|d\xi d\eta$$

where

$$J(G) = \begin{bmatrix} \frac{\partial x}{\partial \xi} & \frac{\partial y}{\partial \xi} \\[2mm] \frac{\partial x}{\partial \eta} & \frac{\partial y}{\partial \eta} \end{bmatrix} = \begin{bmatrix} -2\pi(1-\eta)\sin 2\pi\xi & 2\pi(1-\eta)\cos 2\pi\eta \\[2mm] -\cos 2\pi\xi & -\sin 2\pi\xi \end{bmatrix}$$

$|J(G)| = 2\pi(1-\eta)$, determinant of Jacobian of $G(\xi, \eta)$, geometry mapping. $J(G)_2^{-1}$ is the second row of $J(G)^{-1}$. For $1 \leq i \leq N, N+1 \leq j \leq N+M$, the bilinear form in A_2 can be calculated as follows

$$\begin{aligned} a(\nabla\varphi_i, \nabla\varphi_j) &= \epsilon \iint_\Omega \nabla\varphi_i \nabla\varphi_j - \frac{\partial \varphi_i}{\partial y}\varphi_j \, dxdy \\ &= \iint_{\hat{\Omega}} (J(G)^{-1}\nabla(N_i(\xi)M_i(\eta)))^T (J(G)^{-1}\nabla(N_j(\xi)\varphi_0(\eta)))|J(G)|d\xi d\eta \\ &- \iint_{\hat{\Omega}} (J(G)_2^{-1}\nabla(N_i(\xi)M_i(\eta)))(N_j(\xi)\varphi_0(\eta))|J(G)|d\xi d\eta \end{aligned}$$

Numerical Simulation

Simulation 1

We consider 1-dimensional convection-diffusion problem.

$$\epsilon \triangle u + (1+\epsilon)\nabla u + u = 0, \quad 0 < x < 1 \tag{27}$$

$$u(0) = 0, \quad u(1) = 1$$

Equation (27) can be solved exactly to get

$$u(x) = \frac{1}{e^{-1} - e^{-1/\epsilon}}(e^{-x} - e^{-x/\epsilon})$$

This $u(x)$ is used to investigate the errors of the proposed schemes.

By the boundary layer analysis, we get the boundary layer approximation.

$$u_i = C(1 - e^{-x/\epsilon}), \quad x = O(\epsilon)$$

Table 3: 1D Perturbed Convection-Diffusion equation, Enriched PU-IGA and general IGA Maximum error comparison, P- refinement, $\triangle h = 0.1$ $\epsilon = 0.001$

Degree	DOF	NO Enrichment	Enrichment
2	22	1184374133299504.	0.18638906974603708
4	42	1.8064901684905510	6.0128355627853125E-009
6	62	1.182991935043252	5.8175686490358203E-014

Introduce the boundary layer element φ_0 as

$$\varphi_0 = (1 - e^{-x/\epsilon})\psi_1(x)$$

We compare the numerical results of general IGA and enriched PU-IGA by boundary layer element. See the Figure 12 and Table 3 and 4. General IGA does not yield reasonable solution to the problem from the table. One can find the oscillations around boundary layer. With Enriched PU-IGA, we can have accurate solution and can capture the boundary layer effect.
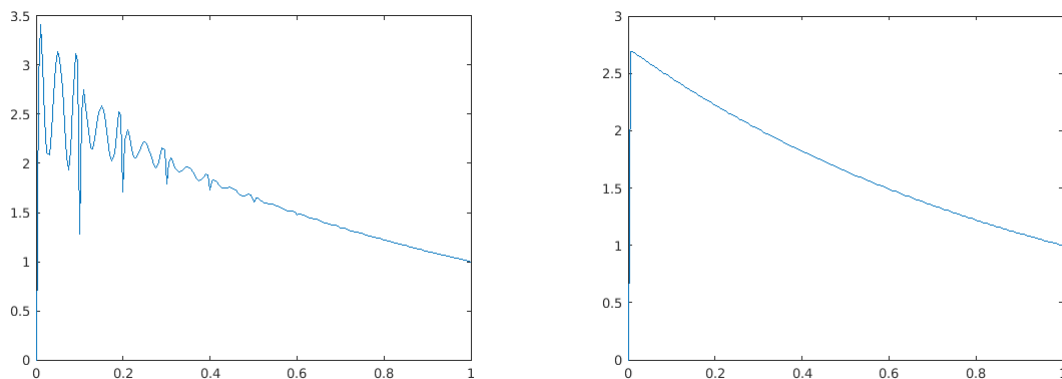
Figure 12: Comparison between general IGA and enriched PU-IGA, $\epsilon = 10^{-3}, N = 62, M = 1, \triangle h = 0.1$, h-refinement

Simulation 2

Perturbed Convection-Diffustion Equation in a circle

Table 4: 1D Perturbed Convection-Diffusion equation, Enriched PU-IGA and general IGA Maximum error comparison, H-refinement, $p = 6$, $\epsilon = 0.001$

$\triangle h$	DOF	NO Enrichment	Enrichment
1	8	4.6265488088990887	0.69128547248598193
0.5	14	5.9244805022950153	0.35385855064367844
0.1	62	1.1829919350432532	5.8175686490358203E-014
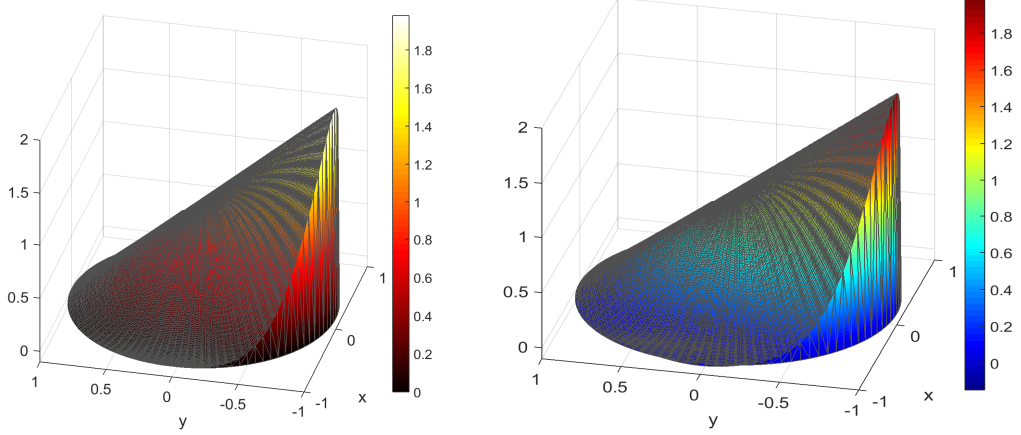
Figure 13: Graphs of numerical solutions obtained by PU-IGA when $\varepsilon = 10^{-3}$(Left) and $\varepsilon = 10^{-5}$(Right).

We approximate the following exact solution u of (3.1)

$$u(x, y) = \begin{cases} (1 - x^2)^2(-y + \sqrt{1 - x^2} + \frac{\epsilon + \sqrt{1 - x^2}}{(1 - x^2)^{3/2}}), & \text{in } \Omega \\ \\ 0 & \text{on } \partial\Omega \end{cases}$$

The corresponding f can be found from (3.1) and it turns out that $f = (1 - x^2)^2 + O(\epsilon)$. See [27]. With the derived the boundary layer element and basis functions, we implement the enriched PU-IGA scheme and present the numerical result.

Relative error in percent in the l-norm $\| \cdot \|_l$ is defined by

$$\|err\|_{l,rel}(\%) = \frac{\|u_{ex} - u^h\|_l}{\|u_{ex}\|_l} \times 100.$$
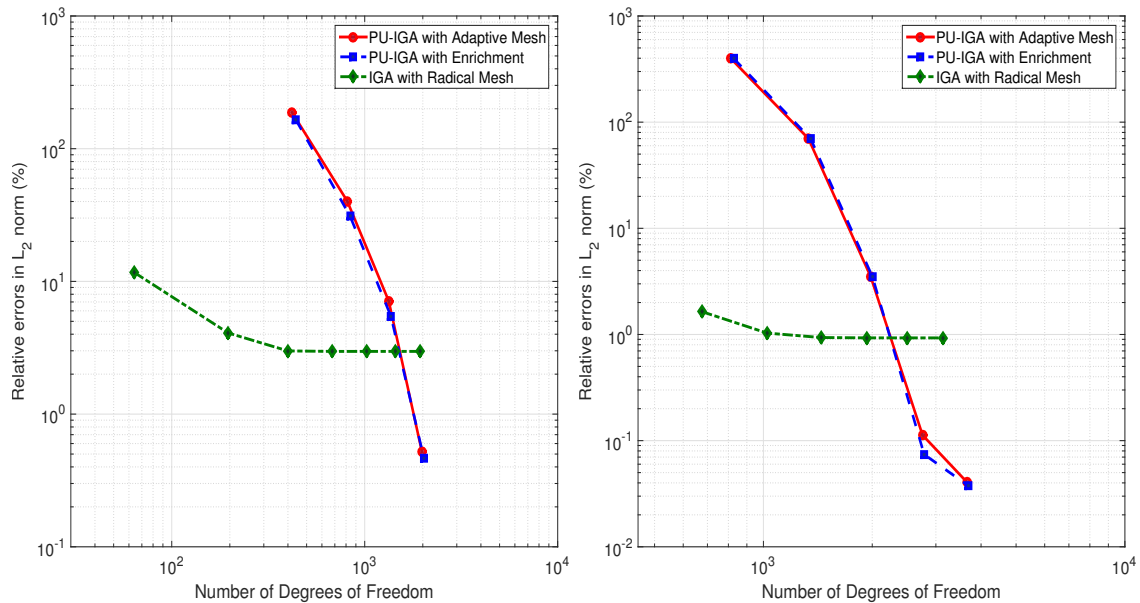
Figure 14: (Left) Relative errors in percent when $\varepsilon = 10^{-3}, a - \delta = 0.05, b = 0.5, \delta = 0.01$. (Right) Relative errors in percent when $\varepsilon = 10^{-4}, a - \delta = 0.005, b = 0.5, \delta = 0.001$.

Results of the enriched PU-IGA using $\mathcal{V}$ as a approximation space are shown in Fig. 13 and Fig. 14, and Table 5, in which we observe the following.

1. The proposed Enriched PU-IGA yields better results with lower degree of freedom than the enriched FEM of [27], as shown in Table 5. We compared our results with those in Table 1 of [27].

2. The authors in [27] used piecewise linear basis functions for enriched FEM, whereas we use high order B-spline basis functions constructed through either the p-refinement or the k-refinement . Thus, Enriched PU-IGA requires more quadrature points than the enriched FEM of [27] for numerical integration. If no internal knots are repeated in the k-refinement of IGA, the support of a B-spline function of degree p covers $p + 1$ (non-void) knot spans for extreme cases

Hence, the integral domain of a B-spline function of degree p can be divided into $p + 1$ intervals for accurate integrations. Therefore, we cannot claim that the total computing time of our method is shorter than that of the enriched FEM used in [27].

For the results in Table 5, we use the p-refinement of IGA in which internal knots are repeated $(p - 1)$ times and hence supports of corresponding B-splines consist of two knot spans. For a comparison of computing time between PU-FEM and PU-IGA, suppose each piecewise linear basis function consists of four 2-dimensional shape functions in FEM. We use B-splines of degrees $p = 10$ and $q = 10$ in the framework of the p-refinement of IGA. Then we may use one Gauss point per shape function in FEM, whereas we use six Gauss points per B-spline function of degree 10 on each knot span. Thus we have the following.

- The number of function evaluations is $9217 \times 4 = 36,868$ in FEM, whereas the number of function evaluations is $3692 \times 36 \times 4 = 531,468$ in the proposed method. Here 9217 and 3692, respectively, are degrees of freedom shown at the last row of Table 5. That is, since the polynomials of degree 10 have more terms than linear polynomials, the proposed method requires much more function evaluations than Enriched FEM for numerical integrations. Since both enriched IGA and enriched FEM use a similar boundary layer function as an enrichment, extra Gauss points used for evaluations of enrichment functions and PU functions are not counted.

By the same reasons, if we assume that the bandwidths k of IGA and FEM are

similar (refer to [60] for detailed discussion of bandwidth), then we have the following.

- The Cholesky factorization costs $9217(k^2 + 3k)$ flops for the enriched PU-FEM and $3692(k^2 + 3k)$ flops for the enriched PU-IGA, respectively. That is, the enriched PU-FEM requires more flops for the factorization than the proposed method.

3. In both cases where $\varepsilon = 10^{-3}$ as well as $\varepsilon = 10^{-4}$, PU-IGA yields numerical solutions with relative error 0.00038, which is as small as ε. Since we compare PU-IGA solutions with approximate true solution that satisfies the stiff convection-diffusion equation only upto ε, it has no meaning to pursue more accurate solutions than those in the column "enriched PU-IGA" and " PU-IGA adaptive" of Table 5.

4. PU-IGA with adaptive k-refinement and Enriched PU-IGA by the boundary layer function are compared as follows:

- We use B-splines of high order ($6 \le p \le 12$) as basis functions for both approaches. As shown in Table 5, the enriched PU-IGA yields accurate solution at low cost (dof = 2784).

- For PU-IGA with adaptive mesh shown in Fig. 14, we choose Ω_3^* to be almost as small as the boundary layer zone and insert knots adaptively for the k-refinement of the radial direction basis $\widetilde{M}_l^C(\eta), 1 \le l \le q + 1$. In other words, using the PU function Ψ_2, basis functions of high degree are

enriched PU-IGA		PU-IGA adapt msh		Hong et al.[27]		IGA with radical msh	
dof	$\|err\|_{L^2,rel}(\%)$	dof	$\|err\|_{L^2,rel}(\%)$	dof	$\|err\|_{L^2,rel}(\%)$	dof	$\|err\|_{L^2,rel}(\%)$
1352	69.56	1332	70.01	1516	5.77	400	4.067
2004	3.480	1980	3.516	2347	5.01	1024	1.031
2784	0.074	2756	0.113	4130	4.43	1936	0.929
3692	0.038	3660	0.041	9217	3.39	3136	0.929

Table 5: Relative error in percent when $\varepsilon = 10^{-4}$. The results in the third column are relative errors in percent by enriched FEM reported in [27].

constructed inside the boundary layer zone. Relative errors in the last row of the column " PU-IGA Adapt msh" of Table 5 show that PU-IGA with adaptive mesh is as good as Enriched PU-IGA enriched with boundary layer function.
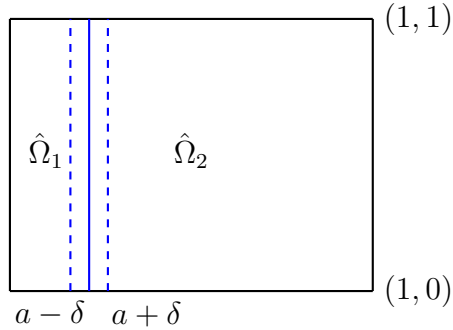
Figure 15: Schematic diagram of subdomains in the reference domain. $\hat{\Omega}_1 = [0, a] \times [0, 1], \hat{\Omega}_2 = [a, 1] \times [0, 1]$, where $a = 0.1$ and $\delta = 0.05$. The supports of PU functions with flat-top, Ψ_1 and Ψ_2, are $\hat{\Omega}_1^* = [0, a + \delta] \times [0, 1] = \text{supp}(\Psi_1)$, and $\hat{\Omega}_2^* = [a - \delta, 1] \times [0, 1] = \text{supp}(\Psi_2)$.

Simulation 3

Perturbed Convection-Diffustion Equation in a square

To present the effectiveness of the proposed enriched PU-IGA, we compare the

performance of enriched PU-IGA with other numerical methods. For a simplicity, we test it with a singularly perturbed convection-diffusion problem with mild boundary layer effect.

Let us consider a singularly perturbed convection-diffusion problem with an exponential layer at the outflow boundary and two characteristic layers. A problem like this is given by

$$-\varepsilon\Delta u - bu_x + cu = f \quad \text{in } \Omega = (0,1)^2, \tag{28}$$

$$u = 0 \quad \text{on } \partial\Omega$$

where $b = 2 - x$, $c = 3/2$, $\varepsilon = 10^{-2}$, and f is calculated from the following solution of (28)

$$u(x,y) = \left(\cos\frac{\pi x}{2} - \frac{e^{-x/\varepsilon} - e^{-1/\varepsilon}}{1 - e^{-1/\varepsilon}}\right) \frac{(1 - e^{-y/\sqrt{\varepsilon}})(1 - e^{-(1-y)/\sqrt{\varepsilon}})}{1 - e^{-1/\sqrt{\varepsilon}}}$$

The function has an exponential boundary layer at $x = 0$, two characteristic boundary layers at $y = 0$ and $y = 1$, respectively.

To find the inner approximation, we introduce a boundary-layer coordinate given as

$$\bar{x} = \frac{x}{\epsilon^\alpha}$$

When using this boundary-layer coordinate, (28) transforms to

$$-\epsilon^{1-2\alpha}\frac{\partial^2 u}{\partial\bar{x}^2} - \epsilon\frac{\partial^2 u}{\partial y^2} - 2\epsilon^{-\alpha}\frac{\partial u}{\partial\bar{x}} + \bar{x}\frac{\partial u}{\partial\bar{x}} + 2/3u(\epsilon^\alpha\bar{x}, y) = f(\epsilon^\alpha\bar{x}, y)$$

The boundary condition is

$$u(0, y) = 0$$

The leading terms are

$$-\epsilon^{1-2\alpha}\frac{\partial^2 u}{\partial \bar{x}^2}, \quad -2\epsilon^{-\alpha}\frac{\partial u}{\partial \bar{x}} = 0$$

By the dominant balancing, $\alpha = 1$. With this we have the following problem to solve:

$$-\frac{\partial^2 u}{\partial \bar{x}^2} + 2\frac{\partial u}{\partial \bar{x}} = 0$$

The general solution of this problem is

$$u_i(x, y) = C(1 - e^{-2\frac{x}{\epsilon}})$$

where C is a constant that we could find by matching condition. We use use $\varphi_0(x)$

as

$$\varphi_0(x) = 1 - e^{-2\frac{x}{\epsilon}}$$

In this simulation, the parameter domain and the physical domain are both $[0, 1] \times [0, 1]$ and the geometric mapping G is the indentity mapping. For the results in Table 6 and Fig. 16, we use the following parameters and PU-functions:

We divide the reference domain, $\hat{\Omega} = [0, 1] \times [0, 1]$ into two subdomains shown in the Fig. 15:

$$\hat{\Omega}_1 = [0, a] \times [0, 1], \quad \hat{\Omega}_2 = [a, 1] \times [0, 1], \text{ where } a = 0.1.$$

Two PU-function with flat-top are defined by

$$\hat{\Psi}_1(\xi, \eta) = \psi_{[0,a]}^{(\delta,1)}(\xi) \times \eta \quad \text{and} \quad \hat{\Psi}_2(\xi, \eta) = \psi_{[a,1]}^{(\delta,1)}(\xi) \times \eta,$$

where $\delta = 0.05$. Then the supports of $\hat{\Psi}_1$ and $\hat{\Psi}_2$, respectively, are $[0, a + \delta] \times [0, 1]$ and $[a - \delta, 1] \times [0, 1]$.

The refinements, B-splines, and an enrichment function used to get the results in Fig. 16 are as follows:

1. For the result of " *PU-IGA* ", we use two different sets of basis functions in the ξ-direction:

   (i) the scaled B-splines $\hat{N}_{k,p+1}^{[0,a+\delta]}(\xi) \cdot \psi_{[0,a]}^{(\delta,1)}(\xi), k = 1, \ldots, n_1$ that are B-spline functions corresponding to an open knot vector on $[0, a + \delta]$, scaled by the PU function $\psi_{[0,a]}^{(\delta,1)}(\xi)$.

   (ii) the scaled B-splines $\hat{N}_{l,p+1}^{[a-\delta,1]}(\xi) \cdot \psi_{[a,1]}^{(\delta,1)}(\xi), l = 1, \ldots, n_2$, that are another set of B-splines corresponding to an open knot vector on $[a - \delta, 1]$, scaled by the PU function $\psi_{[a,1]}^{(\delta,1)}(\xi)$.

2. For the result of " *Enriched PU-IGA* " of Table 6 and Fig. 16, we use the following basis functions:

   (i) By the boundary layer analysis, we get $\phi_0(\xi) = 1 - e^{-2\xi/\varepsilon}$. On the boundary layer zone $[0, a + \delta] \times [0, 1]$, we use the enrichment functions $H_j(\xi, \eta)$ defined by

   $$H_j(\xi, \eta) = \left(\phi_0(\xi) \cdot \psi_{[0,a]}^{(\delta,1)}(\xi) \right) \times M_j(\eta), \quad 0 \leq j \leq p,$$

   as well as

   $$\left(\hat{N}_{k,p+1}^{[0,a+\delta]}(\xi) \cdot \psi_{[0,a]}^{(\delta,1)}(\xi) \right) \times M_j(\eta), \quad 2 \leq k \leq n_1, \quad 0 \leq j \leq p,$$

   where $M_j(\eta), j = 0, 1, \ldots, p$, are Bézier functions of degree p.

Because of the enrichment function $\phi(\xi)$, it is not necessary to use B-splines corresponding to a fine mesh on the boundary layer zone.

(ii) On $[a - \delta, 1]$, we construct B-splines by the k-refinement of IGA in the ξ-direction. For example, the set of Bézier polynomials, defined on $[a - \delta, 1]$, of degree p is refined by inserting equally spaced p knots and scaled by the PU function $\psi_{[a,1]}^{(\delta,1)}(\xi)$.

3. For the result of *"IGA with radical mesh refinement"*, we use B-splines obtained by the k-refinement by inserting n_ξ knots:

$$r_i = \left(\frac{i}{n_\xi + 1}\right)^{1/3}, \; i = 1, \ldots, n_\xi,$$

where the number of knots, n_ξ, is increased as the p-degree is elevated.

4. For the result of *" IGA "*, we use the k-refinement of IGA in both ξ- and η-directions.

Even though the boundary layer effect is not very strong (since $\varepsilon = 10^{-2}$), from the results shown in Table 6 and Fig. 16, we observe the following:

1. Enriched PU-IGA is superior over any other methods (including streamline diffusion techniques).

2. One can use only one patch with sufficiently large number of knot insertions in the k-refinement of IGA to get similar results to enriched PU-IGA. However, in such case, the degrees of freedom become much lager.
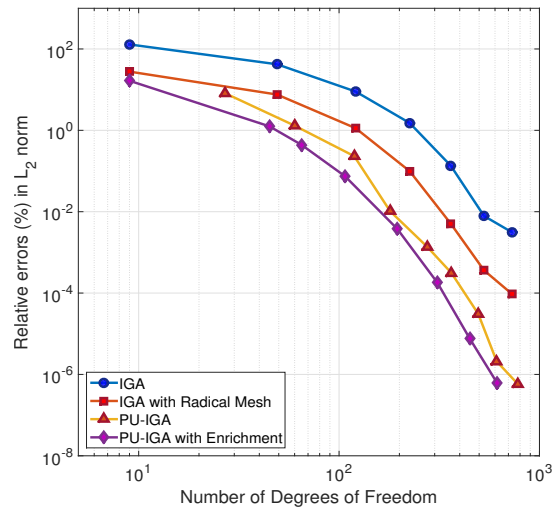
Figure 16: Relative errors in L^2-norm in percent from results obtained by IGA, PU-IGA, Enriched PU-IGA, and IGA with radical mesh.

IGA		PU-IGA		Enrich PU-IGA		IGA with Rad msh	
dof(p-deg)	$\|err\|_{L^2,r}(\%)$	dof	$\|err\|_{L^2,r}(\%)$	dof(p-deg)	$\|err\|_{L^2,r}(\%)$	dof	$\|err\|_{L^2,r}(\%)$
121(6)	8.98E-0	119	2.32E-2	65(4)	4.39E-1	121	1.13E-0
225(8)	1.52E-0	180	1.02E-2	107(6)	7.47E-2	225	9.93E-2
361(10)	1.35E-1	275	1.38E-3	195 (8)	3.81E-3	361	5.07E-3
529(12)	7.84E-3	364	3.10E-4	309 (10)	1.80E-4	529	3.60E-4
729(14)	3.12E-3	495	3.08E-5	449 (12)	7.59E-6	729	9.50E-5
		612	2.08E-6	615 (14)	6.14E-7		

Table 6: Relative errors in L^2-norm in percent of numerical solutions obtained by IGA, PU-IGA, Enriched IGA, and IGA with radical mesh refinement when $\varepsilon = 10^{-2}$.
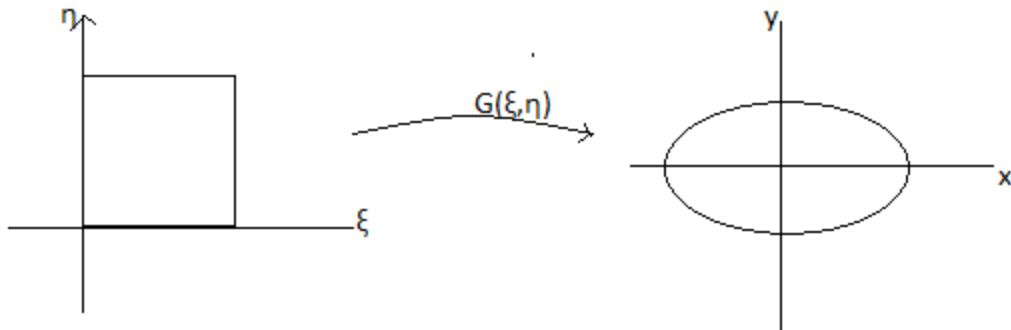
Figure 17: Ellipse Geometry Mapping

4.6 Singulary perturbed convection-diffusion equation on an ellipse domain

We consider the same convection-diffusion problem on a different domain, an ellipse domain.

$$
\begin{cases}
-\epsilon \triangle u - u_y = f(x,y) & \text{in } \Omega \\[2em]
u = 0 & \text{on } \partial\Omega
\end{cases}
$$

where $0 < \epsilon \ll 1$, Ω is an ellipse centered at $(0,0)$ and one radius along the x-axis is 2r and the other along the y-axis is r. The function f is as smooth as needed.

The geometry mapping $G : \hat{\Omega} \longrightarrow \Omega$ is defined by

$$
G(\xi, \eta) = (x(\xi, \eta), y(\xi, \eta) = (2(1 - \eta) \cos 2\pi\xi, (1 - \eta) \sin 2\pi\xi)
$$

where $\eta = 1 - r, r$ is the distance to the origin along the y-axis and $2\pi\xi$ is the polar angle from origin of the ellipse. We define the reference domain $\hat{\Omega} = [0, 1] \times [0, 1]$ and divide the domain into two patches, $\hat{\Omega}_1 = [0, 1] \times [0, b + \delta]$ and $\hat{\Omega}_2 = [0, 1] \times [b - \delta, 1]$. See Figure 17.

To find the boundary layer element, we pullback the problem (5.1) on to the reference space. Using the stretched variable, $\bar{\eta} = \frac{\eta}{\epsilon^\alpha}$. we obtain the transformed equation

of (5.1).

$$\frac{3\epsilon}{4\pi(1-\epsilon^\alpha\bar\eta)}\sin 2\pi\xi\cos 2\pi\xi\frac{\partial\hat u}{\partial\xi}-\frac{\epsilon}{4\pi^2(1-\epsilon^\alpha\bar\eta^2)}\left(\frac14\sin^2 2\pi\xi+\cos^2 2\pi\xi\right)\frac{\partial^2\hat u}{\partial\xi^2}$$

$$+\frac{\epsilon^{1-\alpha}}{1-\epsilon^\alpha\bar\eta}\left(\frac14\sin^2 2\pi\xi+\cos^2 2\pi\xi\right)\frac{\partial\hat u}{\partial\bar\eta}+\frac{\epsilon^{1-\alpha}}{2\pi(1-\epsilon^\alpha\bar\eta)}\sin 2\pi\xi\cos 2\pi\xi\frac{\partial^2\hat u}{\partial\bar\eta\partial\xi}$$

$$-\epsilon^{1-2\alpha}\left(\frac14\sin^2 2\pi\xi+\cos^2 2\pi\xi\right)\frac{\partial^2\hat u}{\partial\bar\eta^2}-\frac{1}{2\pi(1-\epsilon^\alpha\bar\eta)}\cos 2\pi\xi\frac{\partial\hat u}{\partial\xi}+\epsilon^{-\alpha}\sin 2\pi\xi\frac{\partial\hat u}{\partial\bar\eta}=\hat f$$

Dominating terms are

$$-\epsilon^{1-2\alpha}\left(\frac14\sin^2 2\pi\xi+\cos^2 2\pi\xi\right)\frac{\partial^2\hat u}{\partial\bar\eta^2},\quad \epsilon^{-\alpha}\sin 2\pi\xi\frac{\partial\hat u}{\partial\bar\eta}$$

Therefore a consistent scaling is possible if we select $\alpha=1$. Because we are interested only in the leading-order approximation, we obtain

$$-\left(\frac14\sin^2 2\pi\xi+\cos^2 2\pi\xi\right)\frac{\partial^2\hat u}{\partial\bar\eta^2}+\sin 2\pi\xi\frac{\partial\hat u}{\partial\bar\eta}=0$$

The general solution is

$$u_i=C_1+C_2 e^{\frac{\sin 2\pi\xi}{1/4\cos^2 2\pi\xi+\sin^2 2\pi\xi}\bar\eta},\quad 1/2<\xi<1$$

Because the boundary layer is located near $\eta=0$, we apply the boundary condition $\hat u=0$ at $\eta=0$, and so

$$u_i=C_1\left(1-e^{\frac{\sin 2\pi\xi}{1/4\cos^2 2\pi\xi+\sin^2 2\pi\xi}\frac{\eta}{\epsilon}}\right),\quad 1/2<\xi<1$$

We modify the boundary layer approximation to get our boundary layer element. Choose $\xi=3/2$ for numerical simulation and we can get the boundary layer element

$$\varphi_0=1-e^{-\frac{\eta}{\epsilon}}$$

With proposed Enriched PU-IGA, we expect to get an accurate solution on ellipse domain too.

CHAPTER 5: SINGULARLY PERTURBED PARABOLIC EQUATION IN A CIRCLE

5.1   Introduction

We consider the two-dimensional singularly perturbed heat equation of the form

$$
\begin{cases}
\frac{\partial u}{\partial t} - \epsilon \triangle u = f, & \text{in } \Omega \times (0, T) \\[2ex]
u(x, y, t) = 0, & \text{on } \partial\Omega \times (0, T) \\[2ex]
u(x, y, 0) = u_0(x, y), & \text{on } \Omega
\end{cases}
\tag{29}
$$

where $0 < \epsilon \ll 1$ is the heat conductivity and Ω is the unit circle centered at (0, 0). The functions f and u_0 are assumed to be sufficiently regular. We also assume the compatibility condition

$$
u_0 = 0 \quad \text{on } \partial\Omega
$$

The numerical methods for singularly perturbed problems have been studied in many articles. [58], [59], [63] and [64] proposed numerical methods for stationary convection-diffusion equations using finite element methods. One can find numerical results for parabolic type problems in [9], [12], [33], [39] and [69]. In those articles the authors utilized mesh refinement near the boundary layer. Furthermore, for the parabolic type cases, the authors mainly focused on the finite difference methods in a unit interval or rectangular domains and this did not address the issue of the curved boundary in the context of time dependent problems. In [29], the author approxi-

mates problem (29) using a quasi-uniform triangulation and P_1 finite element space enriched with boundary layer correctors constructed near the circular boundary. In this paper, we similarly aim to approximate problem (29) using B-spline based Isogeometric Finite Element space enriched with boundary layer approximation constructed near the boundary layer. We avoid the costly mesh refinements at the boundary by enriching the Finite Element Space. Boundary layer element multiplied by Partition of Unity with flat-top does not affect out of boundary layer zone.

We introduce the boundary layer element based on the boundary layer analysis similar to that of [29]. Incorporating the boundary layer element, we obtain the proposed NURBS based enriched Finite Element space to be used in the numerical simulations with the coarsest mesh. We present the results of our numerical simulations using B-spline based PU-IGA Finite Element method with the enrichment element.

For the time-dependent problems, the mesh refinement is costly since we need to solve the linear system at each time step. Avoiding mesh refinement, [29] approached the problem in classical Finite Element setting. In this paper, we solve the problem similarly in Enriched PU-IGA setting without mesh refinement. We believe this Enriched PU-IGA used in this paper should also be applicable to many other types of time-dependent singularly perturbed problems such as reaction-diffusion equations.

The concept of enriched space and boundary layer element was first introduced in [26]. The authors of [5] and[6] introduced independently a similar concept for the one-dimensional equations. Especially in [6], the authors studied the numerical analysis of the one-dimensional time-dependent problem. In [16, 18], and [19] the authors presented the numerical methods for the two-dimensional stationary convection dif-

fusion equations using the finite element methods and finite volume methods in a rectangular domain. Lately, in [12, 14] and [20], the time-independent equations were considered in a circular domain.

5.2   Discretization

The semi-discrete analogue of (29) will be based on the variational formulation :

Find $u(t) \in V$, $t \in I$ such that

$$(\dot{u}(t), v) + a(u(t), v) = (f(t), v) \quad \forall v \in V, \ t \in I \tag{30}$$

$$u(0) = u^0$$

Now, let V_h be a finite-dimensional subspace of V with basis $\{\varphi_1, \varphi_2, ..., \varphi_N, \varphi_{N+1}, ..., \varphi_{N+M}\}$. We get the following *semi-discrete* analogue of (30): Find $u_h(t) \in V_h$, $t \in I$, such that

$$(\dot{u}_h(t), v) + a(u_n(t), v) = (f(t), v) \quad \forall v \in V_h, \ t \in I \tag{31}$$

$$(u_h(0), v) = (u^0, v) \quad \in V_h$$

In the classical *backward Euler* method for the semi-discrete problem (31) we seek approximations $u_n^h \in V_h$ of $u(., t_n), n = 0, ..., N$, satisfying

$$(\frac{u_h^n - u_h^{n-1}}{k_n}, v) + a(u_h^n, v) = (f(t_n), v) \quad \forall v \in V_h, n = 1, 2, , .., N \tag{32}$$

$$(u_h^0, v) = (u^0, v) \quad \forall v \in V_h$$

The classcial time-discretization method, the backward Euler method satisfies stability condition so is stable regardless of the size of the time steps k_n, namely this

method is *unconditionally stable.*

5.3   Boundary Layer Analysis

The formal limit problem(unperturbed problem) of (29), namely when $\epsilon \longrightarrow 0$, is

$$
\begin{cases}
\frac{\partial u}{\partial t} = f, & \text{in } \Omega \times (0, T) \\[2mm]
u(x, y, 0) = u_0(x, y) & \text{on } \Omega
\end{cases}
\tag{33}
$$

We find the explicit solution

$$
u_{outer}(x, y, t) = u_0(x, y) + \int_0^t f(x, y, s) ds
$$

Define a geometry Mapping $G : [0, 1] \times [0, 1] \longrightarrow \Omega$ by

$$
G(x, y) = ((1 - \eta) \cos 2\pi\xi, (1 - \eta) \sin 2\pi\xi)
$$

To investigate the boundary layer in the circular domain, we pull back the (29) on to the parameter space by the geometry mapping, G. Using the change of variables, we obtain

$$
\frac{\partial u}{\partial x} = -\frac{\sin 2\pi\xi}{2\pi(1 - \eta)} \frac{\partial \hat{u}}{\partial \xi} - \cos 2\pi\xi \frac{\partial \hat{u}}{\partial \eta}
$$
$$
\frac{\partial u}{\partial y} = -\frac{\cos 2\pi\xi}{2\pi(1 - \eta)} \frac{\partial \hat{u}}{\partial \xi} - \sin 2\pi\xi \frac{\partial \hat{u}}{\partial \eta}
$$

$$
\begin{aligned}
\triangle u &= \frac{\partial^2 u}{\partial x^2} + \frac{\partial^2 u}{\partial y^2} \\[2mm]
&= \frac{\partial^2 \hat{u}}{\partial \eta^2} - \frac{1}{1 - \eta} \frac{\partial \hat{u}}{\partial \eta} + \frac{1}{(1 - \eta)^2} \frac{\partial^2 \hat{u}}{\partial \xi^2}
\end{aligned}
$$

(29) becomes

$$\frac{\partial u}{\partial t} - \epsilon \triangle u = \frac{\partial \hat{u}}{\partial t} - \epsilon \frac{\partial^2 \hat{u}}{\partial \eta^2} - \frac{\epsilon}{4\pi^2(1-\eta)^2} \frac{\partial^2 \hat{u}}{\partial \xi^2} + \frac{\epsilon}{1-\eta} \frac{\partial \hat{u}}{\partial \eta} = f(G(\xi, \eta))$$

We look for the expansion of u at fist order:

$$u \simeq u_{outer} + u_{inner}$$

where u_{outer} is the solution of (33) and u_{inner} is the first order boundary layer approximation. Setting $f = 0$ in (29), we introduce the stretched variable to find the boundary layer approximation.

$$\bar{\eta} = \frac{\eta}{\epsilon^\alpha}$$

(4.1) is transformed to

$$\frac{\partial \hat{u}}{\partial t} - \epsilon^{1-2\alpha} \frac{\partial^2 \hat{u}}{\partial \bar{\eta}^2} - \frac{\epsilon}{4\pi^2(1-\epsilon^\alpha\bar{\eta})^2} \frac{\partial^2 \hat{u}}{\partial \xi^2} + \frac{\epsilon^{1-\alpha}}{1-\epsilon^\alpha\bar{\eta}} \frac{\partial \hat{u}}{\partial \bar{\eta}} = 0$$

The coefficients of the terms in the differential equation are

$$1, \quad \epsilon^{1-2\alpha}, \quad \epsilon, \quad \epsilon^{1-\alpha}$$

To determine α, we estimate these magnitudes by dominant balancing. The dominating terms are

$$\frac{\partial \hat{u}}{\partial t} - \epsilon^{1-2\alpha} \frac{\partial^2 \hat{u}}{\partial \bar{\eta}^2} = 0$$

A consistent scaling is possible if we select $\alpha = \frac{1}{2}$. Thus, the reasonable thickness of the boundary layer is $\alpha = \frac{1}{2}$. We obtain the equations for boundary layer approxi-

mation:

$$
\begin{cases}
\frac{\partial u}{\partial t} - \frac{\partial^2 u}{\partial \bar{\eta}^2} = 0, & \text{in } \Omega \times (0, T) \\[2mm]
u(0, t) = -u_{outer} & \text{at } \bar{\eta} = 0 \\[2mm]
u(x, 0) = 0 \\[2mm]
u \longrightarrow 0, & \text{as } \bar{\eta} \longrightarrow \infty
\end{cases}
\tag{34}
$$

See [29]. The solution of (34) is

$$
u_i = -\int_0^t I(\eta, t - s) \frac{\partial u_{outer}}{\partial t}(\xi, 0, s) ds
$$

where

$$
I(x, t) = erfc(\frac{x}{\sqrt{2\epsilon t}})
$$

$$
erfc(z) = 1 - erf(z) = \sqrt{\frac{2}{\pi}} \int_z^\infty \exp(-\frac{y^2}{2}) dy
$$

$$
erf(z) = \sqrt{\frac{2}{\pi}} \int_0^z \exp(-\frac{y^2}{2}) dy
$$

See [10]

5.4 Error Estimates for fully discrete approximations

This is an error estimate for the backward Euler scheme with V_h piecewise linear from [32]

Theorem Let U^n be the numerical solution of (32) and u is the solution of (29) for $n = 1, ..., N$, then there is a constant C such that

$$
\|u(t_n) - U^n\| \leq C(1 + \log(\frac{t_n}{k_n})^{1/2})(\max_{m \leq n} \int_{I_m} \|\dot{u}(s)\| ds + \max_{t \leq n} h^2 \|u(t)\|_{H^2(\Omega)}) \tag{35}
$$

Absorbing the almost bounded logarithmic quantity in the constant C, and using the trivial fact that

$$\int_{I_n} \|\dot{u}(s)\| ds \leq k_n \|\dot{u}\|_{\infty, I_n}$$

where $\|v\|_{\infty, J} = \sup_{s \in J} \|v(s)\|$ We can write (35) alternatively as follows

$$\max_{t \in I} \|u(t) - U(t)\| \leq C(\max_{n \leq N} k_n \|\dot{u}\|_{\infty, I_n} + \max_{t \in I} h^2 \|u(t)\|_{H^2(\Omega)}) \tag{36}$$

5.5   Numerical Simulations

We present the results of numerical simulations of (29) using the general IGA and Enriched PU-IGA.

Modified Boundary Layer Element

We do not use the boundary layer approximation directly since the term $I(\eta, t - s)$ is not convenient for the integration. Instead, We modify the boundary layer approximation for numerical simulation.

$$u_{inner} \sim \int_0^t I(x, t - s) ds, \qquad f \text{ is bounded}$$

$$= \int_0^t 1 - \frac{1}{\sqrt{\pi \epsilon t}} e^{-\frac{x^2}{4\epsilon t}} ds$$

$$\sim 1 - \frac{1}{\sqrt{\pi \epsilon t}} e^{-\frac{x^2}{4\epsilon t}}, \qquad t \text{ is bounded}$$

We simply the boundary layer element φ_0 for numerical simulation:

$$\varphi_0(x, t) = (1 - e^{-\frac{x^2}{4\epsilon t}}) \psi_1(x)$$

where $\psi_1(x)$ is PU with flat-top which makes the boundary layer element not affect the outer zone.

<div align="center">Simulation 1: One-Dimensional Example</div>

We present a simple one-dimensional example To compare the numerical solution with the exact solution, we consider the following equations:

$$u_t - \epsilon u_{xx} = f(x,t), \quad (0,1) \times (0,T)$$

$$u(0,t) = u(1,t) = 0, \quad t \in (0,T)$$

$$u(x,0) = u^0(x), \quad x \in (0,1)$$

We choose the exact solution u as

$$u = t(1 - e^{-\frac{x}{\sqrt{\epsilon}}} \cos(\frac{x}{\sqrt{\epsilon}}))(1 - \cos(\frac{1-x}{\sqrt{\epsilon}})e^{-\frac{1-x}{\sqrt{\epsilon}}})$$

Hence, f is computed from the (29).

We have two boundary layers at each boundary. Similarly, we could derive the boundary layer element at $x = 1$. Since ϕ_0 depends on time, for each time step, we need to calculate different boundary layer element. To improve computational efficiency, we introduce the modified time-independent boundary layer elements ϕ_0 and ϕ_1 such that

$$\phi_0(x) = 1 - \exp(-\frac{x^2}{4\epsilon})\psi_1(x) \tag{37}$$

$$\phi_1(x) = 1 - \exp(-\frac{(1-x)^2}{4\epsilon})\psi_3(x) \tag{38}$$

where ψ_1 and ψ_3 partition unity functions are used to avoid the singularity of ϕ at

Table 7: Enriched PU-IGA and IGA Maximum errors, H- refinement, $p = 12$

$\triangle$h	DOF	No Enrichment	Enrichment
1	13	0.60845711245515210	2.0256926718709600E-002
0.5	25	0.35453147267928342	6.8586187221852946E-003
0.1	121	2.0443482651402722E-002	6.4348526507274073E-013

$x = 0$ and $x = 1$.

$$
\psi_1(\eta) = \begin{cases} 0, & \text{if } \eta \in [a + \delta, 1] \\[2ex] \phi^R_{g_2}\left(\frac{\eta - (a - \delta)}{2\delta}\right), & \text{if } \eta \in [a - \delta, a + \delta] \\[2ex] 1, & \text{if } \eta \in [0, a - \delta] \end{cases}
$$

$$
\psi_3(\eta) = \begin{cases} 0, & \text{if } \eta \in [0, b - \delta] \\[2ex] \phi^L_{g_2}\left(\frac{\eta - (b + \delta)}{2\delta}\right), & \text{if } \eta \in [b - \delta, b + \delta] \\[2ex] 1, & \text{if } \eta \in [b + \delta, 1] \end{cases}
$$

where

$$
\begin{cases} \phi^R_{g_2}(x) = (1 - x)^2(1 + 2x) \\[2ex] \phi^L_{g_2}(x) = (1 + x)^2(1 - 2x) \end{cases}
$$

We present the results of numerical simulation of (29) using the general IGA and Enriched PU-IGA, which is enriched by the boundary layer element by boundary layer analysis. In Figures 18 and 19, we observe that general IGA produce oscillations near the boundary, however, with Enriched PU-IGA the boundary layer elements capture the sharp transition near the boundary. According to Tables 7 and 8, we observe that the errors of Enriched PU-IGA is much smaller than that of general IGA.
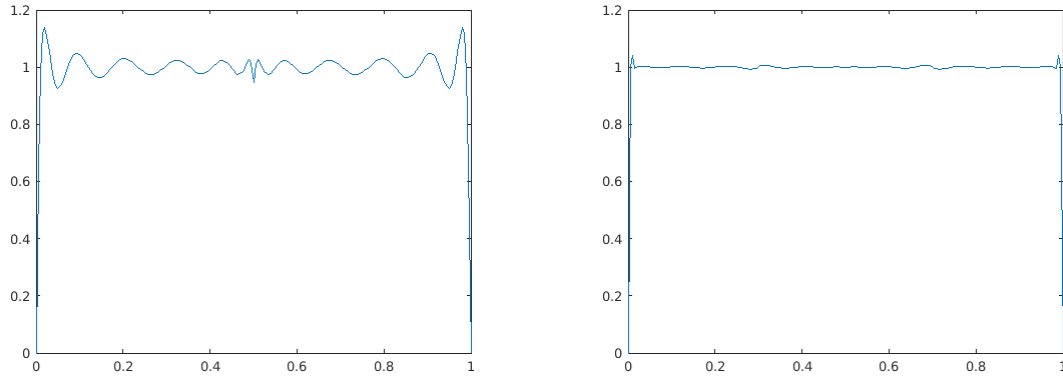
Figure 18: Comparison between IGA and Enriched PU-IGA, $\epsilon = 10^{-5}, N = 25, M = 2, \triangle h = 0.5$, h-refinement
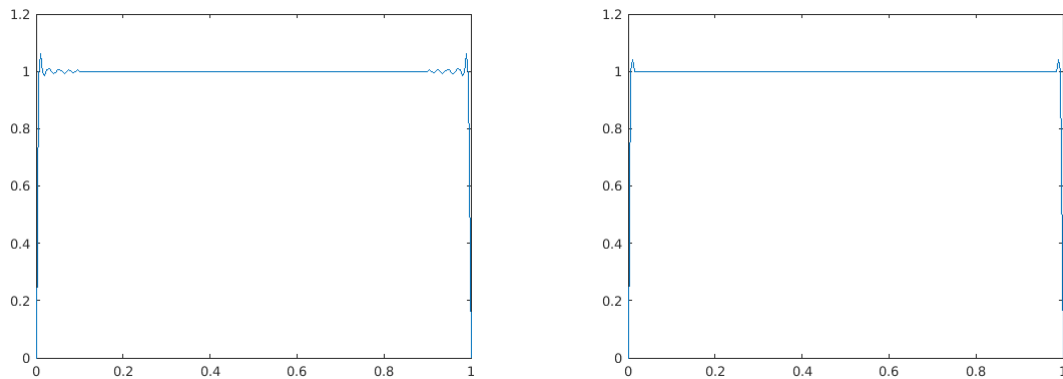
Figure 19: comparison between IGA and Enriched PU-IGA, $\epsilon = 10^{-5}, N = 121, M = 2, \triangle h = 0.1$, h-refinement

1D Error estimates for IGA

Consider this problem for error estimate

$$u = e^{-xt}(1 - e^{-\frac{x}{\sqrt{\epsilon}}}\cos(\frac{x}{\sqrt{\epsilon}}))(1 - \cos(\frac{1-x}{\sqrt{\epsilon}})e^{-\frac{1-x}{\sqrt{\epsilon}}})$$

We use the boundary layer elements (37) developed in the last section. We calculate the convergence rate for h and k, by

$$\frac{\log \frac{e_{i+1}}{e_i}}{\log \frac{t_{i+1}}{t_i}}$$

Table 8: Enriched PU-IGA and IGA Maximum errors, K- refinement, $p = 12$

$\triangle$h	DOF	No Enrichment	Enrichment
1	15	0.60845711245515210	2.0256926718709600E-002
0.1	24	0.12410087048350116	8.6750421698587044E-003
0.01	114	1.3111940128840427E-004	6.2950588269217178E-005

Table 9: H-refinement in space direction, Error and convergence rate with $p = 1$, $\triangle k = 0.001$

$\triangle$h	DOF	Error	Convergence Rate
1	2	0.86719158608753943	0.56577648602290742
0.5	3	0.58586743917746709	1.2734234229268424
0.1	11	7.5459621590306891E-002	1.9739747308538562
0.05	21	1.9208304413022126E-002	1.9825994760155063
0.01	101	7.9015350227129577E-004	1.9609085209372052
0.005	201	2.0296407621556156E-004	

where e_i is error at the time level t_i.

The numerical results show that the space convergence rate is about 2 and time convergence rate is about 1. See the Table 9 and 10. The results support the Theorem 35.

Table 10: H-refinement in time direction, Error and convergence rate with $p = 1$, $\triangle h = 0.01$

$\triangle$k	DOF	Error	Convergence rate
1	101	0.15387596258839775	0.84659173615218630
0.5	101	8.5569946676072428E-002	0.93983918732470273
0.1	101	1.8853928667987407E-002	0.97872058935658002
0.05	101	9.5670403064213039E-003	0.98369693616531739
0.01	101	1.9642777850752413E-003	0.96873175100314268
0.005	101	1.0036576763091665E-003	

CHAPTER 6: FOURTH ORDER ELLIPTIC EQUATIONS CONTAINING SINGULARITIES

6.1   Introduction

We consider the two-dimensional 4th order equations on cracked disk.

$$
\begin{cases}
\triangle^2 u = f \quad \text{in } \Omega \\[2mm]
u(1,\theta) = \frac{\partial u}{\partial n}(1,\theta) = 0 \quad \text{on } \partial\Omega \\[2mm]
u(r,0) = u(r,2\pi) = 0 \\[2mm]
\frac{\partial u}{\partial y}(r,0) = \frac{\partial u}{\partial y}(r,2\pi) = 0
\end{cases}
$$

where Ω is the cracked unit disc centered at $(0, 0)$. The equation satisfy clamped boundary conditions.

The numerical approximation of high order Partial Differential Equations(PDEs) represents a challenging task for the classical Galerkin Finite Element methods due to the need to use trail and test functions featuring high degree of continuity. This issue has been addressed by adapting existing Finite Element schemes or developing new numerical schemes. Specifically, the Discontinuous Galerkin(DG) [57] and local Discontinuous Galerkin(LDG) methods in [15] were developed and adapted for solving high order PDEs. Analogously, non-conforming discretizations have been used to achieve the needed global regularity [11]. Ad hoc techniques as continuous discontinuous finite element approximations for fourth order PDEs have been developed

in [19] in order to overcome the issue of defining C^1-continuous basis for arbitrary shaped elements in dimensions greater than one. Currently, the golden standard in the framework of the standard Galerkin method with Lagrangian basis functions, consists in resorting to mixed formulations [20]. Spectral or pseudo-spectral domain decomposition techinigues have also been used to approximate fourth order PDEs [54]. Isogeometric Analysis(IGA) is a recently developed computational methodology in [16] aiming at closing the existing gap between Computed Aided Design (CAD) and Finite Element Analysis (FEA). Based on the isogeometric paradigm, for which the same basis functions used to present the known geometry are then used to approximate the unknown solution of the PDEs, IGA has been successfully used for the numerical approximation of a wide range of problems providing accurate and efficient solutions. Moreover, IGA provides advantages in the numerical approximation of high order PDEs within the framework of the standard Galerkin formulation, since in IGA globally smooth basis functions can be eventually used. Besides the possibility of offering simplified refinements procedures, IGA allow to exactly represent geometries in engineering design.

However, NURBS or B-spline functions do not satisfy the boundary conditions for the fourth order differential equations. Also the standard refinements of IGA do not yield reasonable solutions to fourth-order equations containing singularities.

In this work, B-splines are modified minimally to satisfy the given boundary conditions using Partition of Unity with flat-top. To handle singularities on the cracked domain, the modified B-spline functions are enriched by singular functions that resemble the singularities of the fourth-order equation.

However, these kind of enrichment methods (GFEM or X-FEM) have to deal with large condition numbers of stiffness matrix and integrals of singular functions. In other words, the Galerkin method in the framework IGA have a stiffness matrix with large condition number and standard quadrature rules does not give accurate integrals of derivatives of enrichment functions.

In this work, we propose a mapping method that overcome these drawbacks of enriched IGA. This proposed mapping method has same result as the enrichment methods with minimal condition number and without singular integrals. The mapping method is developed for one-dimensional problem and is extended to the second-dimensional fourth-order equations on a cracked disk. In the frame of FEM, a mapping method for the elasticity equations on cracked domain, was introduced in [42]. Also, in the frame of IGA, a mapping method for second order PDEs with singularities was introduced [48]. We generalize the proposed mapping method introduced in [48] and apply it to fourth-order equation containing singularities.

The outline of this chapter is as follows. In section 2, we present mapping method scheme for one-dimensional problem and test this approach to fourth-order equation with singularity. In section 3, This mapping method scheme is developed and tested for second dimensional problems on cracked domain. Conclusions follow.

6.2   Enriched PU-IGA and PU-IGA with Mapping Method

Consider the following model problem with clamped boundary conditions

$$
\begin{cases}
u^{(4)}(x) = f(x) & \text{in } (a,b) \\
u(a) = u'(a) = 0 & \\
u(b) = u'(b) = 0 &
\end{cases}
\tag{39}
$$

Let $\mathcal{V} = \{w \in H^2(a,b) : w, w' \in H_0^1(a,b)\}$ be the function space. Multiplying the equation by an arbitrary function $v \in \mathcal{V}$ and integrating over the interval, we have

$$
\int_a^b u^{(4)} v \, dx = \int_a^b u^{(2)} v^{(2)} \, dx = \int_a^b f v \, dx \quad \forall v \in \mathcal{V}
$$

Thus the variational equation is

$$
\mathcal{B}(u,v) \equiv \int_a^b u^{(2)} v^{(2)} \, dx = \int_a^b f v \, dx \equiv \mathcal{F}(v), \quad \forall v \in \mathcal{V}
$$

We construct an example of a fourth-order equation containing singularity of the type x^α. To determine how strong the intensity of singularity α is allowed, we prove the following lemma.

Lemma 2. Suppose $v \in H_0^2(a,b), \;\; 0 \leq a < b$. Then

$$
(1) \quad |v(x)| < C x^{1.5} \tag{40}
$$

$$
(2) \quad \left| \int_a^b x^{\alpha-4} v(x) dx \right| < \infty \quad \text{if } \alpha > 1.5. \tag{41}
$$

Proof. (1)

$$
\text{Since} \quad v(x) \in H_0^2(a,b), \quad v'(x) \in H_0^1(a,b),
$$

$$
\text{then} \quad |v'(x)| < C x^{0.5}, \quad C \in \mathbb{R} \quad \text{by Theorem 7.17 in [21]}
$$

Hence we have

$$|v(x)| = |\int_a^x v'(t)dt| \leq C \int_0^x t^{0.5}dt \leq Cx^{1.5}.$$

(2)

$$\left| \int_a^b x^{\alpha-4}v(x)dx \right| \leq C \int_0^b x^{\alpha-4}x^{1.5}dx$$

For this to be integrable, $\alpha - 4 + 1.5 > -1$

Therefore, $\alpha > 1.5$ $\qquad\qquad\qquad\qquad\qquad\qquad\qquad\qquad\qquad$ □

We use the Enriched PU-IGA which is developed for the singularly perturbed problems, to solve the fourth-order equation with singularities. In singularly perturbed problems, we do not know the boundary layer functions so that we approximate the boundary layer functions and use the approximation as enrichment function. We approximate the boundary layer function on the reference domain not on physical domain. We add the boundary layer approximation and push-forward them to the physical domain to construct the Finite Element Space.

Here, we consider the problem whose singular solution is already known, like crack singularities. We propose two ways to solve the fourth-order equations containing singularities. First, we add singular functions into the Finite Element Space directly. We call this Enriched PU-IGA. Secondly, to get the singular function on the physical domain, we construct a particular Mapping from the reference domain onto the physical domain to generate singular functions on the physical domain. We call this approach PU-IGA with Mapping Method.

The k-refinement, the p-refinement, the reduced p-refinement of IGA for Enriched PU-IGA. Since the fourth-order derivative of singular functions are highly singular, a

special treatment, substitution method are needed for integrals of singular functions. Enriched PU-IGA gives accurate solution, but yields large condition numbers.

In PU-IGA with Mapping Method, the singular functions are generated through a particular mapping. Hence this method does not have a large condition number nor integrals of singular functions.

Enriched PU-IGA

We present the detail scheme of enriched PU-IGA for fourth-order equation with singularities. For simplicity, we assume that the physical domain is the same as the reference domain. Therefore, B-spline functions $\hat{N}_{i,p+1}(\xi)$ and its push-forward $N_{i,p+1}(x)$ onto the physical domain are same.

Consider a fourth-order equation containing singularities ξ^α and $\xi^{\alpha/2+1}$ with $1.5 < \alpha < 2$ (due to Lemma 2).

I. Divide the domain

We divide the domain into singular zone $[0, 0.4]$ and non singular zone $[0.3, 1]$.

II. Construct C^1-continuous B-spline functions

We compare p-refinement and k-refinement of Enriched PU-IGA. Consider the following two open knot vectors that correspond to the p-refinement and the k-refinement, respectively,

$$\Xi^p = \left\{ \underbrace{0,..,0}_{p+1}, \underbrace{0.1,..,0.1}_{p-1}, \underbrace{0.2,..,0.2}_{p-1}, .., \underbrace{0.8,..,0.8}_{p-1}, \underbrace{0.9,..,0.9}_{p-1}, \underbrace{1,..,1}_{p+1} \right\} \quad (42)$$

$$\Xi^k = \left\{ \underbrace{0,\ldots,0}_{p+1}, \quad 0.1, \quad 0.2, \quad \ldots \quad 0.8, \quad 0.9, \quad \underbrace{1,\ldots,1}_{p+1} \right\}. \quad (43)$$

Then we have at least C^1-continuous B-spline functions for p-refinement and kB-

refinement, respectively,

$$\mathcal{V}^p \;=\; \{N_{k,p+1}(x) \mid k = 1, \ldots, 10p - 8\} \tag{44}$$

$$\mathcal{V}^k \;=\; \{N_{k,p+1}(x) \mid k = 1, \ldots, p + 10\} \tag{45}$$

III. Boundary Conditions

To satisfy the clamped boundary conditions at both ends with the B-spline func-

tions (44) and (45). We consider the following two approaches.

- **Discarded** The first two and the last two B-spline functions from (44) and (45)

  are discarded.

$$\mathcal{V}_I^p \;=\; \left\{ N_i(\xi) : 3 \le i \le 10p - 10 \right\} \tag{46}$$

$$\mathcal{V}_I^k \;=\; \left\{ N_i(\xi) : 3 \le i \le p + 8 \right\} \tag{47}$$

- **Modified** The first two and the last two B-spline functions from (44) and (45)

  modified by PU functions with flat-top as follows:

$$^p N_i^*(\xi) \;=\; \begin{cases} N_i(\xi) \times \psi^R(\xi + 0.02), & \text{if } i = 1, 2, \\[2mm] N_i(\xi) \times \psi^L(\xi - 0.45), & \text{if } i = 10p - 9, 10p - 8 \end{cases}$$

$$^k N_i^*(\xi) \;=\; \begin{cases} N_i(\xi) \times \psi^R(\xi + 0.02), & \text{if } i = 1, 2, \\[2mm] N_i(\xi) \times \psi^L(\xi - 0.45), & \text{if } i = p + 9, p + 10 \end{cases}$$

Now modified $\mathcal{C}^1$-continuous B-spline approximation functions for the p-refinement

and the k-refinement, respectively, are as follows:

$$\mathcal{V}_{\text{II}}^p = \mathcal{V}_I^p \cup \{^pN_1^*, {^pN_2^*}, {^pN_{10p-8}^*}, {^pN_{10p-9}^*}\} \tag{48}$$

$$\mathcal{V}_{\text{II}}^k = \mathcal{V}_I^k \cup \{^kN_1^*, {^kN_2^*}, {^kN_{p+9}^*}, {^kN_{p+10}^*}\}$$

where

$$\psi^R(\xi) = \begin{cases} 0 & \text{if } \xi \leq 0.02 \\ N_5^{pu}(\xi) + N_6^{pu}(\xi) & \text{if } 0.02 \leq \xi \leq 0.06 \\ 1 & \text{if } 0.06 \leq \xi \end{cases}$$

$$\psi^L(\xi) = \begin{cases} 1 & \text{if } \xi \leq 0.5 \\ N_7^{pu}(\xi) + N_8^{pu}(\xi) & \text{if } 0.5 \leq \xi \leq 0.55 \\ 0 & \text{if } 0.55 \leq \xi \end{cases}$$

where N_j^{pu} is B-spline function corresponding to the knot vector:

$$\Xi^{pu} = \left\{ \underbrace{0, .., 0}_{4}, \underbrace{0.02, 0.02}_{2}, \underbrace{0.06, 0.06}_{2}, \underbrace{0.5, 0.5}_{2}, \underbrace{0.55, 0.55}_{2}, \underbrace{0.8, 0.8}_{2}, \underbrace{1, .., 1}_{4} \right\}$$

IV. Approximation Space

Two singular enrichment functions, ξ^α and $\xi^{\alpha/2+1}$, are added to the basis functions listed above. We define a modified and enriched C^1-continuous approximation as union of scaled enrichment functions and the list of basis functions in (48)

Enriched p-refinement of PU-IGA

Construct two PU functions with flat-top ψ_2, ψ_2^*, by the B-spline functions generated by the knot vector Ξ^p. We divide the domain into two patches which are the

supports of these two PU functions. The local approximation functions on the two patches are the same set of B-splines generated by Ξ^p. Additionally, two enrichment functions are added. Notice that the two PU functions change as the p-degree varies.

The two PU functions ψ_2 and ψ_2^* are constructed by;

$$\psi_2(\xi) \;=\; \sum_{j=1}^{3p-1} N_j^p(\xi) = \begin{cases} 1 & \text{if } 0 \le \xi \le 0.3, \\[2ex] N_{3p-2}^p(\xi) + N_{3p-1}^p(\xi) & \text{if } 0.3 \le \xi \le 0.4, \\[2ex] 0 & \text{if } 0.4 \le \xi \end{cases}$$

$$\psi_2^*(\xi) \;=\; 1 - \psi_2(\xi)$$

Enrichment functions N_i^s are scaled by PU function ψ_2 ;

$$N_i^s(\xi) = \begin{cases} \xi^\alpha \times \psi_2(\xi), & \text{if } i = 1, \\[2ex] \xi^{\alpha/2+1} \times \psi_2(\xi), & \text{if } i = 2. \end{cases}$$

Now define a modified and enriched $\mathcal{C}^1$-continuous approximation space as follows:

$$\begin{aligned} \mathcal{V}_{\text{rich}}^p \;=\; & \{N_1^s, N_2^s\} \;\cup\; \{\psi_2(\xi)N_k(\xi) : 1 \le k \le 4p-2, \; N_k(\xi) \in \mathcal{V}_{\text{II}}^p\} \\[2ex] & \cup \; \{\psi_2^*(\xi)N_k(\xi) : 3p-2 \le k \le 10p-8, \; N_k(\xi) \in \mathcal{V}_{\text{II}}^p\} \end{aligned} \tag{49}$$

Note that the number of basis functions used in this approach

$$\text{card}(\mathcal{V}_{\text{rich}}^p) = 11p - 5$$

This approach yields large matrix condition numbers. Hence, in order to reduce the size of condition numbers, next consider another approach which reduces a number of B-spline basis functions in the singular zone, the support of ψ_2. Moreover, since the maximum error occurs over the common non flat-top zone $[0.3, 0.4]$ of two

PU functions ψ_2 and ψ_2^*, choose PU functions that have smaller non flat-top zone $[0.35, 0.4]$.

Reduced, enriched p-refinement of IGA

Consider

$$\Xi^p = \Big\{ \underbrace{0, \ldots, 0}_{p+1}, \underbrace{0.1, .., 0.1}_{p-1}, \underbrace{0.2, .., 0.2}_{p-1}, \underbrace{0.3 + \delta^*, .., 0.3 + \delta^*}_{p-1}, \underbrace{0.4, .., 0.4}_{p-1}, \ldots, \underbrace{0.9, .., 0.9}_{p-1}, \underbrace{1, .., 1}_{p+1} \Big\},$$

Choose $\delta^* = 0.05$

$$\tilde{\psi}_2(\xi) = \begin{cases} 1 & \text{if } 0 \leq \xi \leq 0.3 + \delta^*, \\ N_{3p-2}(\xi) + N_{3p-1}(\xi) & \text{if } 0.3 + \delta^* \leq \xi \leq 0.4, \\ 0 & \text{if } 0.4 \leq \xi, \end{cases} \tag{50}$$

This $\mathcal{C}^1$-continuous PU function varies with p-degree

$$N_i^s(\xi) = \begin{cases} \xi^\alpha \times \tilde{\psi}_2(\xi), & \text{if } i = 1, \\ \xi^{\alpha/2+1} \times \tilde{\psi}_2(\xi), & \text{if } i = 2, \\ \xi^2 \times \tilde{\psi}_2(\xi), & \text{if } i = 3. \end{cases} \tag{51}$$

The corresponding approximation space is as follows:

$$\mathcal{W}_{\text{rich2}}^p = \{N_1^s, N_2^s, N_3^s\} \cup \{N_k(\xi) : 3p \leq k \leq 10p - 8, N_k(\xi) \in \mathcal{V}_{II}^p\}.$$

Let us note the following:

1. $\text{card}(\mathcal{W}_{\text{rich2}}^p) = 7p - 4 \ll \text{card}(\mathcal{V}_{\text{rich}}^p) = 11p - 5$.

2. $1 = \sum_{k=1}^{10p-8} N_k(\xi) = \sum_{i=1}^{3p-1} N_i(\xi) + \sum_{k=3p}^{10p-8} N_k(\xi) = \tilde{\psi}_2(\xi) + \sum_{k=3p}^{10p-8} N_k(\xi)$ on $[0, 1]$.

3. Numerical examples, Table 11, show that condition numbers are reduced by

half, however accuracy is also decreased by more than two orders of magnitude.

Next, consider the third approach which multiply enrichment functions to all the B-spline basis functions using the partition of unity property of B-spline functions.

PU-FEM like Enriched p-refinement of IGA

The B-spline functions generated by the open knot vector Ξ^p become $\mathcal{C}^1$-continuous PU functions that varies with p-degree. Like PU-FEM, include the enrichment functions multiplied by these B-spline PU functions.

$$\mathcal{W}^p_{\text{rich3}} = \{N_k(\xi) : 1 \leq k \leq 10p - 8, N_k(\xi) \in \mathcal{V}^p_{\text{II}}\} \bigcup$$
$$\left\{ \xi^\alpha \times N_k(\xi), \quad \xi^{\alpha/2+1} \times N_k(\xi), \quad : k = 1, \ldots, 3p - 1 \right\}$$

We observe the followings from numerical tests:

1. $\text{card}(\mathcal{W}^p_{\text{rich3}}) = 2(3p - 1) + (10p - 8)$.

2. The condition numbers are large and the accuracy is not as good as the enriched p-refinement approaches P1 and P2 above.

Enriched k-refinement of IGA

Since the B-spline functions generated by the knot vector Ξ^k are highly regular, consider two $\mathcal{C}^2$-continuous PU functions defined as follows:

$$\psi_3(\xi) = \begin{cases} 1 & \text{if } 0 \leq \xi \leq 0.3, \\ (4 - 10x)^3(600x^2 - 330x + 46) & \text{if } 0.3 \leq \xi \leq 0.4, \\ 0 & \text{if } 0.4 \leq \xi \end{cases}$$
$$\psi_3^*(\xi) = 1 - \psi_3(\xi).$$

Two enrichment functions are scaled by this PU function with flat-top.

$$N_j^s(\xi) = \begin{cases} \xi^\alpha \times \psi_3(\xi), & \text{if } j = 3 \\ \xi^{\alpha/2+1} \times \psi_3(\xi), & \text{if } j = 4 \end{cases}$$

The modified and enriched $\mathcal{C}^{p-1}$ approximation space is as follows:

$$\mathcal{V}_{\text{rich}}^k = \{N_3^s, N_4^s\} \cup \{\psi_3(\xi)N_i(\xi) : 1 \leq i \leq p+4, \; N_i(\xi) \in \mathcal{V}_{\text{II}}^k\}$$

$$\cup \; \{\psi_3^*(\xi)N_i(\xi) : 4 \leq i \leq p+10, \; N_i(\xi) \in \mathcal{V}_{\text{II}}^k\} \tag{52}$$

Note that

1. $\text{card}(\mathcal{V}_{\text{rich}}^k) = 2p + 13 \ll card(\mathcal{V}_{\text{rich}}^p) = 11p - 5$

2. Numerical example shows that the condition numbers are about a half of the enriched p-refinement of IGA (P1 approach) because the degree of freedom is smaller.

Both enriched p-refinement and k-refinement of IGA yield accurate solutions. However, their condition numbers are large. Moreover, since enrichment functions and their derivatives are singular, these methods fail to give reasonable solutions without special treatment for accurate integrals.

V. Special Treatment for singular integration

We use substitution function to treat singular integration.

1. Let $T(x) = x^\beta$ be an substitution function, whose mapping size β is determined by the strongest singular term.

$$\int_{[a,b]} ((\xi^\alpha)'')^2 d\xi = C \int_{[a,b]} \xi^{2(\alpha-2)} d\xi = C \int_{T^{-1}([a,b])} x^{2(\alpha-2)\beta} x^{\beta-1} dx$$

I choose β so that

$$2(\alpha-2)\beta + \beta - 1 \geq 0$$

$$\beta \geq \frac{1}{2\alpha - 3}$$

2. Since $\alpha = 1.6$, I select a substitution function $T : [0, 0.4^{1/5}] \longrightarrow [0, 0.4]$ defined

   by

   $$\xi = T(x) = x^5 \tag{53}$$

   Then this substitution function converts a singular integral to a regular integral.

   For example,

   $$\int_0^{0.3} [(\xi^{1.6})''] d\xi = \int_0^{0.3^{1/5}} 0.96(T(x)^{-0.4})5x^4 dx = \int_0^{0.3^{1/5}} 4.8x^2 dx$$

3. p-**refinement of PU-IGA** For $N_j, N_i^s \in \mathcal{V}_{rich}^p$ of (49), we compute the bilinear

   form as follows:

   $$\mathcal{B}(N_i^s, N_j) = \sum_{k=0}^{3} \int_{a_k}^{a_{k+1}} N_j^{(2)}(T(x))(N_i^s)^{(2)}(T(x))5x^4 dx$$

   $$\mathcal{F}(N_i^s) = \sum_{k=0}^{3} \int_{a_k}^{a_{k+1}} f(T(x))(N_i^s(T(x))5x^4 dx$$

   $$\text{where} \quad a_i = T^{-1}(i), \quad i = 0.1, 0.2, 0.3, 0.4$$

4. k-**refinement of PU-IGA** For $N_j, N_i^s \in \mathcal{V}_{rich}^k$ of (52), we compute the bilinear

form as follows:

$$
\begin{aligned}
\mathcal{B}(N_i^s, N_j) &= \sum_{k=0}^{3} \int_{a_k}^{a_{k+1}} N_j^{(2)}(T(x))(N_i^s)^{(2)}(T(x))5x^4 dx \\
\mathcal{F}(N_i^s) &= \sum_{k=0}^{3} \int_{a_k}^{a_{k+1}} f(T(x))(N_i^s(T(x))5x^4 dx \\
\text{where} \quad a_i &= T^{-1}(i), \quad i = 0.1, 0.2, 0.3, 0.4
\end{aligned}
$$

Enriched PU-IGA with Mapping Method

In the section, we propose a mapping method that overcome large condition number and singular integration caused by adding enrichment functions directly to the approximation spaces. The proposed mapping method generates singular functions through a push forward mapping from the reference domain onto the singular zone. Hence, it has as small condition number as that of general IGA. Moreover, singular integrals do not appear in computation of stiffness matrices.

The mapping generating the enrichment functions depends on the singularities of problems.

Consider a fourth order equation whose true solution is

$$
u(x) = x^{1.6} - 2x^{1.8} + x^2,
$$

which is singular at the left end of the physical domain $\Omega = [0, 1]$. We assume that the physical domain is the same as the reference domain.

I. Partition of the physical domain into a singular zone and a regular zone:

We consider two mappings to build singular basis functions on a singular zone $\Omega_{sing} = [0, 0.5]$ and regular basis functions on a regular zone $\Omega_{reg} = [0.4, 1]$,

$$F : \hat{\Omega} = [0, 1] \longrightarrow \Omega_{sing}, \qquad G : \hat{\Omega} = [0, 1] \longrightarrow \Omega_{reg},$$

defined by

$$x = F(\xi) \quad = \quad 0.5 \cdot \xi^5 \tag{54}$$

$$x = G(\xi) \quad = \quad 0.6\xi + 0.4 \tag{55}$$

Then we have

$$G^{-1}(x) \quad = \quad \frac{x - 0.4}{0.6}, \quad G^{-1}([0.4, 0.5]) = [0, 1/6], \quad F^{-1}([0.4, 0.5]) = [0.8^{0.2}, 1]$$

The selection of F depends on the strength of singularity. The mapping (54) corresponds to the intensity of singularity $\alpha = 1.6$. The inverse mapping $\xi = F^{-1}(x)$ brings

$$\xi^8, \xi^9, \xi^{10}, \xi^{15}, \xi^{20}, \ldots \xi^{5k}$$

in the reference domain to

$$(2x)^{1.6}, (2x)^{1.8}, (2x)^2, (2x)^3, (2x)^4, \ldots, (2x)^k$$

in the physical domain. These functions satisfy the clamped boundary conditions at $x = 0$.

Note that push-forwards $\xi^k, k \leq 7$ through F mapping are not acceptable basis

functions in the physical domain.

$$\xi^k \circ F^{-1}(x) = (2x)^{k/5} < (2x)^{7/5} = (2x)^{1.4}$$

By Lemma 3.1, this cannot be basis function on the physical domain.

II. $\mathcal{C}^1$-continuous PU functions with flat-top

Let us define two PU functions on the physical domain as follows:

$$\psi_4(x) \quad = \quad \begin{cases} 1 & \text{if } 0 \le x \le 0.4 \\ (5 - 10x)^2(20x - 7) & \text{if } 0.4 \le x \le 0.5 \\ 0 & \text{if } 0.5 \le x \le 1 \end{cases} \tag{56}$$

$$= \quad \begin{cases} 1 & \text{if } x \in [0, 0.4] \\ N_{5,4}(x) + N_{6,4}(x) & \text{if } x \in [0.4, 0.5] \\ 0 & \text{if } x \in [0.5, 1] \end{cases}$$

$$\psi_4^*(x) \quad = \quad 1 - \psi_4(x) \tag{57}$$

$$\hat{\psi}_4(\xi) \quad = \quad \psi_4 \circ F, \quad \hat{\psi}_4^*(\xi) = \psi_4^* \circ G. \tag{58}$$

where $N_{k,4}(x)$, $1 \le k \le 14$ are the B-spline functions corresponding to the following knot vector

$$\{\underbrace{0 \ldots 0}_{4}, \underbrace{0.2, 0.2}_{2}, \underbrace{0.4, 0.4}_{2}, \underbrace{0.5, 0.5}_{2}, \underbrace{0.6, 0.6}_{2}, \underbrace{0.8, 0.8}_{2}, \underbrace{1 \cdots 1}_{4}\}.$$

Note that

$$\psi_4(x) + \psi_4^*(x) = 1, \quad \forall x \in \Omega$$

$$\hat{\psi}_4(\xi) + \hat{\psi}_4^*(\xi) \neq 1, \quad \forall \xi \in \hat{\Omega}$$

These are not PU functions on the reference domain.

The physical and the reference domains are partitioned as follows:

$$\Omega = [0, 0.4] \cup [0.4, 0.5] \cup [0.5, 1],$$

$$\hat{\Omega}_F = [0, 0.8^{0.2}] \cup [0.8^{0.2}, 1], \quad \hat{\Omega}_G = [0, 1/6] \cup [1/6, 1]$$

Non flat-top zones of $\hat{\psi}_4$ and $\hat{\psi}_4^*$ are $[0.8^{0.2}, 1]$ and $[0, 1/6]$ respectively.

III. Basis functions on the reference domain

$$\hat{\mathcal{V}}_F = \hat{\psi}_4(\xi) \times \{\hat{M}_1 = \xi^8, \hat{M}_2 = \xi^9, \hat{M}_{1+k} = \xi^{5k}, k = 2, 3, 4\} \tag{59}$$

$$\hat{\mathcal{V}}_G^p = \hat{\psi}_4^*(\xi) \times \{\hat{N}_{k,p+1}(\xi) : k = 1, \ldots, 2p - 1\} \tag{60}$$

where $\hat{N}_{k,p+1}(\xi)$ are B-spline functions corresponding to the following knot vector:

$$\Xi = \{\underbrace{0 \cdots 0}_{p+1}, \underbrace{1/p+1}_{1}, \underbrace{2/p+1}_{1}, \cdots, \underbrace{p/p+1}_{1}, \underbrace{1 \cdots 1}_{p+1}\}. \tag{61}$$

The push-forwards of these basis functions (59) through F resemble the singularities.

The last two B-spline functions were discarded to satisfy the clamped boundary conditions for $\hat{\mathcal{V}}_G^p$. We have

$$\text{card}(\hat{\mathcal{V}}_F \cup \hat{\mathcal{V}}_G^p) = 2p + 4$$

IV. Bilinear Form Calculation

We implement this mapping method calculating the bilinear forms and load vectors as follows.

(**F mapping**)

Lemma 3. If $\hat{u}(\xi) = (u \circ F)(\xi)$, then

$$
\begin{aligned}
u_{xx} \circ F &= \hat{u}_{\xi\xi}\left(\left(\frac{dF}{d\xi}\right)^{-1}\right)^2 + \hat{u}_\xi\left(\left(\frac{dF}{d\xi}\right)^{-1}\right)_\xi \left(\frac{dF}{d\xi}\right)^{-1} \\
&= (\hat{u}_{\xi\xi})(16\xi^{-8}) + (\hat{u}_\xi)((-16)\xi^{-5})(4\xi^{-4}) \\
&= 0.16\left(\hat{u}_{\xi\xi}\xi^{-8} - 4\hat{u}_\xi\xi^{-9}\right)
\end{aligned}
$$

(**G mapping**)

Lemma 4. If $\hat{w}(\xi) = (w \circ G)(\xi)$, then

$$
\begin{aligned}
w_{xx} \circ G &= \hat{w}_{\xi\xi}\left(\left(\frac{dG}{d\xi}\right)^{-1}\right)^2 + \hat{w}_\xi\left(\left(\frac{dG}{d\xi}\right)^{-1}\right)_\xi \left(\frac{dG}{d\xi}\right)^{-1} \\
&= \hat{w}_{\xi\xi}\left(\frac{1}{0.36}\right).
\end{aligned}
\tag{62}
$$

Case 1: Bilinear form for two basis functions in $\mathcal{V}_F$

Suppose $u = \hat{u} \circ F^{-1}, v = \hat{v} \circ F^{-1}$, where $\hat{u} = \hat{\psi}_4(\xi) \cdot \hat{M}_k$ and $\hat{v} = \hat{\psi}_4(\xi) \cdot \hat{M}_l$ are

in $\hat{\mathcal{V}}_F$. By Lemma 3 , we have

$$
\begin{aligned}
\mathcal{B}(u,v) &= \left(\int_0^{0.8^2} + \int_{0.8^2}^1\right)(u_{xx}\circ F)(v_{xx}\circ F)|J(F)|d\xi \\
&= (0.16^2)\left(\int_0^{0.8^2} + \int_{0.8^2}^1\right)\left(\hat{u}_{\xi\xi}\xi^{-8} - 4\hat{u}_\xi\xi^{-9}\right)\left(\hat{v}_{\xi\xi}\xi^{-8} - 4\hat{v}_\xi\xi^{-9}\right)|J(F)|d\xi \\
&= (0.16^2)\int_0^{0.8^2}\left((\hat{M}_k)_{\xi\xi}\xi^{-8} - 4(\hat{M}_k)_\xi\xi^{-9}\right)\left((\hat{M}_l)_{\xi\xi}\xi^{-8} - 4(\hat{M}_l)_\xi\xi^{-9}\right)|J(F)|d\xi \\
&\quad +(0.16^2)\int_{0.8^2}^1\left((\hat{\psi}_4\cdot\hat{M}_k)_{\xi\xi}\xi^{-8} - 4(\hat{\psi}_4\cdot\hat{M}_k)_\xi\xi^{-9}\right) \\
&\qquad\cdot\left((\hat{\psi}_4\cdot\hat{M}_l)_{\xi\xi}\xi^{-8} - 4(\hat{\psi}_4\cdot\hat{M}_l)_\xi\xi^{-9}\right)|J(F)|d\xi
\end{aligned}
$$

$$
\begin{aligned}
\mathcal{F}(v) &= \left(\int_0^{0.8^2} + \int_{0.8^2}^1\right)(f\circ F)(v\circ F)|J(F)|d\xi \\
&= \int_0^{0.8^2}(f\circ F)(\hat{M}_l)|J(F)|d\xi + \int_{0.8^2}^1(f\circ F)(\hat{\psi}_4\cdot\hat{M}_l)|J(F)|d\xi
\end{aligned}
$$

where

$$
\begin{aligned}
|J(F)| &= 2.5\xi^4, \\
\hat{\psi}_4(\xi) &= \left(5 - 10\cdot F(\xi)\right)^2\left(20\cdot F(\xi) - 7\right) = (5 - 5\xi^5)(10\xi^5 - 7), \text{ for } \xi \in [0.8^2, 1]
\end{aligned}
$$

Case 2: Bilinear form for two basis functions in $\hat{\mathcal{V}}_G$

Suppose $u = \hat{u}\circ G^{-1}, v = \hat{v}\circ G^{-1}$, where $\hat{u} = \hat{\psi}_4^*(\xi)\cdot\hat{N}_k(\xi)$ and $\hat{v} = \hat{\psi}_4^*(\xi)\cdot\hat{N}_l(\xi)$

are in $\hat{\mathcal{V}}_G$. By Lemma 4, we have

$$
\begin{aligned}
\mathcal{B}(u, v) &= \int_0^1 u_{xx} v_{xx} dx = \left(\int_0^{1/6} + \int_{1/6}^1 \right)(u_{xx} \circ G)(v_{xx} \circ G)|J(G)|d\xi \\
&= (\frac{1}{0.36})^2 \int_{1/6}^1 (\hat{N}_k)_{\xi\xi}(\hat{N}_l)_{\xi\xi}|J(G)|d\xi \\
&+ (\frac{1}{0.36})^2 \int_0^{1/6} (\hat{\psi}_4^* \hat{N}_k)_{\xi\xi}(\hat{\psi}_4^* \hat{N}_l)_{\xi\xi}|J(G)|d\xi
\end{aligned}
$$

$$
\begin{aligned}
\mathcal{F}(v) &= \left(\int_0^{1/6} + \int_{1/6}^1 \right)(f \circ G) \cdot (\hat{v})|J(G)|d\xi \\
&= \int_0^{1/6} (f \circ G) \cdot \hat{N}_l \cdot \hat{\psi}_4^* \cdot |J(G)|d\xi + \int_{1/6}^1 (f \circ G) \cdot \hat{N}_l \cdot |J(G)|d\xi
\end{aligned}
$$

where

$$
\begin{aligned}
|J(G)| &= 0.6 \\
\hat{\psi}_4^* &= 1 - \left(5 - 10 \cdot G(\xi) \right)^2 \left(20 \cdot G(\xi) - 7 \right) \\
&= 1 - (1 - 6\xi)^2(12\xi + 1), \quad \text{for } \xi \in [0, 1/6]
\end{aligned}
$$

Case 3: Bilinear form for mixed type: one in $\hat{\mathcal{V}}_F$ and one in $\hat{\mathcal{V}}_G$

For $\hat{u} \in \hat{\mathcal{V}}_F$ and $\hat{v} \in \hat{\mathcal{V}}_G$, domains of $\hat{u} \circ F^{-1}$ and $\hat{v} \circ G^{-1}$ have non-void intersection $[0.4, 0.5]$. The product of two basis functions

$$
u = \hat{u} \circ F^{-1} = \psi_4(x)(\hat{M} \circ F^{-1}) \text{ and } v = \hat{v} \circ G^{-1} = \psi_4^*(x)(\hat{N} \circ G^{-1}),
$$

vanish except for points in $[0.4, 0.5]$.

Let $\hat{u} = \hat{\psi}_4 \hat{M}$ and $\hat{v} = \hat{\psi}_4^* \hat{N}$. By Lemmas 3 and 4, I have the following:

$$
\begin{aligned}
\mathcal{B}(u,v) &= \int_0^1 \Big((\hat{u} \circ F^{-1})_{xx} (\hat{v} \circ G^{-1})_{xx} \Big) dx \\
&= \int_{0.4}^{0.5} \Big((\hat{u} \circ F^{-1})_{xx} (\hat{v} \circ G^{-1})_{xx} \Big) \circ G \circ G^{-1} dx \\
&= \int_{0.4}^{0.5} \Big((\hat{\psi}_4 \cdot \hat{M} \circ F^{-1})_{xx} \circ G \Big) \cdot \Big((\hat{\psi}_4^* \cdot \hat{N} \circ G^{-1})_{xx} \circ G \Big) \circ G^{-1} dx \\
&= \int_{0.4}^{0.5} \Big((\hat{\psi}_4 \cdot \hat{M} \circ F^{-1})_{xx} \circ G \Big) \cdot \frac{1}{0.36} (\hat{\psi}_4^* \hat{N})_{\xi\xi} \circ G^{-1} d\xi \\
&= \int_{F^{-1}(0.4)}^{F^{-1}(0.5)} \Big(((\hat{\psi}_4 \cdot \hat{M}) \circ F^{-1})_{xx} \circ F \Big) \cdot \frac{1}{0.36} \Big((\hat{\psi}_4^* \hat{N})_{\xi\xi} \circ (G^{-1} \circ F) \Big) |J(F)| d\xi \\
&= \int_{0.8^2}^{1} 0.16 \Big((\hat{\psi}_4 \cdot \hat{M})_{\xi\xi} \xi^{-8} - 4(\hat{\psi}_4 \cdot \hat{M})_{\xi} \xi^{-9} \Big) \cdot \\
&\quad \frac{1}{0.36} \Big((\hat{\psi}_4^* \hat{N})_{\xi\xi} \circ (G^{-1} \circ F) \Big) |J(F)| d\xi \\
\text{where} \quad & (G^{-1} \circ F)(\xi) = \frac{5}{6}(\xi^5 - 0.8)
\end{aligned}
$$

Note that it is necessary to divide integrals over $[0.8^2, 1]$ whenever knots are inserted in $[0, 1/6]$ for the knot vector (61).

6.3   Numerical Results

We test enriched PU-IGA and PU-IGA with the Mapping Method introduced in the previous section to fourth-order equation with singularities. We also test general IGA with modified B-spline functions to a clamped fourth-order equation with smooth solution, to compare condition numbers of Enriched PU-IGA and general IGA.

We use relative error in maximum norm and energy norm to measure the accuracy. The energy norm of $u \in H^2(a,b)$ is defined by

$$
\left\{ \frac{1}{2} \int_a^b u^{(2)} u^{(2)} dx \right\}^{1/2} = \sqrt{\frac{1}{2}\mathcal{B}(u,u)} = \|u\|_{Eng}
$$

Figure 20: Relative Error in the Maximum Norm(Left). Condition numbers versus degrees freedom in semi log scale (Right).

The relative error in the energy norm is

$$\|u - U\|_{Eng,rel}^2 = \left| \frac{\|u\|_{Eng}^2 - \|U\|_{Eng}^2}{\|u\|_{Eng}^2} \right|$$

Example 5. Fourth-order differential equation containing singularities

Suppose

$$u(x) = \left(x^{\alpha/2} - x \right)^2 = x^\alpha - 2x^{\alpha/2+1} + x^2$$

is the true solution of the model problem (39) satisfying the clamped boundary conditions at both ends of $\Omega = (0,1)$.

Then we have

$$u^{(4)}(x) = (\alpha)(\alpha-1)(\alpha-2)(\alpha-3)x^{\alpha-4} - 2(\alpha/2+1)(\alpha/2)(\alpha/2-1)(\alpha/2-2)x^{\alpha/2-3} = f(x)$$

Suppose we select an intensity of singularity $\alpha = 1.6$, then

$$\|u\|_{eng}^2 = 0.304$$

By Lemma 2, we have

$$\left| \int_0^1 f(x)v(x)dx \right| < \infty, \ \ v \in H_0^2(0,1)$$

We test Enriched PU-IGA; p-refinement, reduced p-refinement, k-refinement, and PU-IGA with Mapping Method. We observe the followings:

1. Table 11 shows that enriched p-refinement of IGA yields highly accurate nu-

Table 11: Relative error of numerical solutions of 1D fourth-order equation containing singularities obtained by Enrcihed p-refinement of PU-IGA.

Enriched p-refinement PU-IGA				
DEG	DOF	$\|Err\|_{Max}$	$\|Err\|_{Eng}$	$\kappa(A)$
3	28	1.355E-05	9.727E-05	3.4986E+19
4	39	4.963E-08	5.737E-06	1.7504E+17
5	50	3.814E-09	2.750E-06	6.6324E+17
6	61	3.224E-10	3.917E-06	1.0178E+19
7	72	9.160E-11	1.314E-06	1.6273E+19
8	83	1.546E-10	2.949E-05	2.4194E+18
9	94	5.818E-11	4.083E-06	1.0687E+19
10	105	1.018E-09	4.766E-06	9.1598E+18
Reduced, Enriched p-refinement of PU-IGA				
DEG	DOF	$\|Err\|_{Max}$	$\|Err\|_{Eng}$	$\kappa(A)$
3	17	8.509E-02	1.882E-02	4.4658E+09
4	24	5.265E-02	1.212E-02	4.5521E+09
5	31	1.546E-02	5.160E-03	4.5545E+09
6	38	9.254E-04	1.244E-03	4.4294E+09
7	45	3.674E-04	6.800E-04	4.2640E+09
8	52	1.281E-04	5.002E-04	4.1050E+09
9	59	2.626E-05	2.766E-04	3.9573E+09
10	66	4.297E-06	1.306E-04	3.8204E+09

Table 12: Relative errors of numerical solutions of 1D fourth-order equation containing singularities obtained by Enriched k-refinement of PU-IGA

Enriched k-refinement PU-IGA				
DEG	DOF	$\|Err\|_{Max}$	$\|Err\|_{Eng}$	$\kappa(A)$
3	19	1.504E-05	9.903E-05	1.4983E+10
4	21	2.700E-07	2.197E-06	2.4058E+10
5	23	6.678E-08	1.315E-06	3.6642E+10
6	25	1.037E-08	1.558E-06	5.8168E+11
7	27	1.642E-09	1.738E-06	5.3845E+13
8	29	2.716E-10	1.015E-06	5.6871E+15
9	31	5.867E-11	1.278E-06	6.6014E+17
10	33	2.618E-11	1.126E-06	7.7665E+16

Table 13: Relative errors of numerical solutions of fourth-order equation containing singularities obtained by PU-IGA with Mapping Method and by k-refinement of IGA with no enrichment

PU-IGA with Mapping Method				
DEG	DOF	$\|Err\|_{Max}$	$\|Err\|_{Eng}$	$\kappa(A)$
3	6	7.932E-03	2.510E-03	6.34358E+04
4	7	2.143E-04	1.621E-04	6.35467E+04
5	8	6.833E-06	1.133E-04	6.38121E+04
6	9	1.639E-06	1.137E-04	6.53461E+04
7	10	9.190E-07	1.137E-04	6.95966E+04
8	11	8.392E-07	1.137E-04	7.64534E+04
9	12	6.340E-07	1.137E-04	8.94563E+04
10	13	5.630E-07	1.137E-04	1.16090E+05
k-refinement of IGA without enrichment				
DEG	DOF	$\|Err\|_{Max}$	$\|Err\|_{Eng}$	$\kappa(A)$
3	13	7.339E-02	0.866E-00	5.4460E+03
4	14	3.144E-02	0.785E-00	7.1718E+03
5	15	2.395E-02	0.717E-00	1.1849E+04
6	16	2.035E-02	0.658E-00	1.9012E+04
7	17	1.679E-02	0.605E-00	2.9001E+04
8	18	1.584E-02	0.557E-00	4.2240E+04
9	19	1.433E-02	0.512E-00	5.9166E+04
10	20	1.339E-02	0.468E-00	8.0227E+04

merical solutions of the fourth-order equation containing singularities, however condition numbers are unacceptably large. Even for the reduced p-refinement of IGA in which degree of freedom is much smaller, the condition numbers are still large. Table **??** listed in appendix A, shows that the p-refinement of IGA with no enrichment failed to yield any practical solutions.

2. Table 12 shows that enriched k-refinement of IGA is also able to yield highly accurate numerical solutions. However, the condition numbers are still large. The second half of Table 12 shows that the k-refinement of IGA with no enrichment can not solve singularity problems.

3. The first half of Table 13 shows that the mapping method is able to yield accurate numerical solutions and condition numbers of this method are small.

4. The following condition numbers show that the matrix condition number $\kappa(A)$ does not depend on the regularity of PU functions that much. For k-refinement of X-IGA with degree 10 and degree of freedom 24,

$$\kappa(A) = 1.9814E + 8, \quad \text{PU: } C^1\text{-continuous}$$

$$\kappa(A) = 2.1041E + 8, \quad \text{PU: } C^2\text{-continuous}$$

$$\kappa(A) = 2.1203E + 8, \quad \text{PU: } C^3\text{-continuous}$$

$$\kappa(A) = 7.0361E + 8, \quad \text{PU: } C^4\text{-continuous}$$

The mapping method converts a singular problem to a regular problem. To demonstrate the effectiveness of the mapping method, we show the condition numbers and

accuracy of IGA for a smooth problem.

Example 6. Smooth true solution Suppose

$$u(x) = e^x \left((1-x)^3 x^2 \right)$$

is the true solution of model problem (39) with clamped boundary conditions at both ends of the domain $\Omega = (0,1)$. Then we have

$$
\begin{aligned}
f(x) &= \left(e^x ((1-x)^3 x^2) \right)^{(4)} = -e^x(x+2)(x^4 + 15x^3 + 45x^2 - 31x - 6) \\
u^{(2)}(x) &= e^x(x-1)(x^4 + 8x^3 + 7x^2 - 12x + 2) \\
\|u\|_{Eng}^2 &= 0.315697892048689
\end{aligned}
$$

Relative errors of numerical solutions obtained by IGA using basis functions $\mathcal{V}_{\mathrm{II}}^p$, p-refinement, $\mathcal{V}_{\mathrm{II}}^k$, k-refinement, and $\mathcal{V}_{\mathrm{II}}^h$, h-refinement with fixed $p = 5$, respectively, are shown in Table 14. Their condition numbers are shown in Table 15. The approximation spaces $\mathcal{V}_{\mathrm{II}}^p$ and $\mathcal{V}_{\mathrm{II}}^k$ are defined by (48) and $\mathcal{V}_{\mathrm{II}}^h$ is similarly defined.

The numerical results in Table 14 show that the numerical result from PU-IGA with mapping method yields that high accuracy and that low condition numbers as those of IGA for the smooth solution.

6.4 Two-dimensional fourth order elliptic equations on a cracked disk

We extend the proposed PU-IGA with Mapping Method to deal with the fourth order equation containing singularities to the two dimensional cases.

[23] showed the solution of fourth-order equation in cracked domain with clamped boundary condition along the crack faces.

Table 14: Relative errors of numerical solutions of smooth function without singularities) obtained by IGA . For the h-refinement of IGA, p-degree is fixed to be $p = 5$.

k-refinement			p-refinement		h-refinement (deg=5)		
DEG	DOF	$\|Err\|_{Max}$	DOF	$\|Err\|_{Max}$	h-size	DOF	$\|Err\|_{Max}$
3	13	8.440E-04	22	6.768E-04	1/10	42	2.034E-07
4	14	3.230E-05	32	1.253E-05	1/20	82	3.234E-09
5	15	3.056E-06	42	2.034E-07	1/40	162	1.427E-10
6	16	1.303E-07	52	1.816E-09	1/100	402	4.428E-09
7	17	3.886E-09	62	5.881E-11			
8	18	1.793E-10	72	4.208E-11			
9	19	8.994E-11	82	3.120E-11			
10	20	9.149E-11	92	2.824E-11			
k-refinement			p-refinement		h-refinement (deg=5)		
DEG	DOF	$\|Err\|_{Eng}$	DOF	$\|Err\|_{Eng}$	h-size	DOF	$\|Err\|_{Eng}$
3	13	2.734E-02	22	2.559E-02	1/10	42	4.142E-05
4	14	2.447E-03	32	1.511E-03	1/20	82	1.548E-06
5	15	1.674E-04	42	4.142E-05	1/40	162	1.065E-05
6	16	8.836E-06	52	7.680E-07	1/100	402	6.314E-05
7	17	3.684E-07	62	5.955E-07			
8	18	7.956E-08	72	1.302E-06			
9	19	9.744E-08	82	1.336E-06			
10	20	8.795E-08	92	2.880E-06			

Table 15: Condition numbers of Stiffness matrix of smooth function

Condition numbers							
	k-refinement		p-refinement		h-refinement(deg=5)		
DEG	DOF	$\kappa(A)$	DOF	$\kappa(A)$	h-size	DOF	$\kappa(A)$
3	13	5.44E+03	22	5.36E+04	1/10	42	1.67E+05
4	14	7.17E+03	32	9.54E+04	1/20	82	1.34E+06
5	15	1.18E+04	42	1.67E+05	1/40	162	1.07E+07
6	16	1.90E+04	52	2.90E+05	1/100	402	1.68E+08
7	17	2.90E+04	62	4.52E+05			
8	18	4.22E+04	72	6.68E+05			
9	19	5.91E+04	82	9.52E+05			
10	20	8.02E+04	92	1.31E+06			

If $f \in P_2^k(\Omega)$,   i.e $r^{-k+|\alpha|} D^\alpha f \in L_2(\Omega)$, $|\alpha| \leq k$, then the solution of $\Delta^2 u = f$

in cracked domain Ω is

$$u(r,\theta) \quad = \quad \sum_{1 \leq m < k+5/2} r^{m+1/2}\left(\lambda_m s_m^1 + \nu_m s_m^2\right) + u_{reg}(r,\theta) \tag{63}$$

where

$$s_m^1 \quad = \quad \sin(m+1/2)\theta - \frac{2m+1}{2m-3}\sin(m-3/2)\theta,$$

$$s_m^2 \quad = \quad \cos(m+1/2)\theta - \cos(m-3/2)\theta, \quad u_{reg} \in P_2^{k+4}(\Omega).$$

Here λ_m, ν_m are constants. We construct a test problem from this solution.

Example 7. Consider the fourth order equation $\Delta^2 u = f$ in the cracked unit circular

domain Ω with clamped boundary conditions whose solution is

$$u(r,\theta) = (1-r)^2 r^{1.5}\Big(\sin(1.5\theta) - 3\sin(0.5\theta) + \cos(1.5\theta) - \cos(0.5\theta)\Big).$$

Then

$$u(1,\theta) = \frac{\partial u}{\partial n}(1,\theta) = 0,$$

$$u(r,0) = u(r,2\pi) = 0, \quad \frac{\partial u}{\partial y}(r,0) = \frac{\partial u}{\partial y}(r,2\pi) = 0.$$

$$f(r,\theta) = \Delta^2 u = -r^{-3/2}\Big(24r\cos(\theta/2) - 16\sqrt{2}\sin(3\theta/2 + \pi/4) + 72r\sin(\theta/2)\Big),$$

$$\text{Energy} = \frac{1}{2}\iint_\Omega \Delta u \Delta u = 16.755160678572160.$$

PU-IGA with Mapping Method

I. Divide the physical domain

We partition the physical domain into two subdomains, $\Omega_{sing} = \{(x,y)|0 \leq$
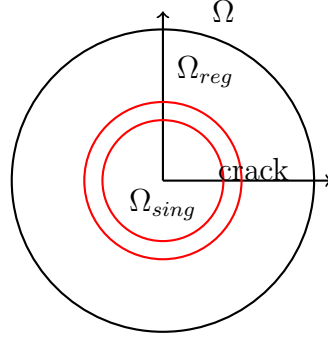
Figure 21: Cracked disk and Patches. $\Omega = \Omega_{sing} \cup \Omega_{reg}$.

$x^2 + y^2 \leq 0.5^2\}$ and $\Omega_{reg} = \{(x, y) : 0.4^2 \leq x^2 + y^2 \leq 1\}$.

II. Geometry Mappings

We construct one geometric mapping onto Ω_{reg}, denoted by G-mapping, and another geometric mapping, denoted by F-mapping, that generate singular functions resembling the singularities.

[G-mapping]

Define a geometric mapping

$$G : \hat{\Omega} = [0, 1] \times [0, 1] \longrightarrow \Omega_{reg}$$

$$G(\xi, \eta) = (0.4 + 0.6\eta)\Big(\cos 2\pi(1 - \xi), \sin 2\pi(1 - \xi)\Big) \tag{64}$$

where $\quad \Omega_{reg}$ has a crack along the positive x-axis.

Then we have

$$G^{-1}(x, y) \;\; = \;\; (\xi(x, y), \eta(x, y))$$

where

$$\xi(x, y) = \begin{cases} \frac{1}{2\pi} \cos^{-1}\left(\frac{x}{r}\right) & \text{if } y < 0 \\ 1 - \frac{1}{2\pi} \cos^{-1}\left(\frac{x}{r}\right) & \text{if } 0 \leq y \end{cases}, \qquad \eta(x, y) = \frac{(r - 0.4)}{0.6}$$

$$r = \sqrt{x^2 + y^2}, \qquad |J(G)| = 1.2\pi\left(0.4 + 0.6\eta\right)$$

[F-mapping]

Next, define a mapping to deal with singularities

$$F : \hat{\Omega} = [0, 1] \times [0, 1] \longrightarrow \Omega_{sing}$$

that maps polynomials to singular functions as follows:

$$F(\xi, \eta) = 0.5\eta^2\left(\cos 2\pi(1 - \xi), \sin 2\pi(1 - \xi)\right) \tag{65}$$

Then

$$F^{-1}(x, y) = (\xi(x, y), \eta(x, y))$$

where

$$\xi(x, y) = \begin{cases} \frac{1}{2\pi} \cos^{-1}\left(\frac{x}{r}\right) & \text{if } y < 0 \\ 1 - \frac{1}{2\pi} \cos^{-1}\left(\frac{x}{r}\right) & \text{if } 0 \leq y \end{cases}, \qquad \eta(x, y) = \frac{r^{1/2}}{\sqrt{0.5}}$$

$$J(F) = \begin{bmatrix} \pi\eta^2 \sin 2\pi(1 - \xi), & -\pi\eta^2 \cos 2\pi(1 - \xi) \\ \eta \cos 2\pi(1 - \xi), & \eta \sin 2\pi(1 - \xi) \end{bmatrix}, \qquad |J(F)| = \pi\eta^3$$

III. C^2-continuous PU functions with flat-top

$$\psi_R(r, \theta) = \begin{cases} 1 & \text{if } 0 \leq r \leq 0.4 \\ \left(5 - 10r\right)^2 \left(20r - 7\right) & \text{if } 0.4 \leq r \leq 0.5 \\ 0 & \text{if } 0.5 \leq r \leq 1 \end{cases} \tag{66}$$

$$\psi_L(r, \theta) = 1 - \psi_R(r, \theta) \tag{67}$$

$$\hat{\psi}_R(\xi, \eta) = \psi_R \circ F$$
$$= \begin{cases} 1 & \text{if } 0 \leq \eta \leq \sqrt{0.8} \\ \left(5 - 5\eta^2\right)^2 \left(10\eta^2 - 7\right) & \text{if } \sqrt{0.8} \leq \eta \leq 1 \\ 0 & \text{if } 1 \leq \eta \end{cases} \tag{68}$$

$$\hat{\psi}_L(\xi, \eta) = \psi_L \circ G$$
$$= \begin{cases} 0 & \text{if } \eta \leq 0 \\ 1 - \left(6\eta - 1\right)^2 \left(1 + 12\eta\right) & \text{if } 0 \leq \eta \leq 1/6 \\ 1 & \text{if } 1/6 \leq \eta \end{cases} \tag{69}$$

Note that

1. ψ_R defined by (66) on the two dimensional physical domain is the same as ψ_4 defined by (56) on the one dimensional physical domain.

2. The choice of non flat-top zone for the PU functions ψ_R and ψ_L is flexible. For a non flat-top zone, one can choose any $[a, b]$ with $0.2 \leq a < b \leq 0.5$ instead of $[0.4, 0.5]$.

3. $\psi_L(r, \theta) + \psi_R(r, \theta) = 1$ for all $(r, \theta) \in \Omega$, but $\hat{\psi}_L(\xi, \eta) + \hat{\psi}_R(\xi, \eta) \neq 1$.

IV. Construction of $\mathcal{C}^1$ basis functions

Basis functions on Ω_{sing}

We assume $p \geq 3$ and $q^* \geq 4$. $\hat{N}_{k,p+1}(\xi)$, $k = 1, 2, \ldots, p+10$, are $\mathcal{C}^{p-1}$-continuous B-splines of degree p, corresponding to an open knot vector

$$S_\xi = \{\underbrace{0 \ldots 0}_{p+1}, \underbrace{\frac{1}{p+1}}_{1}, \underbrace{\frac{2}{p+1}}_{1}, \ldots, \underbrace{\frac{p-1}{p+1}}_{1}, \underbrace{\frac{p}{p+1}}_{1}, \underbrace{1 \cdots 1}_{p+1}\}. \tag{70}$$

We modify them so that they satisfy the clamped boundary conditions. Like the one dimensional case, it can be done by either modifying the the first two and the last two B-splines or discarding these four functions.

Suppose we removed the first two and the last two B-spline functions among $\hat{N}_{i,p+1}(\xi)$, $1 \leq i \leq p+10$, so that the clamped boundary conditions are satisfied at both ends. We define basis function on the reference domain for the mapping F as follows:

$$\hat{\mathcal{V}}_F = \{\hat{N}_{i,p+1}(\xi)(\eta\sqrt{0.5})^l : i = 3, \ldots, p+8; l = 2, 3, 4, 5, 6, 7, 8, \ldots, q^*\},$$

where $q^* \geq 2k+5$, k determined by (63) that depends on the regularity of the source function f.

Then the set $\hat{\mathcal{V}}_F \circ F^{-1}$ generates the crack singularity as well as the complete polynomials of degree $[q^*/2]$ in the radial direction:

$$r, r^{1.5}, r^2, r^{2.5}, r^3, r^{3.5}, \ldots, r^{q^*/2}, \tag{71}$$

where $r^2 = x^2 + y^2$.

Using the PU function ψ_R, we construct basis functions defined on Ω_{sing} as

follows:

$$
\begin{aligned}
\mathcal{V}_F &= (\hat{\mathcal{V}}_F \circ F^{-1}) \cdot \psi_R \\
&= \left\{ \left(\hat{N}_{i,p+1}(\xi) \cdot (\eta\sqrt{0.5})^l \cdot \hat{\psi}_R(\xi, \eta) \right) \circ F^{-1} : \right. \\
&\qquad\qquad\qquad \left. i = 3, \dots, p+8; l = 2, 3, 4, 6, 7, \dots, q^* \right\} \qquad (72)
\end{aligned}
$$

Basis functions on Ω_{reg}

Suppose for $q \geq 3$, $\hat{M}_{k,q+1}(\eta), k = 1, 2, \dots, 2q+1$, are $\mathcal{C}^{q-1}$-continuous B-splines

corresponding to an open knot vector

$$
S_\eta = \{\underbrace{0 \dots 0}_{q+1}, \underbrace{\frac{1}{q+1}}_{1}, \underbrace{\frac{2}{q+1}}_{1}, \dots, \underbrace{\frac{q-1}{q+1}}_{1}, \underbrace{\frac{q}{q+1}}_{1}, \underbrace{1 \dots 1}_{q+1}\}. \qquad (73)
$$

Define basis functions on the reference domain for the mapping G as follows:

$$
\hat{\mathcal{V}}_G = \{\hat{N}_{i,p+1}(\xi) \cdot \hat{M}_{j,q+1}(\eta) : i = 3, \dots, 2p-1; j = 1, \cdots, 2q-1\}.
$$

Now, using the PU function ψ_L, we construct basis functions defined on Ω_{reg} as

follows:

$$
\begin{aligned}
\mathcal{V}_G &= (\hat{\mathcal{V}}_G \circ G^{-1}) \cdot \psi_L \qquad\qquad\qquad\qquad\qquad\qquad\qquad (74) \\
&= \left\{ \left(\hat{N}_{i,p+1}(\xi) \cdot \hat{M}_{j,q+1}(\eta) \cdot \hat{\psi}_L(\xi, \eta) \right) \circ G^{-1} : 3 \leq i \leq 2p-1; 1 \leq j \leq 2q-1 \right\}
\end{aligned}
$$

Note the following feature of basis functions on the physical subdomains Ω_{sing}

and Ω_{reg}.

1. The first two and the last two among $\hat{N}_{i,p+1}, 1 \leq i \leq 2p+1$, were discarded

   in the ξ-direction to satisfy the cramped boundary condition on the crack.

2. The last two among $\hat{M}_{j,q+1}, 1 \leq i \leq 2q+1$, were removed in the η-direction to satisfy the cramped boundary condition on the boundary.

[IV] Approximation Space on Ω

Our approximation space to deal with fourth order partial differential equation on a cracked circular domain Ω is

$$\mathcal{V}_\Omega = \mathcal{V}_G \cup \mathcal{V}_F \tag{75}$$

We observe the following:

- The total number of the degree of freedom is

$$
\begin{aligned}
\operatorname{card}(\mathcal{V}_\Omega) &= \operatorname{card}(\mathcal{V}_F) + \operatorname{card}(\mathcal{V}_G) \\
&= (2p - 3)\Big(6 + q^* - 3\Big) + (2q - 1)\Big)
\end{aligned}
$$

- The intersections of basis functions in $\mathcal{V}_F$ and those in $\mathcal{V}_G$ occur only in the annular region

$$\Omega_{sing} \cap \Omega_{reg} = \{(r, \theta) : 0 < \theta < 2\pi, \quad 0.4 \leq r \leq 0.5\}.$$

V. Bilinear Form We calculate the pullback of the Laplacian on the physical domain onto the reference domain for the stiffness matrix calculation.

Let $\Phi : \hat{\Omega} \longrightarrow \Omega$ be a mapping from the parameter space to the physical space defined by

$$\Phi(\xi, \eta) = (x(\xi, \eta), y(\xi, \eta)),$$

and let

$$\hat{u} = u \circ \Phi, \quad \nabla_x = (\partial_x, \partial_y)^T, \quad \nabla_\xi = (\partial_\xi, \partial_\eta)^T,$$

where u is a differentiable function defined on Ω. Then we have

$$(\nabla_x u) \circ \Phi = J(\Phi)^{-1} \nabla_\xi \hat{u} \quad \text{or} \tag{76}$$

$$
\begin{bmatrix} u_x \circ \Phi \\ u_y \circ \Phi \end{bmatrix} = \frac{1}{|J(\Phi)|} \begin{bmatrix} y_\eta & -y_\xi \\ -x_\eta & x_\xi \end{bmatrix} \begin{bmatrix} \hat{u}_\xi \\ \hat{u}_\eta \end{bmatrix} = \begin{bmatrix} J_{11}^{-1} & J_{12}^{-1} \\ J_{21}^{-1} & J_{22}^{-1} \end{bmatrix} \begin{bmatrix} \hat{u}_\xi \\ \hat{u}_\eta \end{bmatrix}.
$$

Using (76), we have

$$
\begin{aligned}
(\nabla_x u_x) \circ \Phi &= J(\Phi)^{-1} \nabla_\xi (u_x \circ \Phi) \\[2mm]
&= J(\Phi)^{-1} \nabla_\xi (J_{11}^{-1} \hat{u}_\xi + J_{12}^{-1} \hat{u}_\eta) \tag{77}
\end{aligned}
$$

$$
\begin{bmatrix} u_{xx} \circ \Phi \\ u_{xy} \circ \Phi \end{bmatrix} = J(\Phi)^{-1} \begin{bmatrix} (J_{11}^{-1} \hat{u}_\xi + J_{12}^{-1} \hat{u}_\eta)_\xi \\ (J_{11}^{-1} \hat{u}_\xi + J_{12}^{-1} \hat{u}_\eta)_\eta \end{bmatrix}
$$

Similarly, we have

$$
\begin{aligned}
(\nabla_x u_y) \circ \Phi &= J(\Phi)^{-1} \nabla_\xi (u_y \circ \Phi) \\[2mm]
&= J(\Phi)^{-1} \nabla_\xi (J_{21}^{-1} \hat{u}_\xi + J_{22}^{-1} \hat{u}_\eta) \tag{78}
\end{aligned}
$$

$$
\begin{bmatrix} u_{yx} \circ \Phi \\ u_{yy} \circ \Phi \end{bmatrix} = J(\Phi)^{-1} \begin{bmatrix} (J_{21}^{-1} \hat{u}_\xi + J_{22}^{-1} \hat{u}_\eta)_\xi \\ (J_{21}^{-1} \hat{u}_\xi + J_{22}^{-1} \hat{u}_\eta)_\eta \end{bmatrix}
$$

Let $\varphi(x,y) = \hat{\varphi} \circ \Phi^{-1}(x,y)$. Then

$$
\begin{aligned}
(\partial_{xx}\varphi) \circ \Phi &= J_{11}^{-1}\frac{\partial}{\partial\xi}\left(J_{11}^{-1}\frac{\partial}{\partial\xi}\hat{\varphi} + J_{12}^{-1}\frac{\partial}{\partial\eta}\hat{\varphi}\right) + J_{12}^{-1}\frac{\partial}{\partial\eta}\left(J_{11}^{-1}\frac{\partial}{\partial\xi}\hat{\varphi} + J_{12}^{-1}\frac{\partial}{\partial\eta}\hat{\varphi}\right) \\
(\partial_{yy}\varphi) \circ \Phi &= J_{21}^{-1}\frac{\partial}{\partial\xi}\left(J_{21}^{-1}\frac{\partial}{\partial\xi}\hat{\varphi} + J_{22}^{-1}\frac{\partial}{\partial\eta}\hat{\varphi}\right) + J_{22}^{-1}\frac{\partial}{\partial\eta}\left(J_{21}^{-1}\frac{\partial}{\partial\xi}\hat{\varphi} + J_{22}^{-1}\frac{\partial}{\partial\eta}\hat{\varphi}\right) \\
(\partial_{xy}\varphi) \circ \Phi &= J_{21}^{-1}\frac{\partial}{\partial\xi}\left(J_{11}^{-1}\frac{\partial}{\partial\xi}\hat{\varphi} + J_{12}^{-1}\frac{\partial}{\partial\eta}\hat{\varphi}\right) + J_{22}^{-1}\frac{\partial}{\partial\eta}\left(J_{11}^{-1}\frac{\partial}{\partial\xi}\hat{\varphi} + J_{12}^{-1}\frac{\partial}{\partial\eta}\hat{\varphi}\right) \\
(\partial_{yx}\varphi) \circ \Phi &= J_{11}^{-1}\frac{\partial}{\partial\xi}\left(J_{21}^{-1}\frac{\partial}{\partial\xi}\hat{\varphi} + J_{22}^{-1}\frac{\partial}{\partial\eta}\hat{\varphi}\right) + J_{12}^{-1}\frac{\partial}{\partial\eta}\left(J_{21}^{-1}\frac{\partial}{\partial\xi}\hat{\varphi} + J_{22}^{-1}\frac{\partial}{\partial\eta}\hat{\varphi}\right)
\end{aligned}
\tag{79}
$$

It is worthwhile to note that $\Delta\varphi \circ \Phi$ of (79) is different from the simplified form shown in [?] that does not hold for general cases.

For $u, v \in \mathcal{V}_\Omega$, we can calculate the entries in $\mathcal{B}(u,v)$ and $\mathcal{F}(v)$ in a similar manner as those in one-dimensional cases. Let $\triangle_x = \frac{\partial^2}{\partial x^2} + \frac{\partial^2}{\partial y^2}$

Case 1: $\forall u, v \in \mathcal{V}_F$

$$
\begin{aligned}
\mathcal{B}(u,v) &= \int_0^{2\pi}\int_0^{0.5}(\Delta_x u)(\Delta_x v)\,dxdy \\
&= \left(\int_0^1\int_0^{F^{-1}(0.4)} + \int_0^1\int_{F^{-1}(0.4)}^1\right)(\Delta_x u) \circ F \cdot (\Delta_x v) \circ F|J(F)|d\xi d\eta \\
\mathcal{F}(v) &= \left(\int_0^1\int_0^{F^{-1}(0.4)} + \int_0^1\int_{F^{-1}(0.4)}^1\right)f(F(\xi,\eta)) \cdot \hat{v} \cdot |J(F)|d\xi d\eta.
\end{aligned}
$$

Case 2: $\forall u, v \in \mathcal{V}_G$

$$
\begin{aligned}
\mathcal{B}(u,v) &= \left(\int_0^1\int_0^{G^{-1}(0.5)} + \int_0^1\int_{G^{-1}(0.5)}^1\right)(\Delta_x u) \circ G \cdot (\Delta_x v) \circ G|J(G)|d\xi d\eta \\
\mathcal{F}(v) &= \left(\int_0^1\int_0^{G^{-1}(0.5)} + \int_0^1\int_{G^{-1}(0.5)}^1\right)f(G(\xi,\eta)) \cdot \hat{v} \cdot |J(G)|d\xi d\eta.
\end{aligned}
$$

Case 3: $\forall u \in \mathcal{V}_F$ **and** $\forall v \in \mathcal{V}_G$

This calculation of bilinear form is similar to the 1-dimensional counterpart shown in the previous section.

$$
\begin{aligned}
\mathcal{B}(u,v) &= \int_0^{2\pi}\int_0^{0.5} (\Delta_x u)(\Delta_x v)\,dxdy \\
&= \int_0^{2\pi}\int_{0.4}^{0.5} \Delta_x(\hat{u}\circ F^{-1})\Delta_x(\hat{v}\circ G^{-1})\circ G\circ G^{-1}\,dxdy \\
&= \int_0^{2\pi}\int_{0.4}^{0.5} \left(\Delta_x(\hat{u}\circ F^{-1})\circ G\cdot\Delta_x(\hat{v}\circ G^{-1})\circ G\right)\circ G^{-1}\,dxdy \\
&= \int_0^1\int_{F^{-1}(0.4)}^1 \left((\Delta_x(\hat{u}\circ F^{-1})\circ G\cdot\Delta_x(\hat{v}\circ G^{-1})\circ G\right)\circ (G^{-1}\circ F)|J(F)|\,d\xi d\eta \\
&= \int_0^1\int_{F^{-1}(0.4)}^1 \left(\Delta_x(\hat{u}\circ F^{-1})\circ F\right)\cdot\left(\Delta_x(\hat{v}\circ G^{-1})\circ G\right)\circ (G^{-1}\circ F)|J(F)|\,d\xi d\eta
\end{aligned}
$$

where

$$
(G^{-1}\circ F)(\xi,\eta) = (\xi,\ \frac{0.5\eta^2 - 0.4}{0.6})
$$

VI. Numerical Results

Applying the two-dimensional PU-IGA with Mapping Method described above to Example 7, we have the numerical results in Table 16. We observe the followings:

1. Since $u(r,\theta)$ contains singular terms $r^{1.5}, r^{2.5}, r^{3.5}$, we must choose $q \geq 7$ in the approximation space $\mathcal{V}_F$.

2. An approximation space can be enriched by adding the singular functions directly

   $\left(r^{1.5}, r^{2.5}, r^{2.5}\right)\times\left(\sin(1.5\theta) - 3\sin(0.5\theta) + \cos(1.5\theta) - \cos(0.5\theta)\right)$ to get a similar spectral accuracy shown in Table 16. However, this directly enriched

Figure 22: Computed solution by Mapping method(Left). Computed solution without mapping method(Right). True solution(Down center). Figures are computed solutions when B-spline basis functions of degree $p = 5$ are used.

IGA in the physical space will face integrations of singular functions as well as large matrix condition numbers as we observed in the 1-dimensional counterpart.

3. Since this example does not have a regular part, the G-mapping part is not necessary. However, if a domain has n corners and cracks, we have to construct n singular mappings $F_i : \hat{\Omega} \longrightarrow \Omega_i, i = 1, \cdots, n$ and a regular mapping $G : \hat{\Omega} \longrightarrow \Omega \setminus \cup_{i=1}^{n} \Omega_i$ to apply this Mapping Method.

4. [**IGA with no enrichment**] Consider a smooth physical mapping $H : \hat{\Omega} \longrightarrow \Omega$ defined by

$$H(\xi, \eta) = \eta \Big(\cos(2\pi(1 - \xi)), \sin(2\pi(1 - \xi)) \Big)$$

Galerkin method using B-spline basis functions that are push-forwards by this mapping yields the results shown in the second table of Table 16. An adaptive Galerkin method using smooth B-spline basis functions without enrichments, fails to yield any practical solutions.

5. For the cases where condition numbers $\kappa(A)$ of Table 16 are large, we solve the corresponding algebraic systems by MATLAB. The MATLAB solutions are compared with the solutions obtained the direct solver to find out there are virtually no differences.

Table 16: Relative error of numerical solutions of 2D fourth-order equation on a crack domain obtained by PU-IGA with Mapping Method and IGA without enrichment, respectively. $\kappa(A)$ stands for the condition numbers of stiffness matrices.

PU-IGA with Mapping Method				
DEG	DOF	$\|Err\|_{Max}$	$\|Err\|_{Eng}$	$\kappa(A)$
3	169	3.355E-03	2.510E-02	8.7350E+10
4	196	3.111E-04	3.913E-03	3.9621E+11
5	225	3.236E-05	6.008E-04	2.1415E+12
6	256	4.528E-06	7.203E-05	1.0913E+13
7	289	9.877E-07	8.886E-05	4.4463E+13
8	324	1.095E-07	9.155E-05	1.3101E+14
9	361	1.017E-08	9.159E-05	4.5780E+14
10	400	1.900E-09	9.160E-05	2.0502E+15
11	441	3.868E-10	9.160E-05	9.8982E+15
12	484	1.084E-10	9.160E-05	4.8433E+16
IGA without Enrichment				
DEG	DOF	$\|Err\|_{Max}$	$\|Err\|_{Eng}$	$\kappa(A)$
3	169	9.612E-01	9.402E-01	5.2563E+17
4	196	9.885E-01	9.837E-01	2.1325E+18
5	225	9.705E-01	9.598E-01	5.8925E+18
6	256	1.051E-00	1.008E-00	2.2186E+19
7	289	9.685E-01	9.606E-01	6.1723E+19
8	324	1.011E-00	9.917E-01	1.4315E+20
9	361	9.773E-01	9.776E-01	2.4413E+21
10	400	9.849E-01	9.939E-01	1.0948E+22

CHAPTER 7: CONCLUSION AND FUTURE DIRECTIONS

The numerical evidence shows that we found an accurate approximate solution for the convection-diffusion problems and the heat equation with small convection term and small thermal conductivity, respectively. One of the novelties of this research is to compute a non oscillatory numerical solution using Isogeometric analysis combined with boundary layer analysis and avoiding finer mesh in a curved domain. In the future we intend to study elasticity equations.

In order to make local refinement and implementation of enrichment functions simple in the framework of IGA, we introduced partition of unity isogeometric analysis (PU-IGA). Moreover, to maintain resemblances of enrichment functions to singularities in target areas, we adopt the partition of unity with flat-top. Since we implement PU functions in the reference domain divided into several rectangular patches, overlapping parts of the enrichment functions and B-spline basis functions become rectangles in the reference domain. Thus the integrals for stiffness matrices and load vectors become easier and more accurate than before. Moreover, the bandwidth of the stiffness matrix becomes smaller.

In this paper, we tested the proposed method with boundary layer problems on a disk, a square, and a semi infinite domain. The first example shows that the k-refinement with carefully designed knot insertion yields similar results to that obtained by using boundary layer enrichments as approximation functions. Thus, in the

third example, we employed the k-refinement alone with non-uniformly distributed knots insertion in the boundary layer zones to obtain practical solutions at low cost. However, in the second example, comparing enriched PU-IGA with all other methods, we conclude that enriched PU-IGA is superior over other existing numerical methods whenever the boundary layer behavior of the given problem is known.

This enriched PU-IGA is extended to the fourth-order equations with singularities. We encounter some drawbacks of high condition number and singular integrals. We introduce PU-IGA with Mapping Method to overcome the drawbacks. This approach gives accurate solutions as well as smaller condition numbers. The proposed Mapping Method can be extended to handle various types of domain singularities cause by corners and cracks of physical domain.

REFERENCES

[1] Arnold D.N., Falk R.S.,*Edge effects in the Reissner-Mindlin plate theory*, Analytic and Computational Models of Shells. Edited by A. K. Noor, T. Belytschko, and J.C. Simo, ASME 1989.

[2] Babuška I. , Banerjee U., Osborn J.E., *Survey of meshless and generalized finite element methods:A unified approach,* Acta Numerica, Cambridge Press (2003) 1-125.

[3] Bazilevs Y., Beirao Da Veiga L., Cottrell J. A., Hughes T. J. R., Sangalli G., *Isogeometric analysis: Approximation, stability and error estimates for h-refined meshes*, Mathematical Models and Methods in Applied Sciences **16** (2006), 1031–1090.

[4] Bazilevs Y., Calo V., Cottrell J., Evans J., Hughes T. J. R., Lipton S., Scott M., Sederberg T., *Isogeometric analysis using T-splines,* Comput. Methods Appl. Mech. Engrg. 199 (5-8) (2010) 229-263.

[5] Borden M.J., Scott M.A., Evans J.A., Hughes T.J. R., *Isogeometric finite element data structures based on Bézer ext ration of NURBS*, Int. J. Numer. Meth. Engng **87** (2010), 15-47.

[6] Buffa A., Cho D., Sangalli G., *Linear independence of the T-spline blending functions associated with some particular T-meshes,* Comput. Methods Appl. Mech. Engrg. (2010) 1437-1445.

[7] Branco C., Cho D., *Generalized T-splines and VMCR T-meshes,* Comput. Meth. App. Mech. Engrg, 280 (2014) 176-196.

[8] Branco C., Berdinsky D., Cho D., Oh M.J., Kim T.W., *Trigonometric Generalized T-splines,* Compu Meth. App. Mech. Engrg, 268 (2014) 540-556.

[9] Bujanda, B., Clavero, C., Gracia, J.L., Jorge, J.C.: A high order uniformly convergent alternating direction scheme for time dependent reaction-diffusion singularly perturbed problems.. Numer. Math. 107(1), 1-25(2007)

[10] Cannon, J.R: The one-dimensional heat equation

[11] Chen Z. Finite element methods and their applications. Berlin: Springer- Verlag; 2005.

[12] Clavero, C., Gracia, J.L.: A high order HODIE finite difference scheme for 1D parabolic singularly perturbed reaction-diffusion problems. Appl.Math. Comput. 218(9), 5067-5080(2012)

[13] Cottrell JA, Hughes TJR, Bazilevs Y. Isogeometric Analysis: toward integration of CAD and FEA. Chichester, UK: John Wiley & Sons; 2009.

[14] Da Veiga L. , Buffa A., Cho D., Sangalli G., *Analysis suitable T-splines are Dual-compatible,* Compu Meth. App. Mech. Engrg, 249-252 (2012) 42-51.

[15] Cockburn B, Shu CW. The local discontinuous Galerkin method for timedependent convectiondiffusion systems. SIAM J Numer Anal 1998;35: 244063.

[16] Cottrell J. A., Hughes T. J. R. and Bazilevs Y., *Isogeometric analysis: Toward integration of CAD and FEM*, Wiley, 2009.

[17] Dorfel M. R., Juttler B., Simeon B.: *Adaptive isogeometric analysis by local h-refinement with T-splines,* Comput. Methods Appl. Mech. Engrg. 199 (5-8) (2010) 264-275.

[18] Duarte C. A., Oden J. T. : *An hp adaptive method using clouds,* Compu. Meth. App. Mech. Engrg, 139 (1996) 237-262

[19] Engel G, Garikipati K, Hughes TJR, Larson MG, Mazzei L, Taylor RL. Continuous/ discontinuous finite element approximations of fourth-order elliptic problems in structural and continuum mechanics with applications to thin beams and plates, and strain gradient elasticity. Comput Methods Appl Mech Eng 2002;191:433352.

[20] Fortin M, Brezzi F. Mixed and hybrid finite element methods. New York: Springer; 1979.

[21] Gilbarg, D, Trudinger, N.;Elliptic partial differential equations of second order;Berlin ; New York : Springer-Verlag, [1977]

[22] Griebel M., Schweitzer M.A.:*A particle-Partition of Unity Methods Part VII: Adaptivity,* Meshfree Methods for partial Differential Equations III, Lect. Notes in Compu. Science and Engr. 57, Springer 2007

[23] Grisvard, P. Elliptic Problems in Nonsmooth domains, SIAM, 2011

[24] Han W., Meng X.:*Error analysis of reproducing kernel particle method*, Comput. Meth. Appl. Mech. Engrg. 190 (2001) 6157-6181.

[25] Jung C.Y, Temam, R. : Convection-diffusion equations in a circle: The compatible case, Journal de mathematiques pures et appliquees, v96 n1 (2011): 88-10

[26] Jung C.-Y.; Temam R. :Singular perturbations and boundary layer theory for convection-diffusion equations in a circle: the generic noncompatible case, SIAM Journal on Mathematical Analysis, v44 n6 (2012 12 31): 4274-4296

[27] Hong Y., Jung C., Temam R. : *On Numerical approximation of stiff convection-diffusion equations in a circle,* Numer. math. 127(2) (2014) 292-313.

[28] Hong Y., Jung C. , Temam R.: *Singular perturbation of time dependent convection-diffusion equations in a circle,* Nonlinear Analysis, 119 (2015) 127-148.

[29] Hong, Y.: Numerical Approximation of the Singularly Perturbed Heat Equation in a Circle, Springer Science+Business Media New York 2014

[30] Hughes T. J. R., Cottrell J. A., and Bazilevs Y., *Isogeometric analysis: CAD, finite elements, NURBS, exact geometry and mesh refinement*, Comput. Methods Appl. Mech. Engrg. **194** (2005), 4135–4195.

[31] Jeong J.W., *Implementation of reproducing polynomial particle(RPP) shape functions in meshless particle methods for two dimensional elliptic partial differential equations*, PhD dissertation, University of North Carolina at Charlotte, 2008.

[32] Johnson, Claes: Numerical solution of partial differential equations by the finite element method;Cambridge [England] ; New York : Cambridge University Press(1987)

[33] Kopteva, N., Savescu, S.B.: Pointwise error estimates for a singularly perturbed time-dependent semilinear reaction-diffusion problem. IMA J. Number. Anal. 31(2), 616-639(2011)

[34] De Luycker E., Benson D. J., Belytschko T., Bazilevs Y. and Hsu M. C., *X-FEM in isogeometric analysis for linear fracture mechanics*, International Journal for Numerical Methethod in Engrg **87** (2011), 541–565.

[35] Lions, J.L.: Perturbations Singulieres dans les Problemses aux Limites et en Controle Optimal. In Lecutre Notes in Math., vol. 323, Springer, Berlin(1973) (in French)

[36] Li S., Liu W. K. : Meshfree Particle Methods, Springer-Verlag 2004.

[37] Liu W. K., Han W., Lu H., Li S., Cao J.: *Reproducing Kernel Element Method: Part I. Theoretical formulation,* Comput. Methods Appl. Mech. Engrg., Vol. 193 (2004) 933-951.

[38] Li S., Lu H., Han W., Liu W.K., Simkins D. C. Jr. :*Reproducing Kernel Element Method: Part II. Globally Conforming I^m/C^n hierarchies,* Comput. Methods Appl. Mech. Engrg., Vol. 193 (2004) 953-987.

[39] Linss, T., Madden, N. : Analysis of an alternating direction method applied to singularly perturbed reaction-diffusion problems.. Int. J. Number. Anal. Model. 7(3), 507-519(2010)

[40] J David Logan: Applied Mathematics, New York, NY John Wiley & Sons, 2013

[41] Melenk J. M., Babuška I. :*The partition of unity finite element method:Theory and application* , Comput. Methods Appl. Mech. Engr. 139 (1996) 239-314.

[42] Oh H.-S., Babuska: The method of auxiliary mapping for the finite element solutions of elasticity problems containing singularities; Journal of Computational Physics, v121 n2 (1995): 193-212

[43] Oh H.-S., Kim J. G., Hong W.T. *The Piecewise Polynomial Partition of Unity Shape Functions for the Generalized Finite Element Methods,* Comput. Methods Appl. Mech. Engrg. 197 (2008) 3702-3711

[44] Oh H.-S., Kim J.G., Jeong J.W. :*The Closed Form Reproducing Polynomial Particle Shape Functions for Meshfree Particle Methods*, Comput. Methods Appl. Mech. Engrg. 196 (2007) 3435-3461

[45] Oh H.-S., Kim J. G., Jeong J.W. , *The smooth piecewise polynomial particle shape functions corresponding to patch-wise non-uniformly spaced particles for meshfree particles methods,* Comput Mech 40 (2007) 569-594

[46] Oh H.-S., Jeong J.W. , Hong, W.T. *The generalized product partition of unity for the meshes methods,* J Comput Phyics 229 (2010) 100-1620

[47] Oh H.-S. , Jeong J.W. , Kim J. G., *The Reproducing Singularity Particle Shape function for problems containing singularities,* Comput Mech 41 (2007) 135-157

[48] Jeong J. W., Oh H.-S. , Kang S., Kim H., *Mapping Techniques in Isogeometric Analysis for elliptic boundary value problems containing singularities*, Comput. Methods Appl. Mech. Engrg. 254 (2013) 334-352.

[49] Oh H.-S., Kim H., Jeong J. W. *Enriched isogeometric analysis of elliptic boundary value problems in domains with crackes and/or corners,* Int. J. Numer. Meth. Engrg 97 (2014) 149-180.

[50] Oleinik, O.A., Samokhin, V.N.: Mathematical models in boundary layer theory. In: Applied mathematics and mathematical computation. Chapman and Hall, Boca Raton(1999)

[51] O'Malley, R.E.: Singularly perturbed linear two-point boundary value problems. SIAM Rev. 50(3), 459-482(2008)

[52] Ciarlet P. G., *Basic error estimates for elliptic problems*, Handbook of Numerical Analysis, Vol. II, North-Holland, 1991.

[53] Hughes T. J. R., *The finite element method: linear static and dynamic finite element analysis*, Dover, 2000.

[54] Phillips TN. Pseudospectral domain decomposition techniques for the Navier Stokes equations. In: Keyes DE, Chan TF, Meurant G, Scroggs JS, Voigt RG. Fifth international symposium on domain decomposition methods for partial differential equations. SIAM proceedings in applied mathematics; 1992. p. 53140.

[55] Rogers D. F., *An introduction to NURBS*, Academic Press, 2001.

[56] Piegl L. and Tiller W., *The NURBS Book,* 2nd ed, Springer, 1997.

[57] Quarteroni A. Numerical models for differential problems. Milan: Springer-Verlag; 2013

[58] Roos, ,H., Styness, M., Tobiska, L.: Robust Numerical Methods for Singularly Perturbed Differential Equations, Volume 24 of Springer Series in Computational Mathematics, 2nd edition. Springer, Berlin(2008). Convection-diffusion-reaction and flow problems

[59] Roos, H., Uzelac, Z.: The SDFEM for a convection-diffusion problem with two small parameters. Comput. Methods Appl. Math. 3(3), 443-458(2003). (electronic) Dedicated to John J. H. Miller on the occasion of his 65th birthday

[60] Schillinger D., Evans J.A., Reali A., Scott M.A., Hughs T.J.R. : *Isogeometric Collocation: Cost Comparison with Galerkin methods and Extension to Adaptive Hierarchical NURBS Discretization,* Comput. Methods Appl. Mech. Engrg., V. 267 (2013) 170-232.

[61] Strouboulis T., Copps K., Babuska I.: *Generalized Finite Element method*, Comput. Methods Appl. Mech. Engrg., 190 (2001) 4081-4193.

[62] Strouboulis T., Zhang L., Babuska I.: *Generalized Finite Element method using mesh-based handbooks:application to problems in domains with many voids*, Comput. Methods Appl. Mech. Engrg., 192 (2003) 3109-3161.

[63] Stynes, M.: Steady-state convection-diffusion problems. Acta Number. 14. 445-508 (2005)

[64] Stynes, M., Tobiska, L.: The SDFEM for a convection-diffusion problem with a bounary layer: optimal error analysis and enhancement of accuracy. SIAM J. Numer. Anal. 41(5), 1620-1642(2003) (electronic)

[65] Szabo B., Babuska I., Finite Element Analysis, John Wiley, 1991.

[66] Thomas, D.C., Scott, M.A., Evans, J.A., Tew, K., Evans, E.J.: *Bézier Projection: A unified approach for local projection and quadrature-free refinement and coarsening of NURBS and T-splines with particular application to isogeometric design and analysis*, Compt. Methods Appl. Mech. Engrg. 284 (2015) 55-105.

[67] Temme N.M.: *Analytical methods for an elliptic singular perturbation problems in a circle,* J. of Computational and applied Math. 207 (2007) 301-322

[68] Vishik, M.I., Lyusternik, L.A.: Regular degeneration and boundary layer for linear differential equations with small parameter. Uspekhi Mat. Nauk. 12, 3-122(1957)

[69] Viscor, M., Stynes, M. : A robust finite difference method for a singularly perturbed degenerate parabolic problem II. IMA J. NUmer. Anal. 33(2), 460-480(2013)